JULY 1959 VOLUME 1 (1959) No. 2

JOURNAL OF NUCLEAR MATERIALS

JOURNAL DES MATERIAUX NUCLEAIRES

A JOURNAL ON METALLURGY, CERAMICS AND SOLID STATE PHYSICS IN THE NUCLEAR ENERGY INDUSTRY

EDITORS:

R. W. CAHN – BIRMINGHAM, ENGLAND

J. P. HOWE – CANOGA PARK, U.S.A. - P. LACOMBE – PARIS, FRANCE

CONTENTS

NORTH-HOLLAND PUBLISHING COMPANY – AMSTERDAM

EDITORIAL ADVISORY BOARD — CONSEIL DES REDACTEURS

S. AAS (Kjeller, Norway)
K. F. ALDER (Lucas Heights, Australia)
P. ALBERT (Vitry, France)
G. W. ARDLEY (Whetstone, U.K.)
J. E. BURKE (Schenectady, U.S.A.)
R. CAILLAT (Saclay, France)
G. CHAUDRON (Vitry, France)
H. CHISWIK (Argonne, U.S.A.)
A. S. COFFINBERRY (Los Alamos, U.S.A.)
A. H. COTTRELL (Cambridge, U.K.)
R. L. CUNNINGHAM (Ottawa, Canada)
C. DECROLY (Bruxelles, Belgium)
M. D'HONT (Mol, Belgium)
J. D. FAST (Eindhoven, Netherlands)
H. M. FINNISTON (Newcastle, U.K.)
J. FRIEDEL (Paris, France)
E. GEBHARDT (Stuttgart, Germany)
G. B. GREENOUGH (Windscale, U.K.)
E. GRISON (Saclay, France)
R. R. HASIGUTI (Tokyo, Japan)
J. HERENGUEL (Antony, France)
R. KIESSLING (Stockholm, Sweden)
K. LÜCKE (Aachen, Germany)
B. LUSTMAN (Pittsburgh, U.S.A.)
R. MADDIN (Philadelphia, U.S.A.)
P. MURRAY (Harwell, U.K.)
R. MYERS (Sydney, Australia)
J. A. L. ROBERTSON (Chalk River, Canada)
J. A. SABATO (Buenos Aires, Argentina)
K. TANGRI (Bombay, India)
P. VACHET (Paris, France)

Papers or letters should be sent to one of the Editors,

R. W. CAHN (Dept. of Metallurgy, University of Birmingham, Birmingham 15, England).

J. P. HOWE (Atomics International, P.O. Box 309, Canoga Park, California, U.S.A.).

P. LACOMBE (Centre de Recherches Métallurgiques de l'Ecole des Mines, Blvd. St. Michel 60, Paris VI, France)

either directly or through a member of the Editorial Advisory Board.

Les articles ou les lettres devront être envoyés à un des Rédacteurs-en-chef,

R. W. CAHN (Dept. of Metallurgy, University of Birmingham, Birmingham 15, England).

J. P. HOWE (Atomics International, P.O. Box 309, Canoga Park, California, U.S.A.).

P. LACOMBE (Centre de Recherches Métallurgiques de l'Ecole des Mines, 60 Bd. St. Michel, Paris VI, France)

ou directement ou par un membre du Conseil des Rédacteurs.

Papers or letters should be written in English, French or German, with a summary in the appropriate language. Translations of the summary into the two other languages will be added by the Editors.

Les articles ou les lettres devront être rédigés en anglais, français ou allemand avec un résumé dans la langue correspondante. Les traductions du résumé dans les deux autres langues seront ajoutées par les éditeurs.

Instructions to contributors will be found in No. 1 (pp. 111–112).

Les instructions aux auteurs se trouvent dans le No. 2 (pp. 211–212).

Books for review should be sent to one of the Editors.

Les Livres (exemplaires de presse) devront être envoyés à un des Rédacteurs-en-chef.

The Journal of Nuclear Materials will initially be published quarterly.

Le Journal des Matériaux Nucléaires paraîtra initialement tous les trois mois.

The subscription price of a volume of 360 pages is $ 18.00, 130 s., Gld. 68.50 per volume, post-free.

Prix de souscription par volume d'environ 360 pages: $ 18.00, 130 s., Gld. 68.50, franco.

Subscriptions should be sent to the publishers, North-Holland Publishing Company. P.O. Box 103, Amsterdam or to any subscription-agent.

Les abonnements devront être envoyés aux éditeurs, North-Holland Publishing Company, P.O. Box 103, Amsterdam, ou à votre librairie.

No part of this issue may be reproduced in any form, by print, photoprint, microfilm or any other means without written permission from the publisher. Reprints, photoprints or microfilms are obtainable at cost from the publisher.

JOURNAL OF NUCLEAR MATERIALS - 2 (1959) 113–119 - NORTH-HOLLAND PUBLISHING CO., AMSTERDAM

DOSAGE DE L'OXYGENE DANS LE SODIUM

LA METHODE AU MERCURE: SON UTILISATION DANS LE CAS DE TRES FAIBLES TENEURS

L. CHAMPEIX, R. DARRAS et J. DUFLO

Centre d'Etudes Nucléaires de Saclay, Gif-sur-Yvette (S & O), France

Département de métallurgie et chimie appliquée

Service de chimie des solides

Reçu le 12 janvier 1959

La méthode au mercure pour le dosage de l'oxygène dans le sodium est connue depuis une dizaine d'années, elle est probablement la plus utilisée. Nous avons voulu préciser dans quelle mesure elle était valable dans le domaine des faibles teneurs avec une précision acceptable. Nous décrivons en détail l'appareil utilisé pour l'analyse, le mode opératoire, et la méthode d'étalonnage. Nos essais nous ont conduits à adopter la spectrographie de flamme pour le dosage de la soude formée, les erreurs introduites par la présence de chlorure de sodium et de calcium sont discutées. Les résultats obtenus sont examinés du point de vue de la reproductibilité, de la justesse. Moyennant un mode opératoire très soigné, cette méthode permet le dosage de l'oxygène dans le sodium, même à des teneurs inférieures à 10 ppm avec une précision satisfaisante.

The mercury method for the titration of oxygen in sodium has now been known for ten years and is probably the most frequently used. In this paper, the applicability and accuracy of the method in micro-analysis are examined. Details are given concerning the apparatus, its manipulation and its calibration. After testing, flame spectrography was used to titrate the sodium hydroxide formed. The errors due to the presence of sodium chloride and calcium are discussed. Results are examined from the point of view of their reproducibility and accuracy. If great care is taken, this method allows oxygen titration in sodium even at contents below 10 ppm with satisfactory precision.

Die Quecksilbermethode für die Analyse des Sauerstoffes in Natrium ist seit einem Jahrzehnt bekannt und ist wahrscheinlich die meist gebrauchte. Wir wollten die Brauchbarkeit der Methode im Falle eines kleinen Sauerstoffgehaltes nachprüfen. Der Apparat, seine Anwendungsmethode und seine Eichung werden beschrieben. Die Flammenspektrographie des gebildeten Natriumhydroxids hat sich als zweckmässig erwiesen; die von der Anwesenheit des Natriumchlorids und des Kalzium herrührende Fehler werden diskutiert. Die Ergebnisse werden vom Standpunkt der Reproduzierbarkeit und Genauigkeit geprüft. Wenn man sehr sorgfältig arbeitet, kann man weniger als 0.001 % Sauerstoff in Natrium mit genügender Genauigkeit messen.

1. Introduction

Des études assez nombreuses ont montré que la corrosion de divers matériaux (uranium, aciers inoxydables, zirconium, certains réfractaires . . .) par le sodium liquide est fortement accrue s'il renferme des traces d'oxyde: si les aciers inoxydables, par exemple, s'accommodent de la présence de quelques dizaines de ppm d'oxygène, par contre certains métaux comme le zirconium ou le niobium ne semblent compatibles, dans le domaine des températures supérieures à 500° C, qu'avec un sodium contenant moins de 10 ppm d'oxygène. Il est donc extrêmement important pour le développement de ces études et, notamment, la définition précise des conditions d'essais, de disposer d'une

méthode analytique suffisamment sensible.

La méthode au mercure a été la première utilisée par les chercheurs américains vers 1950 pour doser l'oxygène dans le sodium; elle reste probablement encore aujourd'hui la plus utilisée. Le principe est le suivant: l'addition de mercure provoque la formation d'amalgame de sodium liquide sans réagir avec l'oxyde Na_2O solide qui se rassemble à la surface de la phase liquide. Après plusieurs lavages et décantations, l'oxyde — qui se trouve alors à la surface d'une couche de mercure — est transformé en soude par addition d'eau, puis la soude est titrée.

Pepkowitz et Judd [1]), les premiers, citent cette méthode en 1950: ils dosent de 70 à 400 ppm à $\pm$ 50 ppm près.

En 1954, les mêmes auteurs [2]) présentent quelques modifications de détail et indiquent une reproductibilité améliorée à $\pm$ 17 ppm.

En 1951, Williams et Miller [3]) suppriment le gaz inerte utilisé par Pepkowitz et Judd et travaillent sous vide.

D'autres méthodes ont été proposées:
White et Ross [4]) puis Silverman et Shideler [5, 6]) utilisent la réaction du bromure de butyle sur le sodium et opèrent en solution dans l'hexane. La difficulté consiste à obtenir des réactifs suffisamment anhydres pour la sensibilité recherchée.

Humphreys [7]) distille le sodium et dose l'alcalinité sur le résidu.

L'objet de notre travail était de préciser dans quelle mesure la méthode au mercure peut être utilisée dans le domaine des faibles teneurs (au-dessous de 20 ppm) avec une précision acceptable. Nous nous proposons ici de décrire en détail l'appareillage et le mode opératoire utilisés, en insistant sur le problème essentiel du dosage de la soude formée. Puis, nous examinerons les résultats obtenus en ce qui concerne la reproductibilité, la sensibilité et la justesse de la méthode.

2. Appareillage, Réactifs

2.1. Appareil de dosage (fig. 1)

Nous avons modifié le montage de Pepkowitz de manière à travailler sous vide: vide poussé de 10^{-5} mm de mercure pour la partie B et vide primaire de 10^{-3} mm de mercure pour la partie C. Les deux canalisations de vide sont indépendantes.

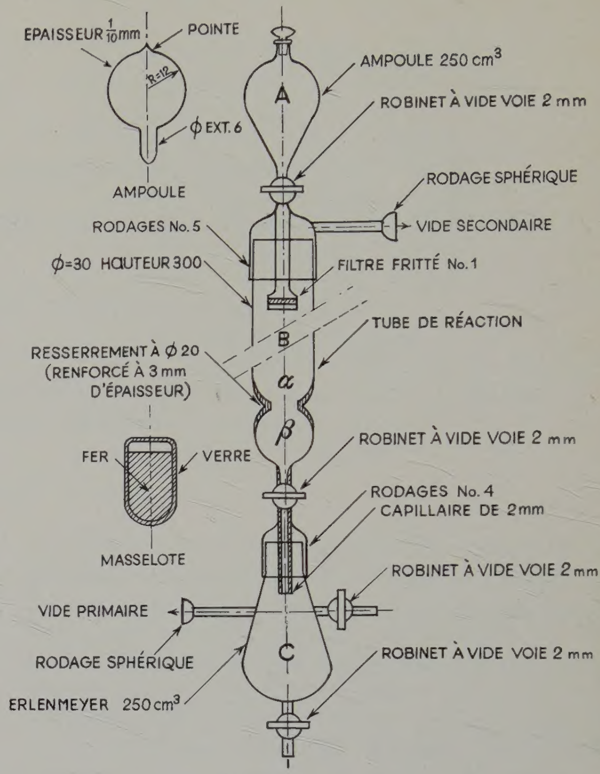

Fig. 1

Nos essais ont été effectués avec des ampoules partiellement remplies de sodium et scellées sous vide. La masselotte en fer doux enrobé de verre, commandée par un électro-aimant, permet de briser ces ampoules dans le tube à réaction de forme appropriée et d'éviter ainsi toute contamination.

La soude formée peut être dosée soit par acidimétrie, soit au spectrophotomètre de flamme.

2.2. Appareil d'oxydation (fig. 2)

Ce dispositif permet d'introduire avant l'analyse une quantité mesurée d'oxygène dans le tube à réaction, puis de recueillir et mesurer le volume d'oxygène qui n'a pas réagi avec le sodium et, ainsi, de préparer des étalons.

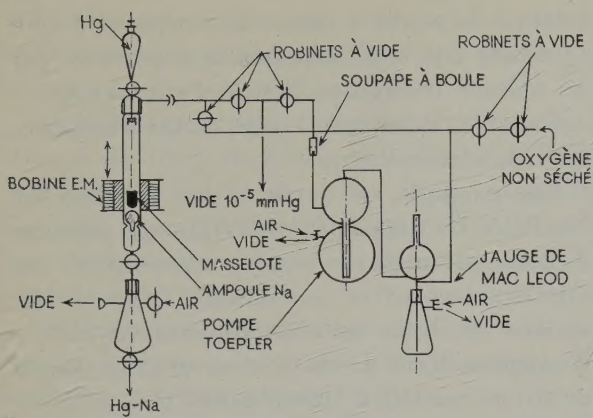

Fig. 2

2.3. Reactifs

Mercure distillé (de l'eau distillée agitée avec ce mercure doit conserver une réaction neutre).

HCl $2N$
NaOH $2N$.

3. Mode Opératoire

1) Préparer les différentes parties de l'appareillage soigneusement nettoyées et séchées.

2) Monter l'appareil.

Eviter tout excès de graisse sur les rodages. Utiliser de préférence la graisse Apiezon N.

3) Mettre l'appareil sous vide.

Un vide de 10^{-5} mm de mercure est maintenu dans le tube à réaction jusqu'à la fin de la manipulation.

4) Flamber le tube à réaction pour éliminer les dernières traces d'eau.

5) Introduire quelques cm³ de mercure dans le tube à réaction, ce qui évite l'obstruction du tube d'écoulement au début de la réaction.

6) Briser l'ampoule de sodium à l'aide de la masselotte.

7) Introduire 20 à 30 cm³ de mercure dans le tube à réaction.

8) Laisser réagir 30 à 40 minutes, afin que tout l'amalgame formé soit homogène et liquide.

9) Faire couler la plus grande partie de l'amalgame dans le réservoir C.

Prendre soin de laisser quelques cm³ au-dessus du robinet pour ne pas entraîner d'oxyde.

10) Reprendre les opérations 7, 8 et 9, dix à quinze fois.

On utilise au total environ 400 cm³ de mercure.

Le temps de réaction est progressivement diminué jusqu'à 5 minutes.

11) De temps à autre, l'amalgame est extrait de l'appareil en cassant le vide en C.

12) Agiter les portions successives d'amalgame avec de l'eau distillée contenant un indicateur de pH. Lorsque cette solution ne présente plus de réaction alcaline, on a du mercure pur, l'extraction est terminée.

13) Laisser quelques cm³ de mercure dans le tube à réaction, afin de ne pas entraîner l'oxyde.

14) Introduire 5 à 10 cm³ d'eau distillée neutre pour dissoudre Na_2O.

15) Casser le vide et soutirer mercure et eau distillée dans un bécher en polythène.

16) Rincer le tube à réaction à l'eau distillée jusqu'à disparition de la réaction alcaline.

Recueiller soigneusement ces eaux de lavage dans le bécher.

17) Doser NaOH formé (voir ci-dessous).

18) Doser le sodium contenu dans l'amalgame pour déterminer le poids de l'échantillon initial: ajouter 50 cm³ de HCl $2N$ puis titrer en retour par NaOH $2N$ en présence de phénolphtaléine.

L'ensemble de ces opérations s'effectue normalement en 6 heures, mais un même opérateur peut mener simultanément 3 ou 4 dosages s'il dispose du nombre correspondent de tubes d'extraction.

4. Détermination de la Quantité de Soude formée

Pepkowitz et Judd titraient la soude formée par de l'acide chlorhydrique en présence de phénolphtaléine.

Nous nous sommes efforcés de comparer les possibilités du dosage acidimétrique, en utilisant un pH mètre et celles du dosage par spectrophotométrie de flamme.

4.1. Dosage acidimetrique

Afin d'évaluer la précision que l'on peut attendre de cette méthode, nous avons tracé, à l'aide d'un pH-mètre, les courbes de titrage de solutions de soude $N/10$ à $N/100\,000$ par des solutions d'HCl N à $N/10\,000$, ce qui correspond à des teneurs de 4 % à 4 ppm d'oxygène dans le sodium, si l'on suppose une prise d'essai de 2 g et l'utilisation de 100 cm³ d'eau pour dissoudre Na_2O.

Ces essais, exécutés à la température ordinaire et au contact de l'atmosphère, ont conduit aux conclusions suivantes concernant ce mode de titrage:

1°) La fin du titrage se situe à un pH d'environ 6.5.

2°) Pour des teneurs de 4 et 0.4 %, la précision est très bonne: une goutte correspond à 0.25 unité de pH.

3°) Pour des teneurs inférieures, les effets de dilution et de carbonatation augmentent notablement l'imprécision du dosage qui peut atteindre $\pm$ 15 à $\pm$ 25 % pour 40 ppm; le titrage devient pratiquement impossible pour 4 ppm.

En conclusion

Le titrage peut être effectué soit au pH-mètre, soit à l'aide d'un indicateur ayant un début de virage voisin de 6.5, le rouge de méthyle par exemple.

Le dosage acidimétrique est valable et commode dans le cas de teneurs élevées (400 ppm). Il reste acceptable entre 400 et 40 ppm, mais devient difficilement utilisable dans le domaine des teneurs inférieures à 40 ppm. Nous verrons que la spectrométrie de flamme est alors préférable.

Remarque: Toutefois, si l'on ne dispose pas de spectromètre de flamme, un dosage acidimétrique est encore possible dans les conditions suivantes:

utiliser un acide de titrage assez concentré (5/1000 N par example) de manière à obtenir un rapport du volume d'acide au volume de solution de soude à titrer de l'ordre de 1/100;

utiliser une burette permettant de titrer par un volume d'acide de l'ordre de 0.5 cm³;

opérer à l'ébullition pour éviter l'influence du CO_2 atmosphérique.

Par exemple, à partir d'une solution de NaOH $N/10$ titrée par HCl $N/10$ en présence de rouge de méthyle, nous avons préparé, par dilutions successives, une solution $5.12 \times 10^{-5}N$: 40 cm³ de cette solution contiennent 32.8 γ d'oxygène. Nous avons titré cette prise d'essai de 40 cm³ par HCl 5/1000 N à 100° C en présence de rouge de méthyle. Les résultats obtenus sont les suivants (volume de solution acide utilisée pour obtenir le virage):

0.42 cm³ – 0.40 cm³ – 0.40 cm³ – 0.37 cm³
soit 0.40 ± 5 %,

ce qui correspond à un titre de $5.0 - 10^{-5}N$, une quantité d'oxygène de 32.0 $\gamma \pm 2$ et une teneur en oxygène de 16 ppm pour une prise d'essai d'un gramme de sodium.

4.2. Dosage du sodium par spectrophotométrie de flamme

La méthode consiste à mesurer la densité de la raie 5 960 Å du sodium. Elle présente un double avantage: elle est sensible (il est possible de déceler moins d'un γ de sodium) et nécessite peu de solution (moins de 5 cm³).

Par exemple, soit une solution de 100 cm³ de soude contenant 8.45 γ d'oxygène (ce qui correspond à 4.2 ppm pour une prise d'essai de 1 g). Cette solution est concentrée à 5 cm³, puis dosée au spectrophotomètre de flamme. Le résultat trouvé est de 8.5 $\gamma \pm 2$ %.

Cependant, l'utilisation de cette méthode spectrophotométrique pose deux problèmes liés à la présence éventuelle de ClNa et de CaO.

a) Présence de ClNa. – Le sodium du chlorure sera dosé au même titre que le sodium de la soude. Si la quantité de ClNa est notable, il convient donc de doser l'ion chlore et d'effectuer la correction.

Cependant, la solubilité de ClNa dans le sodium est très faible. Williams, Grand et

Miller [8]) l'ont trouvée très inférieure à 9 ppm à 400° C, ce qui correspondrait à une erreur de 2 ppm sur la teneur en oxygène.

Par ailleurs, opérant sur du sodium additionné de 10 % de ClNa, puis filtré à 150° C sur verre fritté, nous avons trouvé dans la solution aqueuse de soude 6 ppm de chlore, ce qui correspond à une erreur de 1.3 ppm sur la teneur en oxygène.

On peut donc conclure que, pour du sodium filtré, l'erreur par excès introduite par le chlorure est inférieure à 1.5 ppm.

b) Présence de CaO. — Si une partie de l'oxygène se trouve à l'état de CaO, cet oxyde passera dans la solution de soude, mais ne sera pas dosé.

Dans ce cas, le dosage de l'ion Ca donne évidemment une limite supérieure de l'oxygène présent à l'état de CaO. De toute façon, l'oxyde de calcium n'a pas l'effet corrosif de l'oxyde de sodium; au contraire, certains auteurs préconisent l'addition de calcium pour réduire l'oxyde de sodium et ainsi diminuer la corrosion.

5. Examen Critique de la Méthode

Nous examinerons les résultats obtenus au cours de nos essais de trois points de vue: reproductibilité, sensibilité et justesse, la spectrophotométrie de flamme étant seule retenue pour le dosage final de la soude.

5.1. Reproductibilité

Ce problème est lié au mode de prélèvement des échantillons, qui devrait être réalisé sans altération de la teneur en oxyde, ce qui est souvent très difficile. Aussi, pour limiter au minimum l'influence du facteur prélèvement, nous avons effectué des essais de reproductibilité sur un sodium bien défini, obtenu par distillation ou filtration directe dans les ampoules-échantillons. En effet, ces méthodes sont réputées donner un sodium dont la teneur en oxyde est assez bien reproductible, du moins lorsqu'elles sont mises en oeuvre dans des conditions constantes. Nous donnons ci-dessous le détail des essais effectués et les résultats obtenus:

		Teneur en oxygène
Distillation sous vide à 350° C	5 essais	26 ppm ± 7
Distillation sous vide à 350° C avec addition de copeaux de TiZr dans la cuve en vue de fixer l'oxygène	8 essais	20 ppm ± 4
Filtration à 110° C sur verre fritté n° 1 (diamètre moyen des pores: 90 à 150 μ) sous pression d'argon non purifié	3 essais	63.3 ppm ± 0.8
Filtration à 110° C sur verre fritté n° 2 (diamètre moyen des pores: 40 à 90 μ) sous pression d'argon purifié (sur sodium liquide)	3 essais	7 ppm ± 1.5

En conclusion

le mode de préparation par filtration est préférable;

l'écart d'une détermination avec la moyenne est alors 1.5 ppm;

les écarts observés dans les autres cas ne semblent pas devoir être imputés à la méthode de dosage.

5.2. Sensibilité

Nous n'avons pas dosé moins de 7 ppm en raison de l'insuffisance de nos méthodes de purification du sodium. Mais théoriquement la sensibilité n'est limitée que par la sensibilité du dosage spectrophotométrique du sodium: nous avons vu que cette méthode permet de déceler 1 γ de sodium, soit environ 0.3 ppm d'oxygène dans le sodium.

5.3. Justesse

Nous avons vérifié que des quantités connues d'oxygène ajoutées au sodium étaient bien retrouvées à l'analyse et, d'autre part, que le "blanc" de la méthode était négligeable.

a) *addition d'oxygene*

Exemple n° 1: sodium filtré sur verre fritté n° 1 avec pression d'argon non purifié.

Tableau 1

Essai	Teneur initiale ppm	O_2 introduit ppm	Total théorique ppm	Teneur totale mesurée ppm	Ecart
44				63	
45	Pas d'oxydation			62.5 } 63.3 ± 0.8	
48				64.1	
46	63.3 (a)	30.5	93.8	95.8	+ 2 %
47	63.3 (a)	39.7	103.0	103.6	+ 0.6 %

(a) d'après les essais 44, 45 et 48.

Exemple n° 2 : sodium filtré sur verre fritté n° 2 avec pression d'argon purifié.

Tableau 2

Essai	Teneur initiale ppm	O_2 introduit ppm	Total théorique ppm	Teneur totale mesurée ppm	Ecart
52				6.8	
53	Pas d'oxydation			8.5 } 7.0 ± 1.5	
54				5.8	
55	7.0 (a)	27.7	34.7	33.7	— 3 %
56	7.0 (a)	25.6	32.6	34.7	+ 6 %

(a) d'après les essais 52, 53 et 54.

Remarque : les différentes prises d'essai ne sont probablement pas identiques et la reproductibilité de la méthode de dosage elle-même est peut-être meilleure que ne l'indiquent les chiffres ci-dessus.

b) "Blanc" de la méthode

La réalisation d'un véritable essai à blanc (avec du sodium totalement exempt d'oxygène) n'a pas été possible, aussi avons-nous indiqué sur un graphique (fig. 3) les poids d'oxygène dosés pour des poids croissants de la prise d'essai. Nous avons une droite passant sensiblement par l'origine, ce qui montre bien que l'essai à blanc est négligeable.

6. Conclusions

Ces résultats permettent de conclure à la validité de la méthode au mercure, même pour de très faibles teneurs en oxyde, à condition de prendre certaines précautions et, en particulier, d'utiliser le dosage spectrophotométrique pour les teneurs inférieures à 40 ppm.

Il est possible de doser 7 ppm avec une

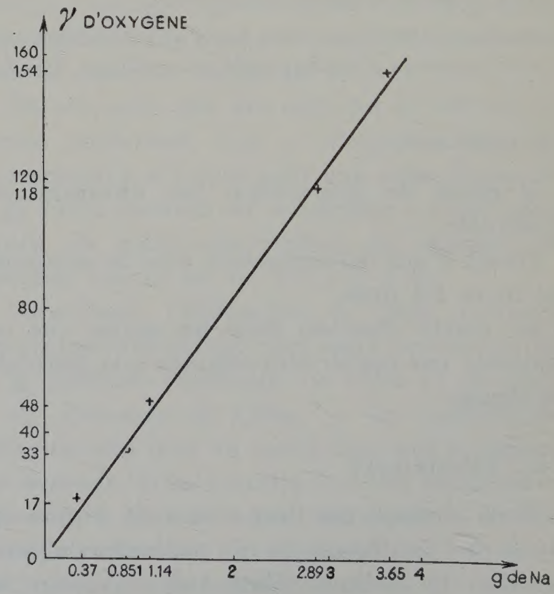

Fig. 3

reproductibilité de $\pm$ 1.5 ppm, mais la sensibilité de la méthode de dosage et l'examen des diverses causes d'erreur (blanc de la méthode, chlorures, etc.) autorisent à penser que des teneurs comprises entre 1 et 7 ppm seraient dosables avec une précision du même ordre. Toutefois, à de telles teneurs, le prélèvement d'un échantillon de sodium sans pollution devient une opération très délicate; cette difficulté constitue probablement le problème majeur à résoudre pour augmenter encore la sensibilité de toute méthode de dosage de l'oxygène dans le sodium.

Bibliographie

1) L. P. Pepkowitz and W. C. Judd, Anal. Chem. 22 (1950) 10
2) L. P. Pepkowitz and W. C. Judd, Anal. Chem. 26 (1954) 246
3) D. D. Williams and R. R. Miller, Anal. Chem. 23 (1951) 1865
4) J. C. White and W. J. Ross, Anal. Chem. 26 (1954) 210
5) L. Silverman and M. Shideler, Anal. Chem. 27 (1955) 1660
6) L. Silverman and M. Shideler, North American Aviation (USA) Report, NAA-SR 1509 (1956)
7) J. R. Humphreys, Amer. Inst. of Chem. Eng. — Nuclear Eng. and Sci. Congress, (1955) Preprint n° 67
8) D. D. Williams, J. A. Grand and R. R. Miller, Naval Research Laboratory (USA) Memorandum Report n° 424 (1955)

JOURNAL OF NUCLEAR MATERIALS - 2 (1959) 120–126 - NORTH-HOLLAND PUBLISHING CO., AMSTERDAM

ETUDE DE L'AUTODIFFUSION DE L'URANIUM EN PHASE γ

Y. ADDA et A. KIRIANENKO

Centre d'Etudes Nucléaires de Saclay, Gif-sur-Yvette (S & O), France

Département de métallurgie et chimie appliquée

Reçu le 12 janvier 1959

L'étude de l'autodiffusion de l'uranium a été effectuée à des températures comprises entre 800 et 1 050° C, à partir de couples de diffusion constitués d'uranium naturel et d'uranium enrichi en U^{234}. Les échantillons ont été sectionnés après traitement, sur un tour de précision, et l'on a mesuré dans une chambre à ionisation, l'émission α (en couche épaisse), de la face sectionnée. A partir des courbes activité-pénétration établies au moyen de cette technique, on a déterminé les coefficients d'autodiffusion de l'uranium en phase γ, ainsi que l'énergie d'activation ($Q = 27.5$ k Cal/at·g) et le facteur de fréquence ($D_0 = 1.8 \times 10^{-3}$ cm^2/sec).

The self-diffusion of uranium was studied at temperatures ranging from 800 to 1 050° C. The diffusion couples used were made of natural uranium and uranium enriched with U^{234}. The samples were sectioned on a precision lathe after treatment. The α-emission of the cut surface was measured by means of an ionisation chamber. The self-diffusion coefficient of uranium in the γ-phase as well as the activation energy ($Q = 27.5$ k Cal/g·at) and the frequency factor ($D_0 = 1.8 \times 10^{-3}$ cm^2·sec) were determined from the activity-penetration curves established by means of this technique.

Die Selbstdiffusion des Urans wurde bei Temperaturen zwischen 800° C und 1 050° C gemessen. Die Proben wurden aus natürlichem Uran und Uran mit U^{234}-Anreicherung hergestellt. Nach der Erhitzung wurden die Proben auf einer Präzisionsdrehbank abgedreht und die aus dem abgedrehten Querschnitt kommende α-Strahlung wurde gemessen. Sowohl der Selbstdiffusionskoeffizient als auch die Aktivierungsenergie ($Q = 27.5$ k. Cal/Mol) und der Häufigkeitsfaktor ($D_0 = 1.8 \times 10^{-3}$ cm^2/sec) wurden mittels wiederholter Messungen dieser Art berechnet.

L'étude de l'autodiffusion est d'une très grande importance théorique. Elle permet en particulier d'établir les processus qui contrôlent le déplacement des atomes dans un réseau métallique déterminé [1]). De plus, l'énergie d'activation d'autodiffusion est, parmi les diverses constantes de diffusion, celle qui semble le mieux se relier aux caractéristiques physiques de l'atome [2, 3]).

Du point de vue pratique, le phénomène de fluage ou celui de frittage étant souvent contrôlé par la diffusion des lacunes, la connaissance des constantes d'autodiffusion (le mécanisme de diffusion étant supposé lacunaire) peut permettre une évaluation correcte de certaines caractéristiques technologiques: la résistance au fluage par exemple.

Enfin, des phénomènes récemment mis en évidence tels que la croissance par cyclage thermique par exemple, semblent être directement sous la dépendance de la diffusion des lacunes.

L'étude de l'autodiffusion de l'uranium, et en particulier, l'influence sur ce phénomène de différents facteurs intervenant dans l'utilisation de l'uranium comme matériau de pile atomique, tels que les éléments d'addition et l'effet de l'irradiation, présentent un intérêt considérable.

La détermination précise des constantes de diffusion nécessitant l'emploi d'isotopes radioactifs, les radioactivités naturelles α et β de l'uranium créent des difficultés supplémentaires et, pour déterminer la concentration de ces isotopes, il faudra en général opérer par différence d'activités.

Les techniques d'étude de l'autodiffusion de l'uranium peuvent être réparties en deux catégories:

celles qui utilisent comme traceur l'U^{235};

celles qui utilisent un émetteur α plus actif (U^{233} ou U^{234}) comme traceur.

Dans le premier cas (recherches effectuées en Grande Bretagne et aux Etats-Unis) un uranium très enrichi en U^{235} (90 % par exemple) est évaporé sur de l'uranium naturel. Après diffusion, la concentration en U^{235} est déterminée, soit par mesure de la densité des traces de fission par autoradiographie, soit par la mesure globale de l'activité γ des produits de fission obtenus lorsque l'uranium est irradié par des neutrons, soit par l'activité d'un élément de fission déterminé.

Nous avons, au début de notre étude, essayé d'utiliser l'U^{235} comme traceur: nos couples étaient constitués par des plaquettes d'uranium naturel soudées à des plaquettes d'uranium appauvri à 0.4 % de U^{235} ou enrichi à 20 % en U^{235}.

Après traitement de diffusion, ces couples, sectionnés perpendiculairement à l'interface de soudage et polis, étaient appliqués contre une plaque nucléaire au cours d'une irradiation par neutrons, et la concentration en U^{235} était déterminée par comptage des traces de fission. Lors de ces essais, nous nous sommes heurtés à de nombreuses difficultés expérimentales et le manque de reproductibilité des résultats nous a conduit à abandonner cette méthode.

Dans la deuxième catégorie d'essais — travaux de Bochvar [4]) et présente étude — les traceurs utilisés sont des émetteurs α très intenses. Bochvar utilise de l'U^{233} pur (émetteur α ayant 1.6×10^5 ans de période), qu'il dépose par évaporation thermique sur de l'uranium naturel.

Après diffusion, la concentration en U^{233} est déterminée, soit par comptage α superficiel après enlèvement de couches successives, soit par autoradiographie d'une section perpendiculaire au front de diffusion et photométrie du noircissement obtenu.

Les métaux utilisés dans notre étude sont de l'uranium naturel (préparé au C.E.A.) et de l'uranium d'origine américaine enrichi à 20 % en U^{235}.

L'activité superficielle α de l'uranium enrichi est 12.9 fois plus élevée que celle de l'uranium naturel. L'analyse spectrographique α montre, en effet, que l'uranium enrichi en U^{235} l'est également en U^{234}; de ce fait, l'activité α provient principalement de l'uranium 234 dont la période est environ 10^4 fois plus courte que celle des autres isotopes, U^{238} et U^{235}.

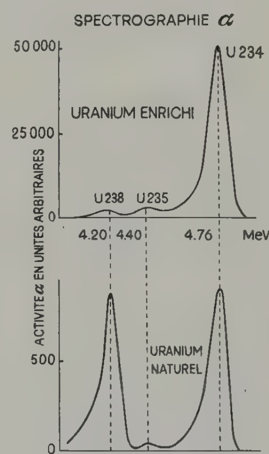

Fig. 1

Le tableau 1 donne la comparaison des deux uraniums utilisés.

La figure 1 donne les spectrographies α comparées des deux métaux.

Les principales impuretés que contiennent ces matériaux sont portées dans le tableau 2.

Tableau 1

		Uranium naturel		Uranium enrichi	
	Période (ans)	Teneur (%)	Activité α	Teneur (%)	Activité α
U 238	4.5×10^9	99.28	100	80	80
U 235	7.1×10^8	0.715	4.5	19.85	125
U 234	2.5×10^5	0.0058	100	0.14	2 435
		100.0	204.5	99.99	2 640

On voit que l'uranium enrichi contient plus d'impuretés que l'uranium naturel et contient notamment plus d'aluminium et de carbone.

TABLEAU 2

Analyses

	Uranium naturel ppm	Uranium enrichi ppm
Fe	55	120
Si	80	175
Cu	20	20
B	0.1	0.25
Ni	10	25
Cr	16	18
Mn	7	8
Al	< 200	10^3
C	100	660

Technique expérimentale

Les couples de diffusion sont sectionnés au tour, parallèlement à l'interface de soudure, et on mesure après chaque passe, dans une chambre à ionisation, l'activité α superficielle de l'échantillon restant.

PREPARATION DES ECHANTILLONS

a) Echantillons de départ: Des cylindres de 1 cm de diamètre et 1 cm de hauteur sont usinés dans l'uranium enrichi et des plaquettes de 1 cm² de section et 4 mm d'épaisseur sont préparées dans l'uranium naturel.

b) Soudure: Après traitement thermique en phase γ, les échantillons sont polis électrolytiquement, puis on les soude, cylindre contre plaquette, en les portant à 600° C pendant 1 heure, sous vide dans une presse à vis suivant une technique décrite antérieurement [5]). On a soin d'interposer des fils de tungstène de 10 μ avant soudure afin de pouvoir facilement repérer l'interface après diffusion. Nous avons vérifié que dans ces conditions les couples présentent une diffusion négligeable.

c) Traitement de diffusion: Les couples sont traités thermiquement sans pression extérieure, à des températures comprises entre 800° C et 1050° C pendant 5 à 24 heures, sous un vide inférieur à 5×10^{-6} mm de mercure (fig. 2).

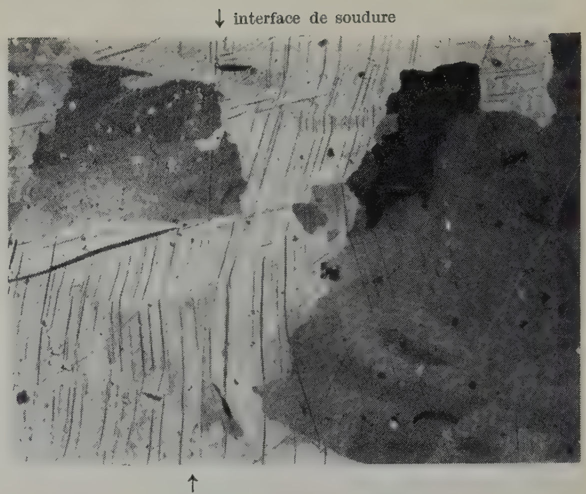

Fig. 2. Diffusion à 800° pendant 15 h.

La figure 2, micrographie au grossissement 100 en lumière polarisée, montre l'interface de soudure et l'aspect de la diffusion après un traitement de 15 h à 800°.

d) Usinage des échantillons et réglage avant sectionnement: le réglage a pour but de rendre l'interface de soudure perpendiculaire à l'axe du tour. Usinage et réglage sont effectués sur un tour de précision spécialement aménagé à cet effet.

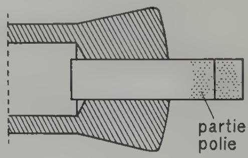

Schéma 1

1°) Tout d'abord, le couple de diffusion est transformé en un cylindre parfait, puis une partie de sa surface est polie mécaniquement à la poudre de diamant (schéma 1). L'échantillon

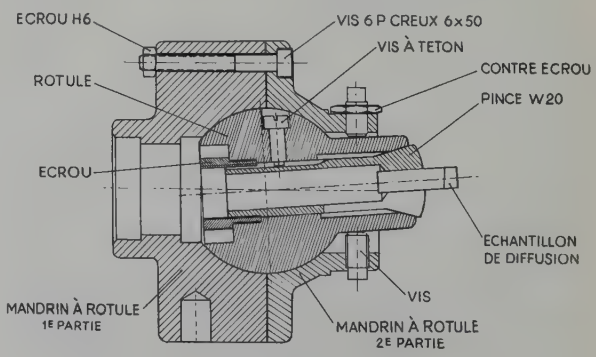

Fig. 3

est alors fixé sur un mandrin spécial (inspiré d'un montage plus simple utilisé par A. D. Le Claire) dont la partie principale est constituée par une rotule ajustée avec précision dans un rodage sphérique (fig. 3). Cette rotule réglable au moyen de 3 vis à pas fin permet de placer l'interface repéré par les fils de tungstène, perpendiculairement à l'axe du tour. Ce réglage est obtenu au moyen d'un microscope (fig. 4) dont l'axe optique est également perpendiculaire à l'axe du tour. En effectuant ce réglage avec des grossissements allant de 30 à 200, on peut

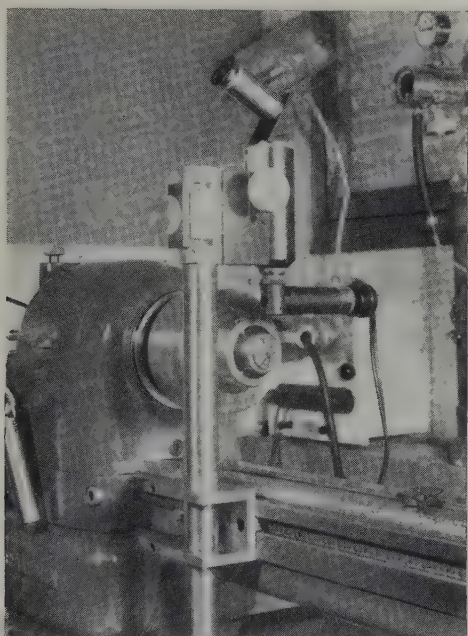

Fig. 4

amener l'interface à 4 minutes du plan qui est rigoureusement perpendiculaire à l'axe du tour (ce qui correspond à un réglage à 5 μ près sur un échantillon de 1 cm de diamètre).

2°) Le couple est usiné sous argon dans une boite étanche en plexiglass, de manière à obtenir un échantillon dont les génératrices sont rigoureusement perpendiculaires à l'interface de soudage (fig. 5).

3°) L'échantillon est alors mis en place, en pince, directement dans la broche du tour. Une butée réglable (fig. 6) située dans cette broche, permet d'enlever à tout moment, l'échantillon

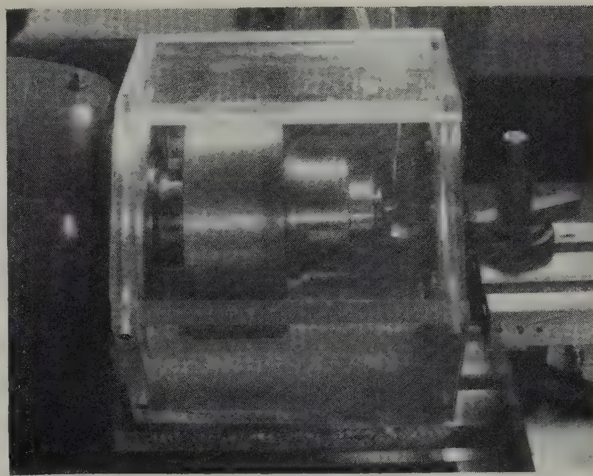

Fig. 5

àour les mesures d'activité, puis de le replacer d 1 micron près.

Microsectionnement et mesures

Le tronçonnage des échantillons est effectué également dans une boite étanche, en plexiglass, permettant la récupération totale des copeaux. L'outil dont l'avance est mesurée avec précision grâce à un comparateur au micron, travaille sous jet d'argon, ce qui permet d'opérer à sec, et d'éviter toute oxydation. Après chaque passe, l'épaisseur de métal enlevé est mesurée à l'aide d'un deuxième comparateur. Nous avons choisi pour nos expériences des épaisseurs

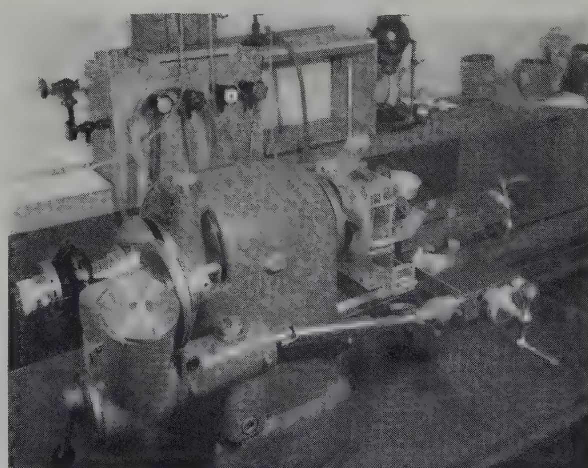

Fig. 6

de 10 à 100 microns, les zones de diffusion variant de 1 à 2.5 mm environ.

Grâce à un dispositif d'avance automatique du chariot les surfaces obtenues sont parfaitement reproductibles.

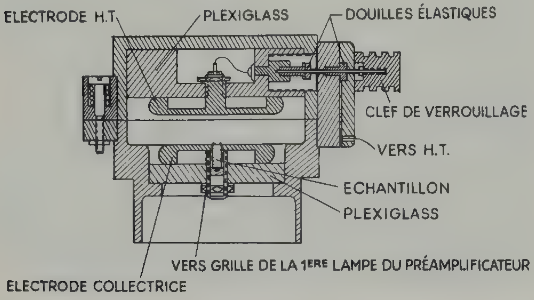

Fig. 7. Chambre d'ionisation.

La mesure de l'émission α de ces surfaces est effectuée dans une chambre à ionisation à impulsions, à électrodes planes et parallèles et à remplissage d'air.

La figure 7 donne le schéma de principe d'une telle chambre à ionisation, transformée pour recevoir des échantillons cylindriques: un puits à fond mobile réglable a été prévu dans l'élec-

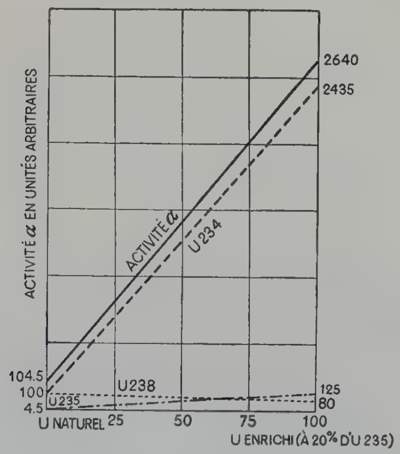

Fig. 8

trode inférieure. Avant d'être placés dans la chambre à ionisation, les échantillons sont enfermés dans un petit cylindre en laiton qui présente au centre de sa face supérieure une ouverture de 3.5 mm de diamètre, ce qui permet de délimiter toujours la même surface, donc le même angle solide d'émission.

Nous avons, entre l'uranium enrichi et l'uranium naturel, un gradient d'activité α correspondant à un gradient de concentrations isotopiques (cf. tableau 2 et fig. 8).

La figure 8 représente les variations d'activité α en fonction du % d'uranium enrichi. Les vitesses de diffusion des trois isotopes sont supposées égales. La droite supérieure correspond à l'activité totale α mesurée. Les trois autres droites se rapportent aux trois isotopes présents.

A partir de l'activité globale, nous pouvons calculer, par une simple règle de trois, l'enrichissement en l'un des isotopes. Pour l'établissement des courbes d'autodiffusion, nous portons:

$$C = \frac{N - N_0}{N_{100} - N_0} \times 100,$$

en fonction de la pénétration.

N est l'activité α mesurée au point d'abscisse x.
N_0 ,, ,, de l'uranium naturel.
N_{100} ,, de l'uranium enrichi.

La figure 9 donne l'une des courbes concentration-pénétration ainsi obtenues pour un traitement de diffusion à 800° C pendant 15 heures.

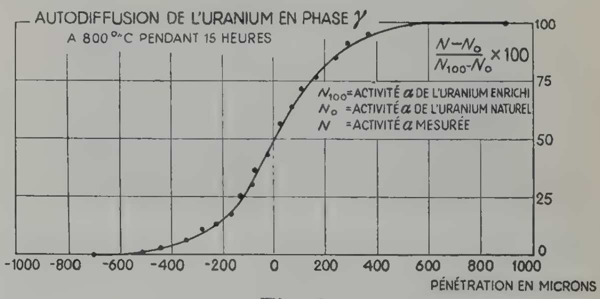

Fig. 9

Pour calculer les coefficients d'autodiffusion, nous avons utilisé l'intégrale de l'équation de diffusion correspondant à nos conditions expérimentales:

$$\frac{C(x,t)}{C_0} = \tfrac{1}{2}\left[1 - \Theta\left(x/2\sqrt{Dt}\right)\right]$$

avec

$$\Theta\left(x/2\sqrt{Dt}\right) = \frac{2}{\sqrt{\pi}} \int_0^{\frac{x}{2\sqrt{Dt}}} e^{-z^2} dz.$$

où z est une variable d'intégration.

$C(x, t)$ défini comme précédemment, représente l'enrichissement en isotope radioactif au point d'abscisse x, par rapport à l'uranium naturel.

C_0, différence de teneur en isotope radioactif entre l'uranium enrichi et l'uranium naturel, est pris égal à 100.

L'utilisation de cette solution de l'équation de Fick est pleinement justifiée, par l'aspect des courbes obtenues en portant sur un graphique C/C_0, en fonction de $x/\sqrt{t}$, en coordonnées Gausso-arithmétiques [6]) (cf. fig. 10).

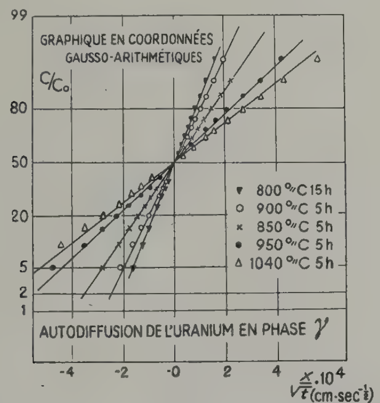

Fig. 10

Les valeurs du coefficient de diffusion pour les températures de 800, 850, 900, 950, 1000 et 1040° C sont portées dans le tableau 3.

La courbe représentant les variations du logarithme du coefficient d'autodiffusion en fonction de l'inverse de la température absolue T°K, étant une droite, nous avons déterminé l'énergie d'activation Q et le facteur de fréquence D_0 (fig. 11).

$$Q = 27.5 \text{ kcal/at}\cdot\text{g}$$
$$D_0 = 1.8 \times 10^{-3} \text{ cm}^2\text{/sec.}$$

Ces valeurs sont en bon accord avec celles, données récemment à la 2ème Conférence de Genève, par les chercheurs russes A. A. Bochvar, V. G. Kuznetsova et V. S. Sergeev [4]), comme le montre le tableau 4.

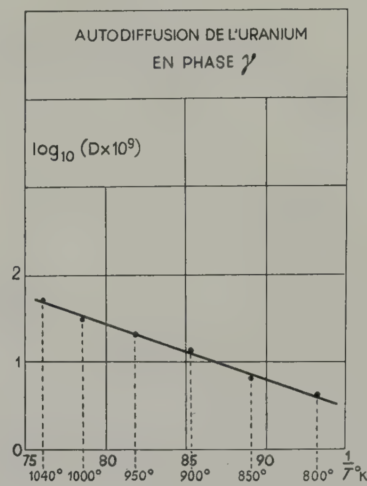

Fig. 11

La valeur basse de l'énergie d'activation ne peut être imputée à la diffusion intergranulaire, étant donné que les essais sont effectués relativement près du point de fusion de l'uranium, et que la courbe log $D = f(1/T)$ est une droite dans tout le domaine de température considéré.

La diffusion superficielle, par ailleurs, ne peut intervenir dans nos expériences, car les échantillons ont leur diamètre réduit de 10 à 8 mm environ, après diffusion, et d'autre part les mesures d'activité α sont faites exclusivement dans la région voisine de l'axe des échantillons.

La figure 12 représente la variation de l'énergie d'activation pour l'autodiffusion en fonction de la température absolue de fusion. La plupart des métaux étudiés, qui appartiennent à des structures diverses, sont portés sur ce graphique dû à Kidson et Ross [7]). On voit que l'énergie d'activation pour l'autodiffusion se relie assez bien à la température de fusion.

Dans le cas de l'uranium, la chaleur d'activation devrait être de 55 à 60 kcal. Une telle

TABLEAU 3

Température ° C	800	850	900	950	1000	1040
D en cm²/sec	5×10^{-9}	7.7×10^{-9}	1.4×10^{-8}	2.2×10^{-8}	3.2×10^{-8}	5.1×10^{-8}

Tableau 4. Résultats

Températures (° C)	A. A. Bochvar *et al.* Comptages α $D \times 10^8$ cm²/sec	A. A. Bochvar *et al.* Par autoradio $D \times 10^8$ cm²/sec	Y. Adda et A. Kirianenko $D \times 10^8$ cm²/sec
800	0.48	0.9	0.5
850	—	—	0.77
900	1.17	2.0	1.4
950	—	—	2.2
1 000	2.8	4.0	3.2
1 040	—	—	5.1
1 050	4.5	—	—
Facteurs de fréquence D_0	1.17×10^{-3} cm²/sec	1.4×10^{-4} cm²/sec	1.8×10^{-3} cm²/sec
Energie d'activation Q en kcal/at·g	26.6	21.0	27.5

différence entre la valeur prévue, et celle obtenue (27.5 kcal/at·g) ne peut être attribuée aux impuretés, car les études de Bochvar ont été faites à partir d'un uranium qui ne contenait pas les mêmes impuretés.

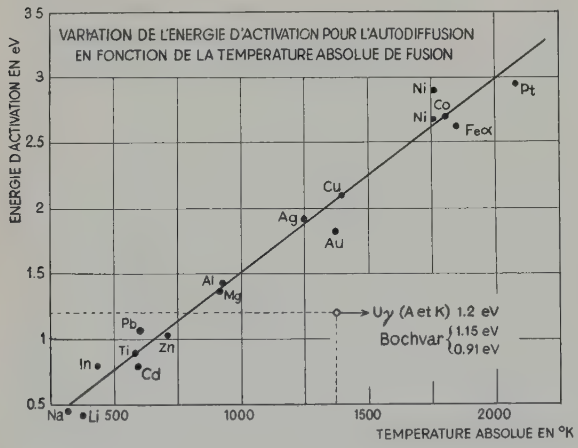

Fig. 12

Il semble donc que cette valeur très faible de la chaleur d'activation puisse être attribuée à un comportement particulier de l'uranium.

Certaines données fondamentales, telles que les caractéristiques élastiques de l'uranium en phase γ faisant défaut, ce comportement semble difficile à expliquer. Leur connaissance permettrait peut-être, partant des considérations théoriques de C. Zener [8]), A. D. Le Claire [9]), et de celles plus récentes de F. S. Buffington et M. Cohen, d'expliquer cette "anomalie" de l'uranium.

Nous tenons à remercier particulièrement Mmes H. Faraggi, A. Garin et J. Olkovsky, ainsi que Monsieur J. Engelman du C. E. N. Saclay, pour leur précieux concours.

Bibliographie

1) H. B. Huntington et F. Seitz, Phys. Rev. **61** (1942) 325
2) A. D. Le Claire, Progress in Metal Physics **1** (1949) 374
3) N. H. Nachtrieb et G. S. Handler, Acta Met. **2** (1954) 797
4) A. A. Bochvar, V. S. Kuznetsova et V. S. Sergeev, 2ème Conférence de Genève (1958) P/2.306
5) Y. Adda, J. Philibert et H. Faraggi, Rev. Metal. **54** (1957) 597
6) L. D. Hall, J. Chem. Physics **21** (1953) 87
7) G. V. Kidson et R. Ross, Conférence Internationale sur l'utilisation des Radioisotopes dans la Recherche Scientifique (1957) UNESCO/NS/RIC 216
8) C. Zener, J. Appl. Phys. **22** (1951) 372
9) A. D. Le Claire, Acta Met. **1** (1953) 438
10) F. S. Buffington et M. Cohen, Acta Met. **2** (1954) 660

JOURNAL OF NUCLEAR MATERIALS - 2 (1959) 127–135 - NORTH-HOLLAND PUBLISHING CO., AMSTERDAM

CATHODIC BOMBARDMENT ETCHING OF NUCLEAR MATERIALS

D. ARMSTRONG, P. E. MADSEN and E. C. SYKES

UKAEA, *Atomic Energy Research Establishment, Harwell, Didcot, Berks., UK*

Received 13 January 1959

A simple apparatus is described for cathodic etching by ionic bombardment. The etching conditions for a variety of metals, alloys and ceramics, including thorium, uranium, uranium carbide and uranium dioxide, are reported.

Un appareil simple est décrit pour réaliser l'attaque cathodique par bombardement ionique. Les conditions d'attaque sont précisées pour divers métaux, alliages et céramiques comprenant le thorium, l'uranium, le carbure d'uranium et le bioxyde d'uranium.

Ein einfacher Apparat wird beschrieben für kathodische Ätzung durch Beschiessung mit Ionen. Die Ätzbedingungen für verschiedene Metalle, Legierungen und keramische Substanzen, u.a. Thorium, Uran, Urankarbid und Urandioxyd wurden festgestellt.

1. Introduction

In recent years cathodic etching by ionic bombardment has been increasingly used to reveal the microstructure of metals and alloys, especially those used in the field of atomic energy. The method has much to commend it, particularly since it seems applicable to practically any metal or alloy, and even to refractory ceramic materials. This paper details operating experience with this technique applied principally to uranium, thorium, and their alloys, but the etching conditions of a variety of other metals were studied to explore the scope of the method.

Several papers [1–15]) on this subject have appeared, particularly since McCutcheon [4]) re-introduced the method in 1949. Inert gases have generally been used for bombardment but Englander, Laniesse and Stohr [16]) experimented with oxygen ions to reveal the microstructure of uranium. Here, however, the structure was shown more by preferential film formation than by surface relief produced by sputtering.

2. Cathodic Etching Apparatus

The cathodic etching apparatus used in this investigation (fig. 1) is generally similar to those described in the literature (e.g. refs. [7,8,9,12])); the dimensions quoted are probably in no way critical. An interesting feature is the inner pyrex tube which ensures an even flow of gas over the anode (and which may be more easily cleaned on removal than the outer tube). No provision was made for water cooling the cathode, but efficient cooling was obtained by placing troughs of liquid nitrogen on the base plate.

The etching chamber was continuously evacuated by a rotary pump, a diffusion pump proving unnecessary. Ordinary cylinder argon was used in preference to krypton or xenon (which would probably have given more rapid etching) on grounds of expense and availability since a continuous flow of gas was employed. No attempt was made to remove the oxygen, but the gas was dried with calcium chloride, phosphorous pentoxide and silica gel.

A variac controlled, half wave rectified unsmoothed high tension supply (very similar to that in an X-ray set) was used. As a safety precaution to prevent anyone from touching the anode when it was live, a vacuum operated switch cut off the current to the high tension transformer if the pressure in the etching chamber exceeded 50 mm Hg.

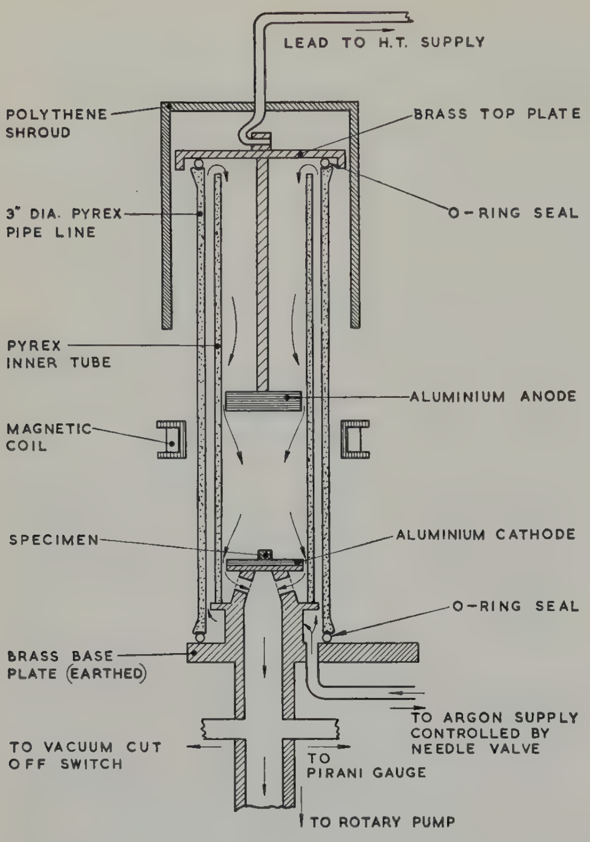

(ARROWS INSIDE APPARATUS INDICATE DIRECTION OF ARGON FLOW)

Fig. 1. Diagram of etching chamber.

Following Newkirk and Martin [12]), we have used a magnetic field of approximately 100 oersted from a coil placed around the etching chamber. The purpose of this coil is to cause the electrons flowing from cathode to anode to follow a (longer) helical path and thus ionize more gas atoms and increase the current flowing to the cathode.

3. Operating Procedure

After some initial trials the following procedure was adopted for etching. The specimen (broken out of its mount if it had been set in plastic) was placed face upwards on the aluminium cathode. The remainder of the cathode was covered with thin zirconium foil, chosen because of its low sputtering rate. The chamber was continuously evacuated and argon was simultaneously admitted through a needle valve to give a constant pressure of 30–50 μ (as measured by a Pirani gauge on the outlet side of the chamber). A voltage of 1–2 kV was then applied across the electrode and the voltage gradually increased to degas the equipment. During this process the gas pressure rose rapidly (to about 80 μ) but it fell after a few minutes, when etching commenced. Some indication of the amount of etching could be obtained from the appearance of the specimen in the apparatus, but generally with a new material two etches were required – the first trial run to find the amount of etching in a given time, and the second with the time correspondingly adjusted. The etching current was most easily controlled by slight alterations in the amount of gas flowing into the etching chamber. The use of a magnetic field reduced the etching time considerably; without it the short etching times quoted could not be attained.

Consistent results were only obtained if the apparatus was thoroughly degassed. Etching times were longer, and the etch often unsatisfactory, if the chamber had been exposed to the atmosphere for some time, or when some new component was introduced. Consequently the apparatus was kept evacuated when not in use. Trouble was frequently encountered from fragments of the mounting plastic embedded in cavities in the specimen decomposing in the discharge and causing staining or preventing etching altogether. This could be avoided if the specimen was wrapped in a very thin metal foil before being mounted in the plastic.

A limitation to the method is the possibility of specimens overheating. Although there is a greater chance of thick specimens getting hot, thermal contact between specimen and cathode seems more important in controlling the specimen temperature; for example specimens with rough bases or with holes drilled in them got very hot. When precautions were observed it was possible to etch specimens without appreciable temperature rises. Fig. 2 shows a specimen of deformed bismuth after cathodic etching. The deformation twins are still present indicating that the specimen temperature cannot

Fig. 2. Deformed bismuth. $\times$ 270.

have exceeded about 100° C. A similar temperature was deduced from etched cadmium and zinc specimens.

Most of the specimens were etched with the surface to be examined parallel to the base, but surfaces almost parallel to the chamber axis could also be etched satisfactorily. Generally only one specimen was etched at any one time, but several specimens of similar composition could be done simultaneously. The only drawback (which may be easily overcome) to this procedure is that a short specimen next to a tall one was often not completely etched, as if it had been shielded.

The mechanical polishing of specimens for cathodic etching should be as good as possible since less cathodic etching is then required to remove the scratches. Specimens for cathodic etching were given a standard preparation-ground on emery papers, and then on rotating wheels covered with diamond impregnated cloth. This sometimes resulted in the formation of a very tenacious surface film (e.g. on some uranium alloys) and then the final preparation was done using alumina as abrasive. Very occasionally an attack polish or an electropolish was employed, but this was avoided when possible in the present tests since some phases or inclusions might be preferentially attacked.

4. Results of Cathodic Etching

The etching conditions for a number of metals and alloys were determined when operating at an argon pressure of 30 μ Hg. The time taken to etch the specimen (after an induction period) and the average voltage and current density used are entered in table 1. Most of the materials studied could be etched under very similar conditions i.e. at an average voltage of $4-5$ kV and average current density of $0.5-0.75$ mA/cm^2 in $2-5$ minutes after an induction period of about 3 minutes. Metals with higher melting points tend to require slightly longer times, and low melting point metals require short etching times and lower etching voltages (about 2 kV average). The etches obtained were good except with a few metals, (e.g. aluminium, magnesium and nickel) where films were present on the surface which did not correspond to the true structure of the material which was also revealed by cathodic etching. It is thought that the films could be avoided by more careful specimen preparation.

In table 1 the etching conditions reported by other workers are also entered. An induction period, generally of the same order as found here, has been reported by most workers. Values of only a few seconds [12]) and over an hour [5, 10]) have also been recorded. The etching times are comparable with those of Newkirk and Martin [12]), Padden and Cain [7]), and Carlson *et al.*[8]), and shorter than the remainder. The etching voltages are similar, but the current densities appear lower in the present investigation. Some of this discrepancy may be due to the fact that the current was averaged over the whole cathode area in this case, whereas in practice there seems to be some concentration of the discharge around the specimen.

When compiling table 1 a standard argon pressure of 30 μ Hg was employed, since it appeared that most rapid etching occurred at

TABLE 1. Comparison of conditions for cathodic bombardment etching

Investigation	This report			Newkirk and Martin [12])				Holland [13])	Padden and Cain [7])		Carlson, Williams, Rogers and Manthos [8])	Other investigators					
Bombarding gas	Argon			Krypton				Argon	Argon		Argon						
Gas pressure	30 μ			8–15 μ					50 μ		15 μ						
Induction period	3 minutes			few seconds					$\frac{1}{2}$–2 minutes		few minutes						
Etching times	2–10 minutes			1–25 minutes				5–60 min.	1–3 minutes		3 minutes						
Time for operation	10 minutes								20 minutes		≈ 45 minutes						
Voltage	2–5 kV			$3\frac{1}{2}$–$4\frac{1}{2}$ kV				2 kV	5 kV		5 kV						
Current density	0.5–0.80 mA/cm²			$1\frac{1}{2}$–2 mA/cm²				1–3 mA/cm²	≈ 4.5 mA/cm²								
Magnetic field	≈ 100 oersted			≈ 100 oersted													
Materials	**kV**	**mA/cm²**	**time (min)**	**kV**	**mA/cm²**	**time (min)**	**press. (μ)**	**time (min)**		**time (min)**		**gas**	**press. (μ)**	**kV**	**mA/cm²**	**time (min)**	**reference**
Aluminium	3–4	0.5–0.65	3						X								
duralumin				4.0	2	20	10										
aluminium-7 % magnesium								20									
Bismuth	2	0.5	$2\frac{1}{2}$					15									
Cadmium	2–2.5	0.5–0.55	2														
30 % cadmium-70 % silver									rapid etch, satisfactory in air								
Cobalt	4–5	0.5–0.75	3														
vitallium												A	25	2		155	McCutcheon and Pahl [5])
Graphetic stellite									X								
Chromium		no success							X								
Copper	4–5.5	0.5–0.65	3–4						X			Ne	30–200	2–25		45–60	Spivak *et al.*[14])
α brass				3.5	1.5	1	8	10									
Copper-nickel									X								
Copper-nickel-iron								5–10									
Copper-2.5 % iron				3.5	2	1	15										
23 % Cu-75 % Ag-2 % Ni												A	25	3.8		15	McCutcheon and Pahl [5])
Iron	4–4.5	0.5–0.65	2														
Medium C steel				4.0	1.5	3	10										
Low C steel											X	A	25	4		60	McCutcheon and Pahl [5])
Pearlitic steel											X						
Stainless steel	4–4.5	0.5–0.65	2	4.5	1.5	3	8		X	4							
Exhaust valve steel (19 % Cr, 8 % Ni, 0.40 % C)												Air	15	4		100	McCutcheon and Pahl [5])
Magnesium	2–3	0.5–0.55	3														
Magnesium-zinc											X						
Molybdenum	4.5–5	0.5–0.80	5														
Nickel	4–4.5	0.5–0.75	5								X						
Electrodeposited coatings								30–60									
Niobium	4.5	0.5–0.80	10														
Palladium	4–4.5	0.5–0.65	3														
Platinum								10									
Silicon	4–5	0.5–0.8	10–20														
Tantalum	4–4.5	0.5–0.7	7														
Titanium	4–4.5	0.5–0.75	6					30									
Tungsten	4–5	0.5–0.8	7														
Thorium	4–5	0.5–0.75	3–5									A+Xe	2	4		45	Morris [10])
Thorium-zirconium	4–5	0.5–0.75	3–5														
Thorium-2 % iron											X						
Thorium-carbon											X						
Uranium	4–4.5	0.5–0.65	3	4.0	2	25	10		X	1–3	X	O Kr	> 15 75	2 3	≈ 16 3	 60	Englander *et al.*[15]) Berlein [9])
Uranium-cobalt	4–4.5	0.5–0.65	3														
Uranium-molybdenum	4–4.5	0.5–0.65	3														
Uranium-niobium	4–4.5	0.5–0.65	3														
Uranium-niobium-molybdenum	4–4.5	0.5–0.65	3														
Uranium-silicon	4–4.5	0.5–0.65	3														
Zirconium	4–5	0.5–0.75	3–6						X		X						
Zirconium-niobium	4–5	0.5–0.75	3–6														
Uranium dioxide	4–4.5	0.5–0.65	3									No details					Cain [11])
Uranium carbide	4–4.5	0.5–0.65	3														
83 % Cr carbide 15 % Ni binder									X								
70 % Cr 30 % alumina									X								

this pressure. More recent work has shown that more rapid etching can be attained if the pressure in the chamber is initially set at 45 μ Hg. The induction period then ranges from $\frac{1}{2}$ to 2 minutes (decreasing with the number of times the apparatus is used) while etching times for optical examination range from $\frac{1}{2}$ to $1\frac{1}{2}$ minutes.

Cathodic bombardment etching may be confidently applied to nuclear materials as most of the metals of interest in reactors have medium or high melting points, and hence the possibility of structural changes occurring as the result of etching is slight.

The conditions for etching uranium and uranium alloys are similar, except that the alloys may require slightly longer times. Both cooling the specimen and drying the gas increase the speed of etching, presumably through slower surface oxidation under these conditions. Despite the low thermal conductivity quite large specimens may be etched without appreciable heating provided good thermal contact with the cathode exists. Cylindrical samples up to $1\frac{1}{4}$ inches in diameter and a half inch thick have been satisfactorily etched.

Fig. 3 shows the cathodically etched structure of recrystallized uranium. The amount of metal removed by bombardment varies considerably with the crystal orientation, so that some boundaries are very clearly defined, and others barely delineated, by the difference of height of adjacent grains. This effect is not limited to uranium, but occurs with most single phase alloys. Fig. 4 shows a similar microstructure in a ternary uranium-molybdenum-niobium alloy retained in the γ (b.c.c.) structure by quenching.

Attempts to use the apparatus for etching by the method of Englander, Laniesse, and Stohr [16]) were not successful, thick black films being invariably produced. These workers, however, used much higher current densities ($\approx$ 15 mA/cm^2) than we could achieve in our apparatus ($\approx$ 2.5 mA/cm^2).

Attempts to get contrast by heating the specimen by ionic bombardment and then admitting air gave erratic results, although

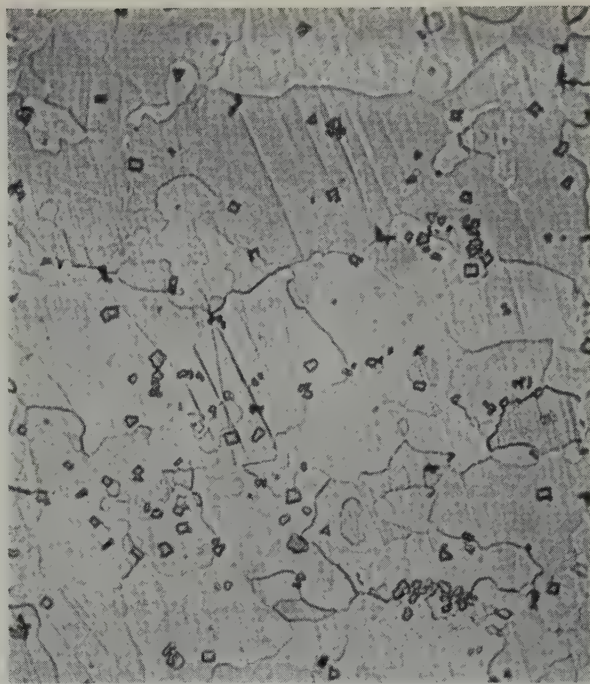

Fig. 3. Recrystallized uranium. $\times$ 400.

good contrast was often obtained, as for example in the microstructure of wrought and partially recrystallized uranium (fig. 5). Sometimes the structure was revealed much more clearly by this means than by polarized light examination; for example fig. 6 shows a recrystallized 'speckled grain' which is visible with only slight contrast under polarized light. Sometimes contrast is produced accidentally by impurities in the argon or by decomposing organic material contained in cavities in the specimen as in the case of the deformed uranium specimen shown in fig. 7. These coatings, if found objectionable, can frequently be removed by re-etching the specimen.

A second phase is frequently shown more clearly by cathodic vacuum etching than by other methods of specimen preparation. Fig. 8 shows a second phase in a ternary uranium-molybdenum-niobium alloy. This was barely visible after chemical etching although its presence was established by X-ray diffraction. The shape of inclusions are generally preserved by cathodic vacuum etching. This is especially valuable when inclusions are to be studied by

Fig. 4. γ phase uranium-molybdenum-niobium alloy × 55.

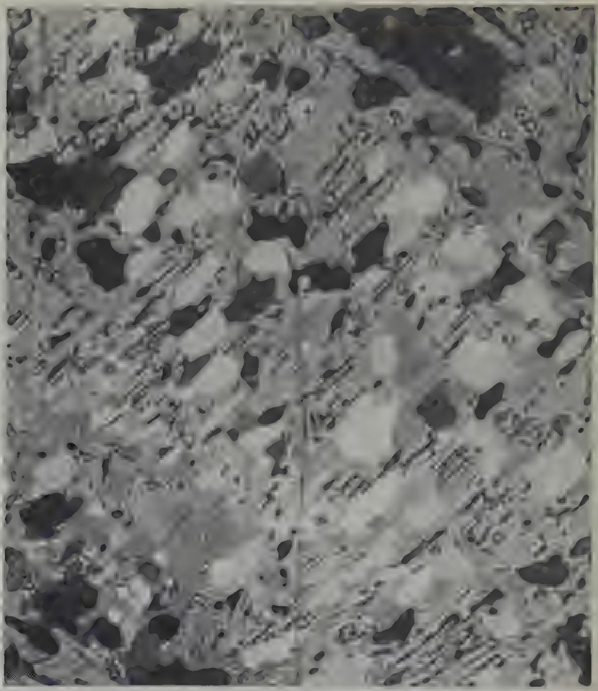

Fig. 6. Uranium showing recrystallized "speckled grain". × 570.

Fig. 5. Wrought and partially recrystallized uranium × 90.

Fig. 7. Slightly deformed uranium with surface film. × 75.

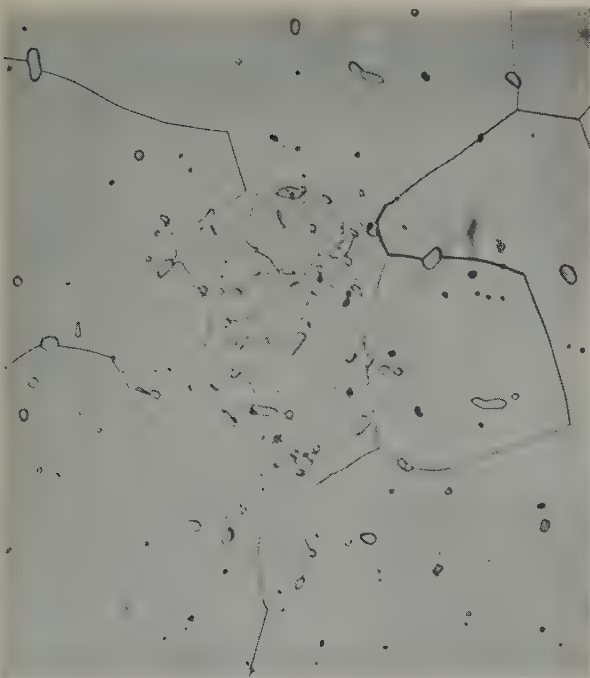

Fig. 8. Ternary uranium-molybdenum-niobium alloy showing second phase. × 270.

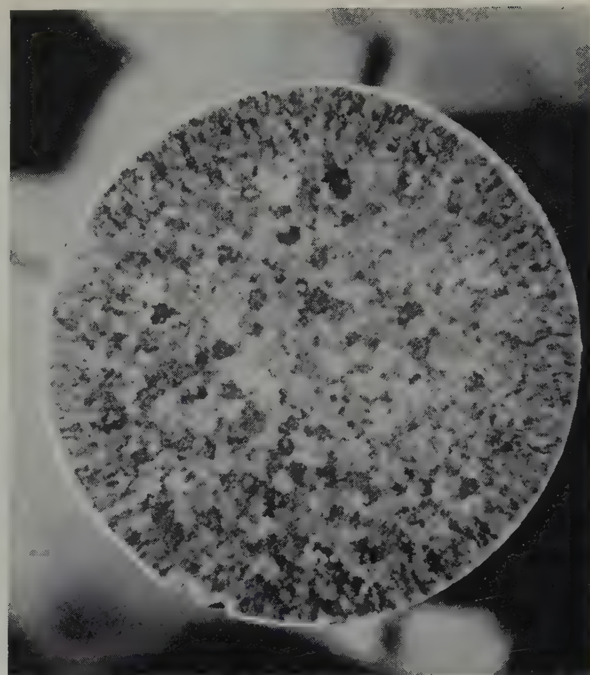

Fig. 10. Cast thorium-aluminium alloy. × 5.

Fig. 9. Electron micrograph of carbide dendrite in uranium. × 10 000.

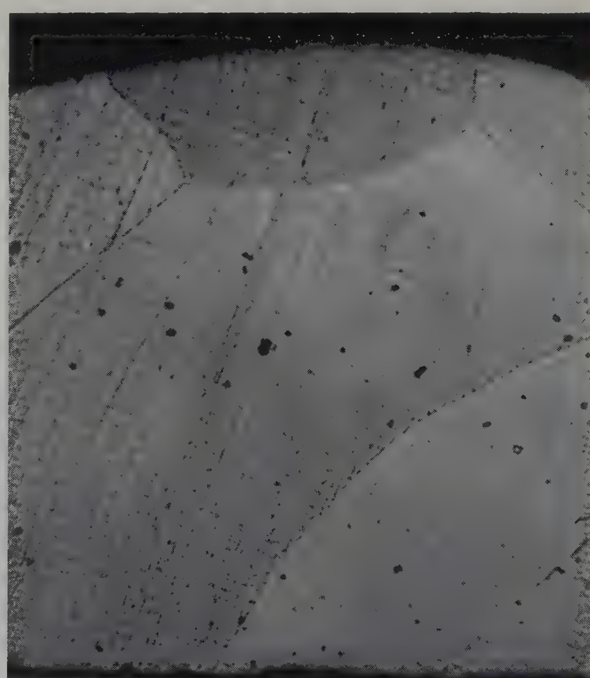

Fig. 11. Cast niobium ingot. × 28.

Fig. 12. Zircaloy sheet. × 150.

electron microscopy since cathodic etching gives a surface suitable for replication and the details on the inclusions are preserved. Fig. 9 is an electron micrograph of a carbide dendrite in uranium. On similar micrographs from surfaces prepared by electropolishing or attack polishing the carbide outline is blurred and the fine detail is absent.

Thorium and thorium alloys can be etched by ionic bombardment under similar conditions to uranium. Cathodic etching is very useful in revealing the grain structure since this is difficult to show by chemical or electrolytic etching without producing false structures. Fig. 10 shows the macrostructure of a thorium-aluminium ingot where the contrast is produced by the different reflectivities of the grains under oblique illumination. The technique of allowing the specimen to heat up and then admitting air to produce a contrasty coating can be applied to thorium and gives consistently good results. The advantages found when cathodically etching uranium alloys—i.e. showing second phases more clearly in optical micrographs and revealing fine precipitates in electron micrographs—have also been found with thorium alloys.

Canning materials such as aluminium, beryllium, magnesium, niobium (fig. 11) stainless steel, zirconium and zircaloy (fig. 12) can all be etched by ionic bombardment. The method is especially useful when composite fuel elements are to be examined, since it is difficult to etch different layers simultaneously by other means.

Cain [11]) and Bierlein *et al.*[15]) have shown that it is possible to etch ceramic fuel materials by ionic bombardment. We have revealed the structure of uranium carbide and uranium dioxide (fig. 13) by this method. Cathodic etching is useful with this latter material since it is very difficult to etch it chemically if its composition departs from stoichiometry.

5. Conclusions

The apparatus described for cathodic bombardment etching in commercial argon has been tested on a variety of materials with melting points ranging from 271° C (bismuth) to 3340° C (tungsten). Satisfactory etches have been obtained in nearly every case.

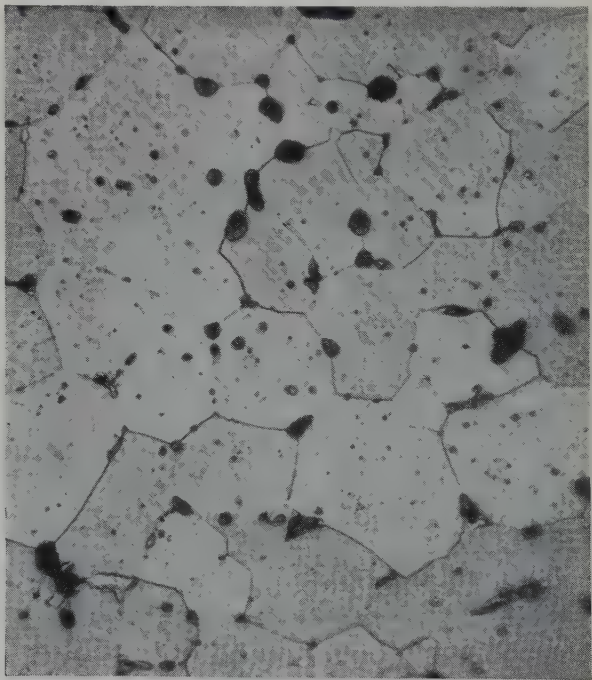

Fig. 13. Sintered uranium dioxide. × 400.

Cathodic etching develops grain boundaries and grain contrast is generally low. Where contrast is required this may often be provided by heat tinting i.e. allowing the specimen to heat up by bombardment and then admitting air. Often contrast is produced during etching, presumably from the impurities in the argon.

Cathodic etching generally leaves the inclusions untouched, so that they are left in relief and their true contours can be appreciated. This is very important when inclusions are to be studied by electron microscopy and the method appears much superior to other preparation techniques. For electron microscopic examination generally perhaps some caution should be exercised since an etch structure has been reported in some metals after prolonged bombardment [17, 18, 14], which may not correspond to the true structure of the material. However no convincing evidence for such a structure has been found on the specimens examined here.

A great advantage of cathodic etching is that practically any metal or alloy can be etched under similar conditions. This is important where the alloy can only be etched with difficulty by conventional chemical or electrolytic means. In investigating new alloy systems in particular much time may be saved in searching for chemical etches.

The present apparatus can deal with several specimens at once, and the short operating time ($\approx$ 10 minutes) compares favourably with other apparatus of its class, and even with chemical etching.

The only serious objection that can be raised to the method is that specimens may get hot enough for structural changes to occur. This effect can be minimised by ensuring good contact between the specimen and the cathode and by keeping the etching time to a minimum. The successful etching of a deformed bismuth specimen indicates that temperatures in a specimen need not exceed $\approx 100°$ C.

Acknowledgements

The authors would like to thank Messrs. F. L. Jagger, V. Haddrell and C. T. E. Hosker, who contributed at various stages to the development of the apparatus. They would also like to thank many colleagues for providing specimens, Mr. I. MacDonald for photomicrography, and Dr. H. M. Finniston and Dr. G. K. Williamson for encouragement and advice.

References

1) W. Feltknecht, Helvetica Chim. Acta 7 (1924) 825
2) C. S. Smith, J. Inst. Met. **38** (1927) 133
3) L. Belladen and M. Martino, La Metallurgia Italiana **21** (1929) 18
4) D. M. McCutcheon, J. Appl. Physics **20** (1949) 414
5) D. M. McCutcheon and W. Pahl, Metal Progress **56** (1949) 674
6) H. Tsuchikura, Kagaku (Science) **21** (1951) 419
7) T. R. Padden and F. M. Cain, Metal Progress **108** (1954) 66
8) A. J. Carlson, J. T. Williams, B. A. Rogers and E. J. Manthos, Iowa State College (U.S.A.) Report, I.S.C. 480 (1954).
9) T. K. Bierlein, Hanford (U.S.A.) Report, HW-34390 (1955)
10) P. R. Morris, discussion to paper by D. Peterson and D. Westlake, USAED Document, TID-7523 (Part I) (1955) 15
11) F. M. Cain, USAED Document, TID-7523 (Part I) (1955) 75
12) J. B. Newkirk and W. G. Martin, General Electric Research Laboratory (USA) Report 56-RL-1561 (1956); and Trans. A.S.M. **50** (1958) 572
13) L. Holland, Vacuum Deposition and Thin Films (Chapman Hall, 1956) 439–443
14) G. V. Spivak, V. E. Iurosova, I. N. Prilizhaeva and E. K. Pravdina, Bull. Akad. Sci. U.S.S.R. (Physical Series) **20**, 1073 (Columbia Technical Translations). This paper contains references to other Russian work in this field.
15) T. K. Bierlein, H. W. Newkirk and B. Mastel, J. Amer. Ceramic Soc. **41** (1958) 1956
16) M. Englander, J. Laniesse and J. Stohr, Saclay (France) Report CEA 1 (1952); and Le Vide 12 (1957) 215
17) A. Güntherschulze and W. Tollmien, Z. Phys. **119** (1942) 685
18) G. K. Wehner, J. App. Phys. **26** (1955) 1056

JOURNAL OF NUCLEAR MATERIALS - 2 (1959) 136–144 - NORTH-HOLLAND PUBLISHING CO., AMSTERDAM

STAINLESS STEEL CLAD DISPERSION OF BORON IN IRON FOR PRESSURIZED WATER REACTORS †

C. F. LEITTEN, Jr. and R. J. BEAVER

Metallurgy Division

and

A. E. RICHT

Solid State Division, Oak Ridge National Laboratory, Tenn., USA ††

Received 15 January 1959

The Army Package Power Reactor (APPR-1) at Fort Belvoir, Virginia, is currently operating with a control rod which contains a boron-bearing neutron absorber section. This component is a welded rectangular parallelepiped, in which the sides consist of rolled austenitic stainless steel-clad plates incorporating 3 wt % boron in iron. This paper presents details describing the design of the absorber section, selection of materials, fabrication procedures, and results of performance under irradiation. The boron, 90 % enriched in the B^{10} isotope, is added to iron powder in elemental form and shaped into a rectangular core which is sintered to a high density. Roll-cladding with austenitic stainless steel results in a composite plate in which the cladding is bonded to the boron-iron dispersion. Irradiation testing of small specimens of this product in the MTR indicates no significant damage after 4 % burn-up of the B^{10} atoms. Slight swelling appears after 10 % burn-up and after 30 % burn-up the irradiation damage is serious. Although some damage is expected under APPR-1 operating conditions, the control rods have operated smoothly in this reactor through 9 MWy of the expected 15 MWy lifetime.

L'"Army Package Power Reactor" (APPR-1) de Fort Belvoir en Virginie fonctionne couramment avec une barre de contrôle qui contient une section absorbante de neutrons contenant du bore. Cette barre est un parallélépipède soudé de forme rectangulaire dont les faces sont constituées par des tôles appliquées d'acier inoxydable laminées contenant 3 % en poids de bore dans le fer. Ce mémoire présente des détails sur la construction de l'absorbeur, le choix des matériaux, les procédés de fabrication et les performances obtenues sous irradiation. Le bore enrichi à 90 % de l'isotope B^{10} est ajouté à la poudre de fer sous forme élémentaire, on en fait un noyau rectangulaire qu'on fritte à haute densité. Le plaquage par laminage avec l'acier inoxydable austénitique fournit un bloc composite dans lequel le plaquage est lié à la dispersion bore-fer. Les essais d'irradiation des petits échantillons de ce produit dans les réacteurs MTR ne montre pas de dommages importants après une combustion de 4 % des atomes de B^{10}. Un léger gonflement apparaît après une combustion de 10 % et les dommages par irradiation deviennent sérieux après 30 % de combustion. Bien qu'on puisse s'attendre à quelques dommages dans les conditions où le réacteur APPR-1 fonctionne, les barres de contrôle ont bien fonctionné dans ce réacteur pendant 9 MW/a, la durée de vie espérée étant de 15 MW/a.

Der "Army Package Power Reaktor" (APPR-1) in Fort Belvoir, Virginia, arbeitet mit einem Kontrollstab innerhalb dessen ein Neutronenabsorber enthalten ist, der Bor enthält. Dieser Bestandtail ist ein geschweisstes, rechtwinkliges Parallelepiped, dessen mit austenitischen, rostfreien Stahl verkleideten gewalzten Seitenplatten 3 Gew % Bor in Eisen enthalten. Die vorliegende Arbeit enthält Einzelheiten über die Konstruktion dieses Absorbers, Materialauswahl, Herstellung sowie Ergebnisse über sein Verhalten bei Bestrahlung. Das Bor, 90 % mit B^{10} Isotop angereichert, wurde dem Eisenpulver in elementarer Form zugesetzt, die Mischung wurde in eine rechtwinklige Form gebracht und zu hoher Dichte gesintert. Die Verkleidung mit austenitischem, rostfreiem Stahl ergibt eine zusammengesetzte Platte, bei der der rostfreie Stahl und der Kern fest miteinander verbunden sind. Bestrahlungsversuche an kleinen Proben dieses Materials in dem MTR zeigten keine wesentliche Schädigung, nachdem 4 % der B^{10} Atome

† Paper presented at the American Nuclear Society Meeting, Hotel Statler, Los Angeles, California, June 2, 3, 4, and 5, 1958.

†† Operated for the U. S. Atomic Energy Commission by the Union Carbide Corporation.

verbraucht worden waren. Eine leichte Schwellung erscheint bei einem Verlust von 10 % der Bor-Atome und nach einem Verlust von 30 % ist die Strahlenschädigung sehr stark. Obwohl unter den Bedingungen im APPR-1 eine merkliche Schädigung erwartet wurde, arbeiteten die Kontrollstäbe in diesem Reaktor 9 MWJ fehlerfrei bei einer geschätzten Lebensdauer von 15 MWJ.

1. Introduction

The control rods of the Army Package Power Reactor at Fort Belvoir, Virginia, contain a neutron absorber section in the shape of a welded rectangular parallelepiped. The sides of this component consist of composite plates containing 2.8 wt% of elemental boron-10 in iron which are clad with austenitic stainless steel. Although boron has excellent neutron absorption characteristics for this type of thermal reactor, the helium generated by the (n, α) reaction leads to potential irradiation damage, which limits the application of the boron-bearing component. However, at the time of the selection of a neutron absorber material, hafnium was unavailable, and other possibilities such as europium and silver-indium-cadmium alloys were completely undeveloped. Circumstances dictated the selection of boron and subsequently a composite stainless steel-clad plate, containing a dispersion of 3 wt % boron in iron was developed.

It was observed that alloys of boron in this composition range were extremely difficult to fabricate but that powder-metallurgy techniques offered a potential answer to the problem. Iron was, therefore, selected as the matrix material because of its compatibility with boron in this process and boron, enriched in the B^{10} isotope at the 90 % level, was specified to

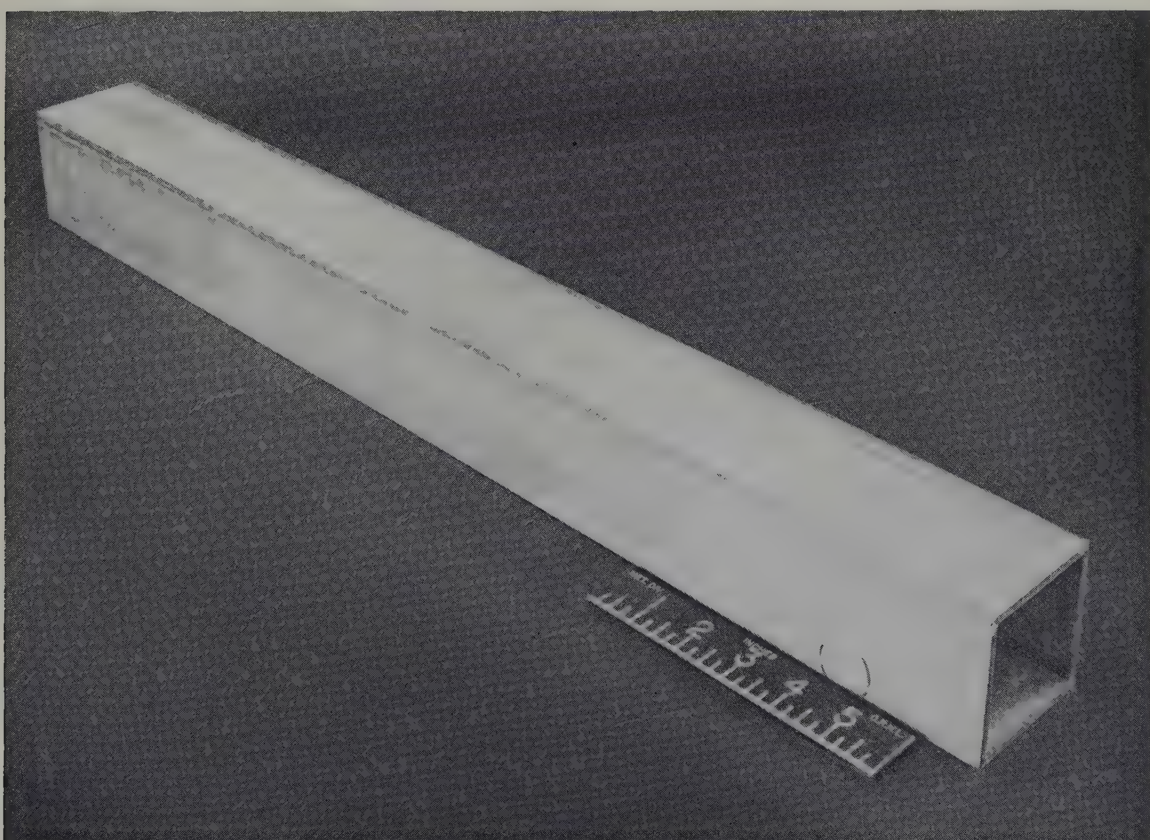

Fig. 1. APPR absorber section.

minimize the concentration of boron in the iron. The corrosion rate of iron in the 232° C, 1 200 psi coolant of APPR-1 necessitated protection of this boron-bearing material by stainless steel, and heat transfer considerations led to development of metallurgical bonding by roll cladding. The work culminated in the manufacture of the seven absorber sections contained in the control rods of the first core of the reactor.

Miniature specimens of the composite plate were prepared for irradiation testing in the MTR under various degrees of burnup, and irradiation damage effects evaluated by post-irradiation examination of dimensional and microstructural changes.

2. Description of Component

As illustrated in fig. 1, the APPR-1 absorber section consists of four plates welded into the shape of a rectangular parallelepiped. Each plate contains a dispersion of 3.2 wt % boron in iron and is clad with austenitic stainless steel. Critical dimensions and other pertinent information are listed in table 1.

TABLE 1

Pertinent data on APPR-1 absorber section

I. Dimensions, inches		
A. Absorber section		
length	$26\frac{1}{16}$	
cross section	2.624 × 2.624	
B. Absorber plates	Boron-bearing section	Over-all
1. Length	$20\frac{3}{4}$	$26\frac{1}{16}$
2. Width	2.214	2.464
3. Thickness	0.090	0.156
II. Materials		
1. Cladding — Type 304L stainless steel		
2. Core	Weight (g)	Weight (%)
Total boron	15.90	3.23
Boron-10	14.10	—
Iron	476.99	96.77
Totals	492.89	100.00

3. Materials Selection

Not only was the desirable material, hafnium, not readily available, but also stainless steel alloys containing boron in the concentration range required were difficult to fabricate, prone to serious irradiation damage, and had questionable corrosion resistance. The concept of incorporating enriched elemental boron in iron by powder metallurgical processing, and roll bonding the dispersion with wrought stainless steel, was conceived as an expedient alternate. This selection of materials appeared to offer the following advantages:

1. Compatibility of boron with iron at required sintering temperatures.
2. Easy fabricability of the dispersion-type material.
3. Corrosion resistance offered by the wrought type 304 stainless steel cladding.
4. Containment of irradiation damage of the boron-bearing dispersion by the high strength ductile austenitic stainless steels.

4. Fabrication

Procedures were developed which led to consistent and reliable methods for powder metallurgical processing of the boron-iron dispersion, and fabrication of roll bonded composite plates. The electrolytic iron and enriched boron powders are separately weighed and blended together for each individual compact, thus affording the advantage of accurate accounting, within 0.2 %, of each gram of boron. The material is cold pressed under 31 tsi, sintered in dry hydrogen at 1 120° C and coined to final size at, again, 31 tsi. The density of the sintered and coined compact is 88 % of theoretical. X-ray diffraction data of the sintered material reveal that the elemental boron combines with the iron to form the iron borides, Fe_2B and FeB. Thus, the final product is in reality a dispersion of iron borides in alpha iron.

Each core compact is clad with wrought stainless steel by roll bonding to result in a composite plate. Simple "picture-frame" procedures [1]) are utilized, in which the compact is

placed within a machined frame, previously provided with an evacuation tube. Cover plates are welded to each side of the frame; the billets are leak detected, evacuated, and sealed. Preheating of the billet prior to rolling is done in a semi-protective hydrogen atmosphere at a temperature of 1100° C for 90 min. Sound metallurgical bonding is achieved with a reduction per pass of 10 % and a total reduction in thickness of 90 %. A transverse section of the fabricated composite is shown in fig. 2. It can be seen that some porosity still exists in the iron-base dispersion. A higher magnified view of a transverse section near the edge is shown in fig. 3. The boron diffusion which occurs can be readily seen, and the grain growth across the interface substantiates the fact that the metallurgical bonding has been achieved. Plates with these characteristics proved to be perfectly sound after being thermally cycled fifty times between 538° C and an ice water quench.

Preliminary investigations indicate that as much as 5 % boron can be incorporated in iron and readily fabricated into composite plates. The limit of rollable boron-iron-base alloys has been reported to be about 3.8 % [2]). In view of preliminary results with the 5 % boron dispersion in iron, there is every reason to believe that the fabrication limit imposed with wrought material can be appreciably extended by powder metallurgy processing.

5. Performance Testing

The mechanical properties of the fabricated boron-iron dispersion, stripped of the cladding, are listed in table 2. It can be observed that the properties in the range from room temperature to 538° C are characterized by high strength, but little ductility.

Irradiation testing of miniature composite

Fig. 2. Cross section of a 3 wt % boron dispersion in iron clad with type 304L stainless steel at 1100° C using a 90 % total reduction. A slight amount of boron diffusion can be observed at the core-clad interface. × 20.

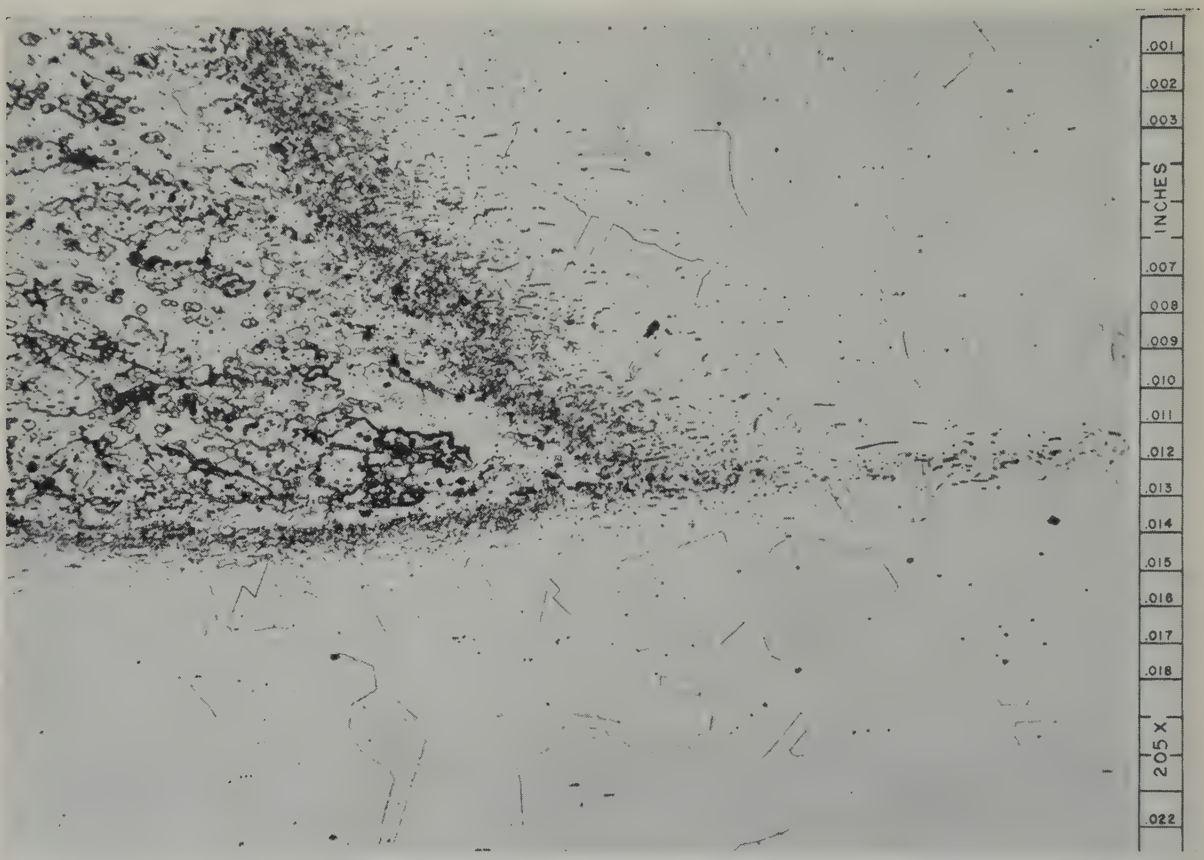

Fig. 3. Core-frame-clad interface of a 3 wt % boron-iron dispersion clad with stainless steel at 1100° C using 90 % total reduction. Note the degree of boron diffusion and the interfacial grain growth. × 205. Cathodic etch.

Table 2

Mechanical properties of fabricated dispersion of 3 wt % boron in iron

Temperature (° C)	Yield strength (0.2 % offset) (psi)	Tensile strength (psi)	Per cent elongation
RT	40 500	42 600	0.5
150	40 000	41 100	0.5
260	39 700	40 000	0.5
400	34 500	39 300	3.0
540	21 500	28 200	5.0
980	3 850	5 050	16.0

plates, containing 1.7, 2.8, and 3.5 wt % B^{10} in iron, was conducted in the Materials Testing Reactor (MTR) to varying degrees of B^{10} burnup. The results of the irradiation tests are listed in table 3. The only change in dimensions was a thickness increase. It is apparent from this table that under MTR temperature conditions (66° C), severe swelling can be expected after a burnup of at least 32.9 % of the B^{10} atoms. It also can be observed that post-irradiation heat treatment caused additional swelling. Since this heat treatment was done at one atmosphere, it is felt that this test is a more severe condition than will be realized in the APPR where the absorber section is under an external pressure of 1 200 psi. Comparison of the results on specimens 60A, 7, and 120A indicates that the swelling increases with increased concentration of B^{10} atoms. The change in thickness is attributed to helium generated by the B(n, α) reaction. Helium was identified in the irradiated samples.

Metallographic examination of the specimen

TABLE 3

Effects of irradiation on composite stainless steel-clad plates containing a dispersion of enriched boron in iron

Plate size: $6\frac{1}{2}$ in. × 1 in. × 0.156 in.

Sample No.	Boron concentration wt % B^{10}	Burnup † % B^{10} atoms	Thickness †† increase (%)		Heat treatment temperature (° C)
			After MTR irradiation at 66° C	After 312 h heat treatment	
6	2.81	4.0	0	0	315
7	2.81	11.5	2.6	10.9	315
8	2.81	17.6	4.5	21.2	315
1	2.81	32.9	34.0	72.4	315
5	2.81	37.0	30.1	—	—
60A	1.67	9.3	1.3	3.2	260
60B	1.67	14.7	2.6	7.7	260
120A	3.50	8.9	10.3	18.6	260
120B	3.50	3.4	1.9	3.8	260

† Burnup based on lithium analysis.
†† Nominal clad-core-clad thicknesses: 0.033-0.090-0.033 in.

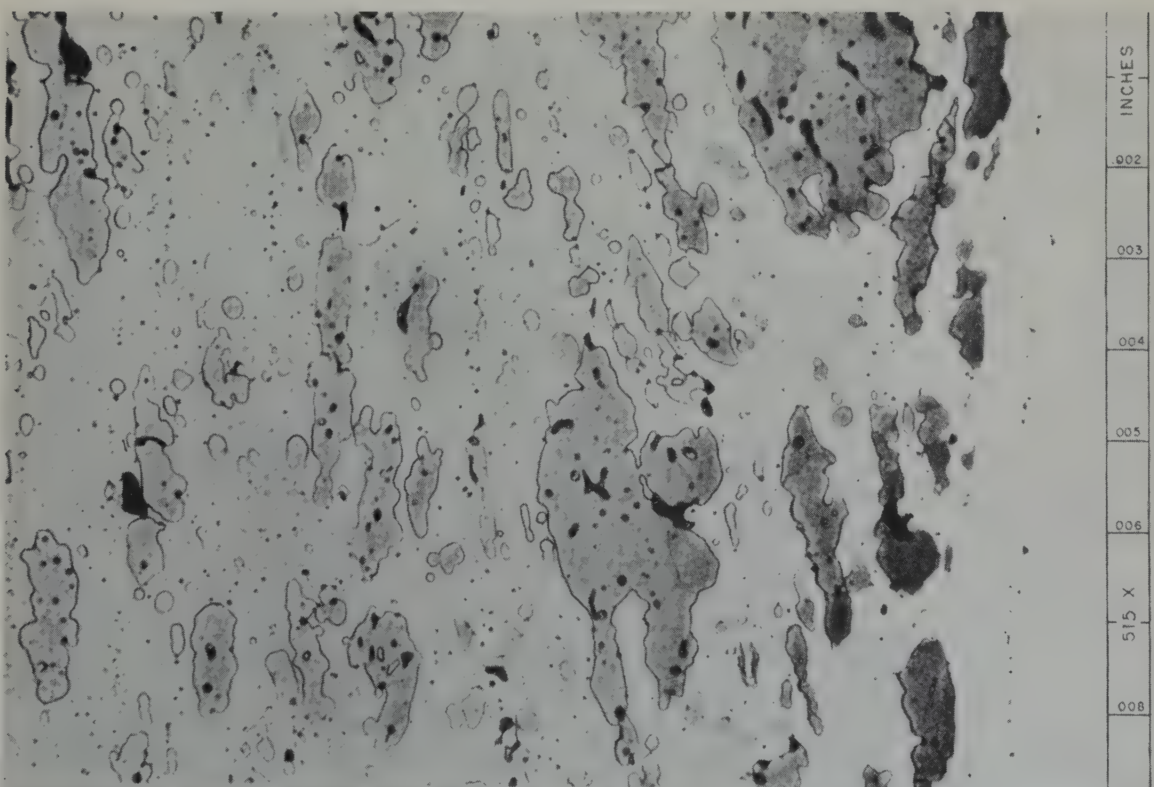

Fig. 4. Microstructure of core adjacent to cladding in the 4 % irradiated sample after being subjected to 312 h of cyclic heating to 315° C. × 515.

clearly reveals that the burnup is confined to a volume adjacent to the borided interface of cladding and core. This phenomenon is evident by the differential attack of the etchant shown in fig. 4. This specimen was subjected to 4 % burnup of the B^{10} atoms and showed no evidence of irradiation damage. The porosity shown is not believed to be a result of irradiation since it appears to be of the same size and magnitude as the voids present in unirradiated material. Fig. 5 illustrates the failure of a specimen which was irradiated to 11 % burnup of the B^{10} atoms. Although the failure occurred during the post-irradiation heat treatment, as shown in fig. 6, the higher magnified view of the region adjacent to the bonded interface reveals the severe damage caused by the irradiation. Fig. 7 illustrates the microstructure

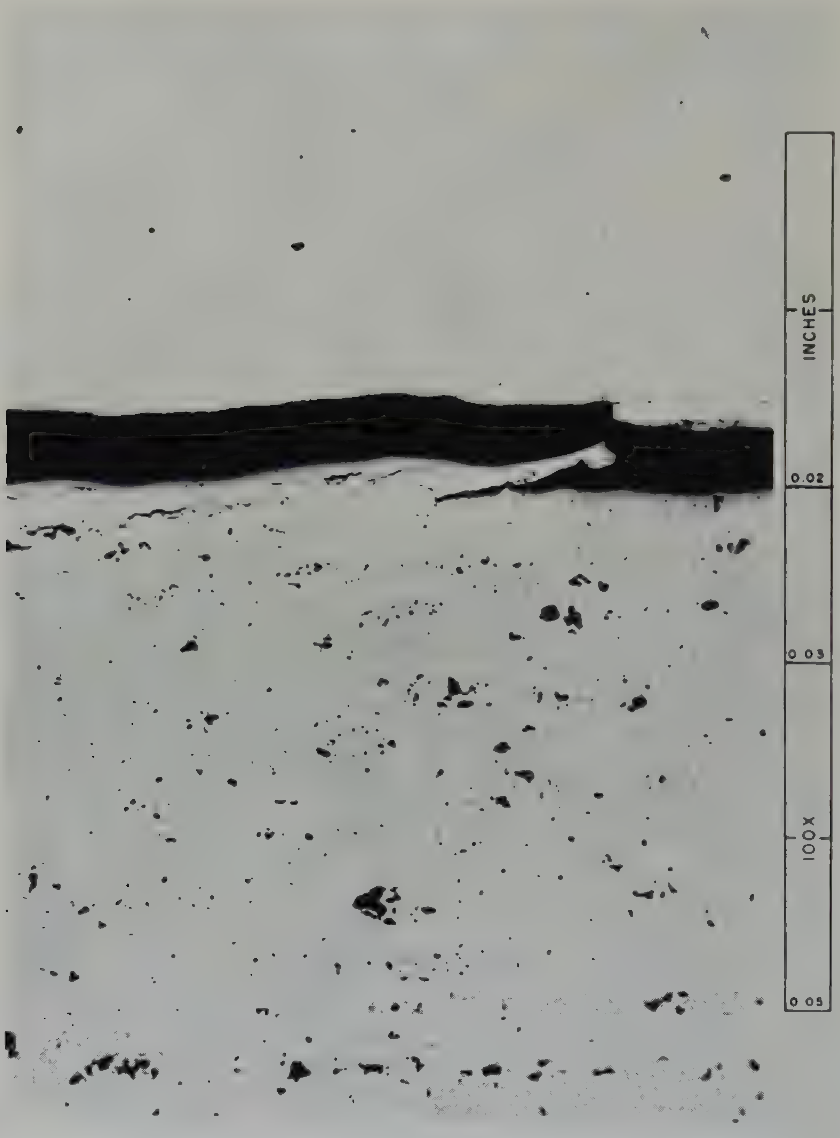

Fig. 5. Cladding separation in the 11 % irradiated miniature sample after being subjected to 312 h of cyclic heating to 315° C. × 100.

Fig. 6. Magnified view of the core adjacent to the cladding as shown in fig. 5. × 515.

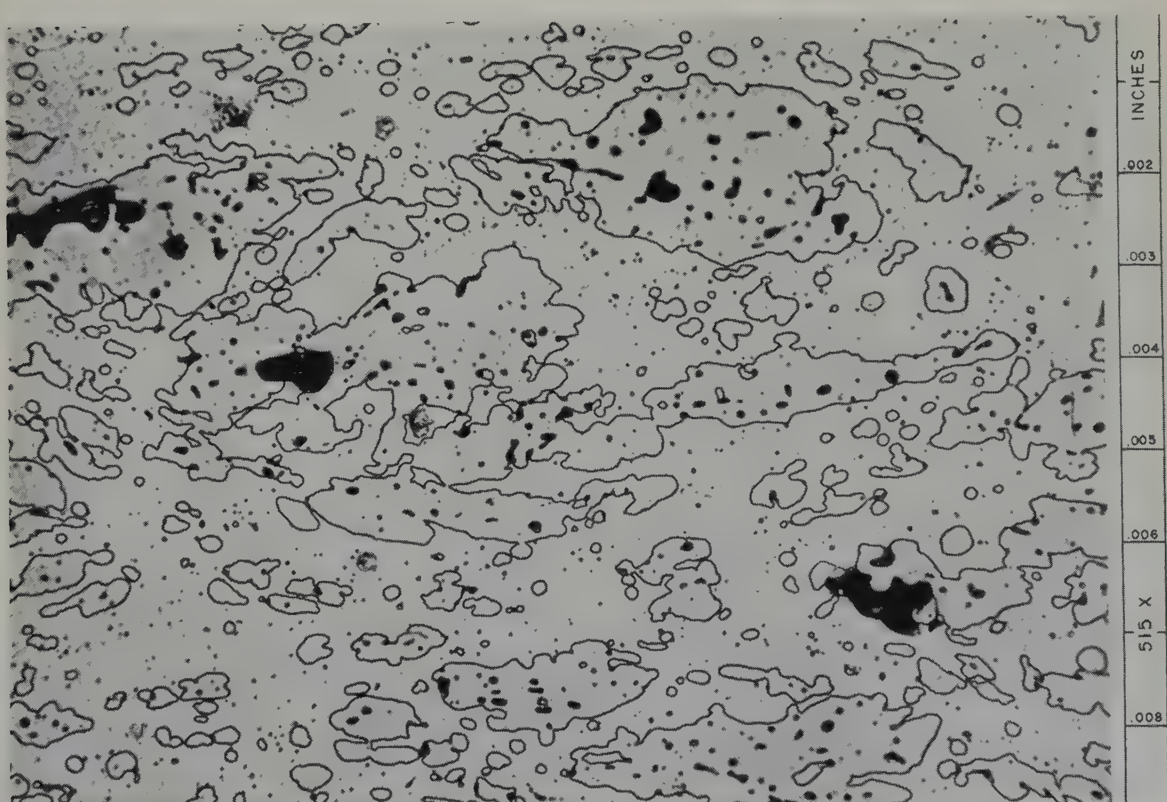

Fig 7. Photomicrograph of the core at the center of the irradiated plate illustrated in fig. 5. × 515.

at the center of this specimen. It is apparent that the self-shielding effect confined the burnup of B-10 atoms to the volume of material adjacent to the bonded interface with ultimate deterioration of the bond and subsequent swelling, particularly after heat treatment at 315° C.

6. Conclusions

1. A dispersion of boron in iron with a concentration of 3 wt % can be readily prepared by powder metallurgical techniques and clad with austenitic stainless steel by roll cladding.

2. Irradiation damage in this composite plate is severest in the region of the boron-bearing iron which is adjacent to the bond interface.

3. Miniature specimens of composite plate, irradiated in the MTR showed no gross dimensional changes after a B^{10} atom burnup as high as 17 %. At a burnup of 33 %, significant swelling occurred.

4. In post-irradiation heat treatments of miniature specimens, the only sample which exhibited no deleterious effects from the irradiation and subsequent heat treatments was limited to a burnup of 4 % of the B^{10} atoms.

5. Preliminary results strongly indicate that the concentration limit of boron in boron-iron alloys can be appreciably extended by powder-metallurgical processing.

References

[1]) J. E. Cunningham and E. J. Boyle, Proc. in Nucl. Energy, Series V (Pergamon Press, London, 1956) 548

[2]) T. H. Middleham, J. R. Rait and E. W. Colbeck, J. Iron and Steel Inst. **187** (1957) 1

JOURNAL OF NUCLEAR MATERIALS - 2 (1959) 145–153 - NORTH-HOLLAND PUBLISHING CO., AMSTERDAM

CORROSION OF ALUMINIUM ALLOYS IN HIGH TEMPERATURE WATER – A SURVEY

KETIL VIDEM

Joint Establishment for Nuclear Energy Research, Lillestrøm, Norway

Received 17 January 1959

In high temperature water aluminium alloys can be attacked in three ways: by grain boundary attack, by accelerated attack and by uniform attack. The grain boundary attack can be prevented by alloying with elements which form phases which are cathodic to aluminium. The beneficial influence is attributed to the exchange currents set up between the aluminium matrix and the phases of alloying elements. The accelerated attack can be controlled by proper fabrication technique and well-balanced additions of alloying constituents, and thus the main corrosion problem is the high uniform corrosion rate. It is proposed that the rate-controlling step in a dynamic system is the dissolution of aluminium oxide, and it is therefore difficult to propose alloys which have a lower corrosion rate than the best present ones. At 230° C in flowing water a corrosion rate of 0.1 mm/year is observed. This is increased to about 0.3 mm/year under boiling at 70 watt/cm². With proper design, aluminium-clad fuel elements might work satisfactorily at this temperature and perhaps even somewhat higher. A short comment is made on the mechanical properties of the corrosion resistant alloys and on the welding of these.

Les alliages d'aluminium peuvent être attaqués de trois façons par l'eau à température élevée: par attaque intergranulaire, par attaque accélérée et par attaque uniforme. On peut empêcher l'attaque intergranulaire par formation d'alliages avec des éléments qui constituent des phases cathodiques par rapport à l'aluminium. Leur influence bénéfique est attribuée aux courants créés entre la matrice d'aluminium et les phases des éléments d'alliages. L'attaque accélérée peut être contrôlée par des procédés de fabrication appropriés et des additions de constituants d'alliages correctement ajustées. Ainsi le problème principal est la grande vitesse de la corrosion uniforme. On suggère que le phénomène qui contrôle la vitesse dans un système dynamique est la dissolution de l'oxyde d'aluminium, et il est donc difficile de proposer des alliages qui ont une plus faible vitesse de corrosion que les meilleurs utilisés actuellement. A 230° C sous l'eau en circulation, on observe une vitesse de corrosion de 0.1 mm par an. Elle atteint 0.3 mm par an sous ébullition à 70 watts par cm². Convenablement disposés, les éléments combustibles gainés d'aluminium pourront être utilisés avec satisfaction à cette température et peut-être même à des températures légèrement plus élevées. Les propriétés mécaniques des alliages résistant à la corrosion et leur soudure sont brièvement commentées.

In heissem Wasser werden Aluminiumlegierungen auf drei Weisen angegriffen: durch Korngrenzenangriff, gleichmässigen Angriff und beschleunigten Angriff. Der Korngrenzenangriff kann durch Zugabe gegenüber Aluminium kathodischer Legierungselemente vermieden werden. Der vorteilhafte Einfluss dieser Elemente wird den elektrischen Strömen zugeschrieben, die zwischen Aluminium und anderen Phasen fliessen. Der beschleunigte Angriff kann durch gute Herstellungsmethoden und wohlgewählte Legierungszugaben kontrolliert werden; es bleibt also der gleichmässige Angriff als wichtigstes Korrosionsproblem. Es wird angenommen, dass in einem dynamischen System die Angriffsgeschwindigkeit durch die Auflösung des Aluminiumoxyds kontrolliert wird und es ist deswegen schwer Legierungen mit besseren Korrosionseigenschaften als die besten jetzigen vorauszusagen. In fliessendem Wasser bei 230° C wurde eine Korrosionsgeschwindigkeit von 0.1 mm pro Jahr gemessen. Bei einem Wärmefluss von 70 Watt/cm² in kochendem Wasser bei 230° C erhöht sich die Geschwindigkeit auf 0.3 mm pro Jahr. Richtig konstruierte, mit Aluminium verkleidete Brennelemente dürften sich bei dieser Temperatur, und sogar bei etwas höheren Temperaturen, gut verhalten. Kurze Bemerkungen werden gemacht über die mechanischen Eigenschaften und das Schweissen von korrosionsbeständigen Legierungen.

1. Introduction

Aluminium appears to be a very attractive material for use in water cooled reactors. It has a low cross section for thermal neutrons, it is cheap, easily available, and it has a well known technology.

In reactors operating at fairly low temperatures, aluminium canning has been widely used for many years. In power reactors which have to operate at higher temperatures to obtain a good thermal efficiency, aluminium has two serious disadvantages; the corrosion resistance in high temperature water is poor, and the creep and tensile strength are low at high temperatures.

In 1955, Draley and Ruther [1, 2]) showed that the corrosion rate could be markedly decreased by addition of 0.5 – 2.0 wt % Ni. Since then the high temperature corrosion of aluminium alloys has been the interest of many research institutes, and much work has been done in order further to improve the properties, the ultimate aim being the development of satisfactory aluminium alloys for use in water cooled power reactors. In what follows, we shall review the conclusions reached on the basis of these researches.

2. Testing Procedures and Results

Autoclave tests were generally used to select the most promising alloys. Specimens of various alloys are usually mounted on racks and the autoclaves are opened at intervals for inspection and measurement. The results obtained in this way led to optimism. It was shown by Huddle and Wilkins [3]) that the destructive grain boundary attack can be prevented by alloying with minor amounts of Ni, Fe, Cu, Co, Mo, W or Ti. The type of alloy (X 8001) originally proposed by Draley and Ruther [1, 2]) (Al with 0.5 – 2 wt % Ni, 0.2 – 0.5 wt % Fe and up to 0.2 wt % Si), has generally been regarded as the most corrosion resistant, and it appears that the percentages of the various constituents are not critical. It has further been shown [4, 5]) that the addition of small amounts of Ti and Be, in addition to Ni and Fe, is beneficial. Promising results have also been obtained with (Al, 10 wt % Si, 1 wt % Ni) [6]) and with (Al, 1 – 2 wt % Ni, 4 – 8 wt % Cu) [7]).

Corrosion rate in autoclaves of alloys of the X 8001 type have been studied by various workers, and some results are shown in table 1.

TABLE 1
Corrosion of X 8001 type aluminium alloys

Corrosion rate (mm/year)	Temperature (°C)	References
0.15 —0.18	350	[8, 11])
0.013—0.06	300	[8, 10, 11, 12])
0.015—0.033	250	[8, 11])

It is seen from the table that the rate is reasonably low even at 350° C, and if the same rate could be obtained under reactor conditions corrosion would not appear to be a serious drawback up to 300° C. A certain spread will be noted in the results reported by the various workers. This can partly be explained by variations in the alloys structure and composition; the main reason is, however, a slight variation in the test conditions.

High purity water was usually added at the beginning of the experiments and was renewed each time the autoclaves were opened. By this procedure the specimens are exposed to water of varying quality, as each filling is gradually contaminated by corrosion products from the aluminium and stainless steel. Accordingly, it was found that the corrosion rate was highly dependent on how often the water has been renewed, on the ratio of surface area of aluminium to water volume and even upon the composition of other specimens in the same autoclave. The reason is clearly the influence of dissolved aluminium. It is felt therefore, that simultaneous testing of specimens of various alloys will result in a lower rate for the most resistant ones than would be found if these were tested in isolation.

Several workers [8, 10, 11, 20]) have foreseen the difficulties arising from the batch-wise replacement of the water, and conducted corrosion tests with a slow flow of fresh water through the autoclaves. Interesting information regard-

ing the corrosion mechanism has been obtained from these experiments. The corrosion rate, however, was found to be dependent upon the rate of replacement of water, and rate data are consequently of limited interest.

To overcome these conditions and simulate reactor conditions more closely, so-called loop tests were carried out, a loop being a closed tube system where specimens are exposed to high temperature water which flows past the specimens at a specified flow rate. The corrosion rate of aluminium alloys in loops was found to be 10–50 times higher than that found in autoclaves. Initially there was a considerable variation in the results obtained by various workers. This could be traced back to differences in the water conditions. The ratio: specimen surface area/volume of water, is of particular importance. In the JENER high temperature loop operating at 230° C, the corrosion rate was increased about 50 times when the ratio of surface area to water volume was decreased from 200 cm^2/l to 0.1 cm^2/l [21]).

In order to obtain data for preliminary estimates of corrosion rates under reactor conditions, the loop tests should be carried out with the same ratio of aluminium surface to water volume and ion exchange flow rate as for the reactors under consideration.

The maximum operating temperature in the JENER loop is 230° C. Various alloys have been tested at this temperature under a linear flow rate of 4 m/sec [21]). To raise the ratio "aluminium surface area/water volume" to 200 cm^2/l, foil of X 8001 was mounted in the loop in addition to the specimens. The flow through the ion exchanger was 10 l/h, and the total water volume 100 l. The resistivity of the water during the test was $0.5-1.0 \times 10^6$ ohm-cm. Almost identical corrosion rates were observed for specimens of the different alloys, i.e. about 0.1 mm/year.

Krenz *et al.*[13]) report that in Chalk River loop tests a corrosion rate of 0.3 mm/year was observed for X 8001 under a linear flow rate of 6–7 m/sec at 270° C. Increasing the area volume ratio from 170 to 360 or 567 cm^2/l did not affect the corrosion rate. Of special interest are the experiments with prefilming of the specimens in autoclaves prior to exposure in the loop. A considerably lower rate was observed for the prefilmed specimens. It is, however, not yet known if this low rate can be maintained for longer periods. Loop tests at Argonne [9]) have been in excellent agreement with the Canadian work.

Scant experimental data are available regarding the effect of heat transfer through the specimen and boiling on the corrosion rate in a dynamic system. In the JENER loop a by-pass system has been used for studying effects of heat transfer on the corrosion. The equipment is shown in fig. 1.

Boiling tests with this equipment have been

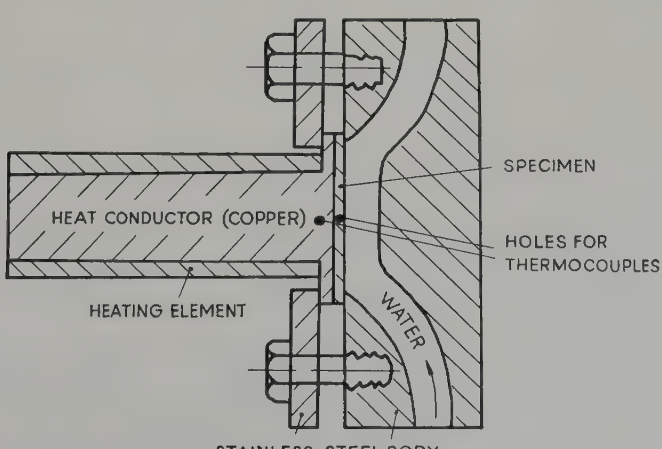

Fig. 1. Equipment for testing aluminium under conditions of heat transfer.

carried out with specimens of various alloys. The flow rate was 2 m/sec and the heat flux 70–80 watt/cm^2. The water was heated from 220° C at the inlet to about 240° C at the outlet. This corresponds to the boiling point at the applied pressure. Foil of X 8001 was introduced into the loop to obtain a surface/water ratio of 200 cm^2/l.

The corrosion rate was found to be about 0.3 mm/year for several alloys. This value is extrapolated from a 3 months' experiment.

Draley *et al.*[8]) have studied the effect of heat transfer at 210° C in autoclaves with continuously refreshed water. The maximum heat flux in their experiment was 6.7 watt/cm^2. The logarithm of corrosion rate was found to be proportional to the square root of the heat flux. Using this relationship and extrapolating to 70 watt/cm^2 gives a corrosion rate of about 0.3 mm/year. The law thus seems to be valid even up to higher heat fluxes.

3. Corrosion Mechanisms

The standard electrode potential of aluminium is +1.66 volt, and it is not possible to protect it by cathodic polarization. The voltage needed would lead to hydrogen evolution and the current would be unacceptably high.

At room temperature protective films are formed in non-complexing solutions with *p*H 4–8.5, and experience with aluminium kitchen utensils shows that corrosion troubles normally are not serious up to 100° C.

3.1. Grain boundary attack

When high purity aluminium is exposed to distilled water at about 120° C a change in the kind of attack is observed. Above this temperature a loose non-adherent film is formed. The corrosion rate is high and the grain boundaries especially are severely attacked. This kind of corrosion has, therefore, been given the name *grain boundary attack*. It should, however, be remembered that the type of attack is somewhat different from what is usually meant by this term, as the rate of general corrosion is also high.

The grain boundary attack on aluminium can be avoided either by anodic polarization of the specimens or by alloying additions.

For anodic polarization a minimum current density has been observed above which the metal is protected, and below which it will suffer grain boundary attack [14]), see fig. 2.

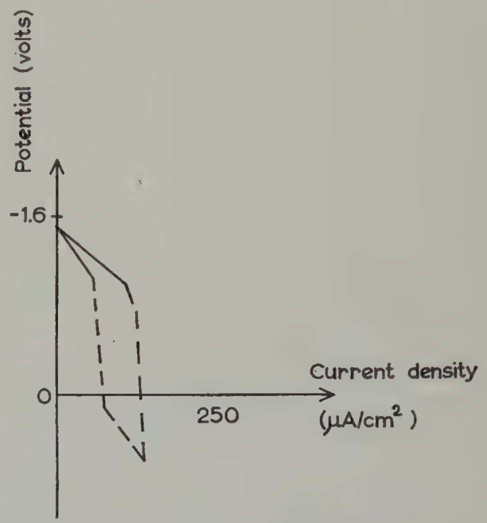

Fig. 2. Voltage versus current density for anodic polarisation of high purity aluminium at 200° C. Pt reference electrode [14]).
——— Grain boundary attack.
. . . . Passivation.

Only alloying elements which form phases with low hydrogen overvoltage have been found to be effective in preventing grain boundary attack. The second phases themselves corrode slowly, and they will be cathodic to the aluminium matrix. The matrix will be polarized anodically, and the current density is sufficient to prevent grain boundary attack.

3.2. Uniform attack

Hunter and Fowle [15]) have shown that when aluminium is oxidized in air or anodized, a duplex corrosion product film is formed. This film consists of a thin protective barrier film adjacent to the aluminium surface and a more permeable bulk film. The same occurs in water. It is reasonable to assume that the *manner* in which aluminium is attacked is determined by the inner film, or barrier layer. The effect of the

anodic polarization is probably to modify the barrier layer in some way.

The barrier layer is found to consist of amorphous alumina, impervious and without pores. It grows by outward diffusion of aluminium ions. After an initial build-up period the film does not further increase in thickness. To keep the thickness constant while aluminium is diffusing out, the barrier layer film must be progressively transformed into bulk film.

The composition of the bulk layer formed in distilled water is dependent upon the temperature. At room temperature it consists of $Al(OH)_3$, above 120° C it is mainly boemite $AlO(OH) = Al_2O_3.H_2O$. At very high temperatures (350° C and above) alumina is formed.

The bulk layer contains pores and cracks, and it must be assumed that this is the reason why the bulk layer thickness does not affect electrical measurement of the barrier layer thickness.

The barrier layer alone does not control the corrosion *rate*. It is found that the corrosion rate decreases with increasing bulk layer thickness, with constant barrier layer thickness. Mass transport is presumably much slower though the barrier layer type of film, for a given thickness, and the reason why the bulk layer overshadows the barrier layer in controlling the corrosion rate must be the much larger thickness of the former.

It is probably not only the thickness, but also the nature, of the bulk layer which is rate determining. According to work by Krenz [19]) a double structure can be observed in the bulk layer: an inner film without microscopic pores, and an outer porous film. The second phases of alloying elements are present in the inner bulk film, but not in the outer. The pattern of the second phases indicate that the inner bulk film is growing inwards, and the outer is most likely the result of a dissolution-reprecipitation process. It is not clear whether these double layers also are present in corrosion films formed at lower temperature.

Dillon and Troutner [11]) have showed that there is a parabolic corrosion/time relationship for tests conducted in autoclaves with slowly replaced water. In loops, however, a linear relationship is found, and the bulk film does not increase in thickness. This could be due either to an abrasion and spalling-off mechanism, or else to a dissolution process. With an abrasion process we would have difficulties in accounting for the area/volume ratio effect, and dissolution of the bulk film appears to be the most probable mechanism.

When a constant film thickness is obtained, the amount of corrosion products formed must be equal to the amount of material removed. The dissolution of oxide from the film is now rate-determining, and the corrosion barriers will be adjusted to a thickness which gives the same rate. Thus a promising line for development of better alloys might be to search for elements which could be incorporated in the bulk film and thereby decrease the dissolution rate. In addition to such constituents, elements forming cathodic sites are required for the prevention of grain boundary attack, as mentioned earlier.

In a stationary state the same amounts of aluminium are transferred through the barrier layer and bulk layer. A relationship between the thickness of the layers should therefore be expected, and e.g., an improved bulk layer should lead to increased thickness of the barrier layer.

The transformation of the barrier layer into the porous boemite bulk layer probably involves a dissolution-precipitation process. During the transformation, aluminium is very likely lost to the solution, in which it will occur in a colloidal or ionic form. A comparatively concentrated solution will be present in the pores, and precipitation will lead to sealing of the remaining film.

If this theory for the corrosion rate is correct, the corrosive power of the water will depend on the rate at which the aluminium is removed from the oxide film. A high flow rate will increase the dissolution process and a high aluminium content in the water is expected to lead to a reduction. The influence of the area/volume ratio is thus understood.

It is not known whether it is the ionic or colloidal aluminium which plays the most important role. Preliminary experiments indicate that it is the colloidal aluminium.

The effect of heat transfer through the metal on the corrosion rate in a pressurized system can be explained by the increased temperature of the corrosion film. In this case it has been observed that the film thickness increases steadily with time, and the temperature of the film with a constant heat flux is therefore increased. If a steady state with constant film thickness and constant rate is reached, the dissolution of film will again be rate-determining, and thus the flow pattern and the properties of the water should be the only important factors. Thermal stresses and thermal shocks could cause spalling-off of the corrosion films, and thereby cause accelerated rate. This is not very likely to be of great importance, as the additional stresses are small compared to those resulting from the film growth itself. The possible effect of a boiling process is a difficult problem and will not be treated here, apart from stating that it is possible that alloys with a resistant phase acting as nucleation sites for the bubbles would be expected to have the better corrosion resistance.

Our present knowledge regarding corrosion mechanisms does not give many indications as to what kind of alloying elements should be added in order to improve the corrosion resistance, apart from the general statement that such elements should reduce the dissolution rate of the film.

A promising line of attack might be the one pointed out by Draley *et al.*[8, 9]) who have shown that additions of H_3PO_4 to the water will decrease the corrosion rate appreciably. The effect is attributed to formation of a bulk layer film of a different composition. In a system with H_3PO_4 additions, a basic aluminium phosphate, augelite, is formed [11]). Maximum inhibiting effect is obtained in systems with a pH as low as 3.8, and even less. At this pH, the concentration of the phosphate ions can be very low and still be effective. Good corrosion resistance has been reported by Draley *et al.*[8]) for 2*S* aluminium with 1 wt % Ni in water with H_3PO_4 at 315° C with a flow rate of 6 m/sec.

The low pH required to protect the aluminium may naturally favour attack of any steel components in a reactor system.

3.3. Other kinds of attack

Alloys which resist the immediate grain boundary attack and undergo reasonably slow uniform corrosion, are susceptible to a third kind of attack – a so-called *accelerated attack* – which sometimes occurs after long exposures and is characterised by a sharp increase in the corrosion rate. Two different explanations have been put forward to account for this behaviour.

The barrier layer thickness of the alloys which are attacked in the grain boundaries is found to be smaller than on the alloys resistant to this kind of attack [11, 21]). Hunter and Fowle [15]) have shown that when aluminium is oxidised in air at 475° C, crystallization of the barrier film occurs after some time. Dillon and Troutner [11]) have therefore proposed that the onset of accelerated attack is caused or accompanied by crystallization of the amorphous barrier layer. After this has happened the barrier layer will not be able to prevent grain boundary attack. The original films are assumed to prevent formation and growth of a new amorphous barrier film, and a rapid grain boundary attack will be the result.

Somewhat against his own theory Troutner [12]) also showed that the inner film is amorphous on alloys which are initially attacked in the grain boundaries. Only experiments with short exposure times were carried out, and it cannot be excluded that crystallization of the barrier layer would occur after long exposure. According to this theory, alloying additions which improve the resistance to accelerated attack stabilize the amorphous form of barrier layer.

Some time after the accelerated attack has started, macroscopic blisters can often be seen on the specimens. These blisters seem to be generated by gas. The commonly accepted explanation of this phenomenon is the one

originally proposed by Draley *et al.*[1, 2, 8, 9]). Hydrogen is discharged from solution in the form of atoms and will be easily picked up by the aluminium metal. The hydrogen atoms diffuse to grain boundaries, voids and lattice defects where they combine in pairs to form molecular gas. As pressure builds up, the metal and the oxide are blown apart, fresh metal is thus exposed and a high corrosion rate results.

When alloys rich in phases with low hydrogen overvoltage suffer this blister attack, the hydrogen is probably taken up via these second phases and diffuses from them to the metal. To reduce blistering in this case, alloying constituents which lower the solubility of the hydrogen in the cathodic phases should be effective. It is possible that Si has such an effect, and preliminary experiments indicate that high silicon alloys are little susceptible to blistering[14]).

The study of the accelerated attack is complicated by the long exposure times needed for its onset, and also because alloys with the same chemical analysis may have surprisingly different properties in this respect.

4. Welding of Corrosion-Resistant Alloys

The Al/Ni/Fe alloys referred to are easy to weld and the welds are satisfactory from a mechanical point of view. It is difficult, however, to make welds which are not preferentially attacked in high temperature water. It has been shown for the Al/Fe/Si alloys that very structure-sensitive properties will result if the iron content is too low[16]). Welding of such material will usually lead to a coarser second phase and a more uneven distribution of it. Relatively poor corrosion resistance will be the result.

Loop tests at 230° C of argon-arc welds on Al, $1-2$ wt % Ni, $0.25-0.8$ wt % Fe alloys have given different results. In some cases the corrosion of welded specimens did not differ from that of unwelded ones, in other cases the areas adjacent to the weld were severely attacked. Anderson *et al.*[20]) have reported that argon arc welds of Al/Ni/Fe alloys performed badly in a loop operating at 260° C. Hot pressure welds, however, were satisfactory.

As-cast Al/high Si/Mg/Ni alloys have been found to have a good corrosion resistance when

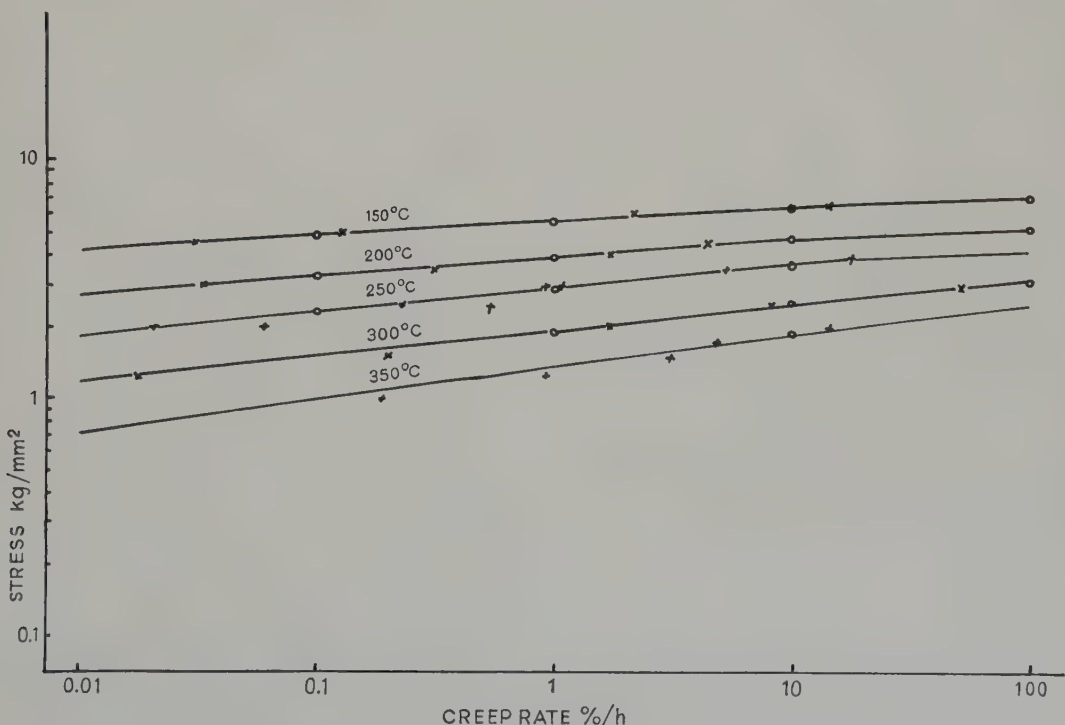

Fig. 3. Creep rate versus stress at various temperatures for Al, 1 wt % Ni, 0.5 wt % Fe (ref. [12])).

joined to Al + 1 wt % Ni alloys. The strength is good, and the melting point low. It may be possible to utilise such material for corrosion-resistant soldering of aluminium alloys.

5. Mechanical Properties of Corrosion-Resistant Alloys

The development work on aluminium alloys for use in water cooled power reactors has mainly been concentrated on improving the corrosion resistance. The mechanical properties of these alloys have not been thoroughly investigated. As has been pointed out above, there are three groups of alloys which show promising corrosion resistance: the Al/Ni/Fe type (0.5 – 2 wt % Ni, 0.2 – 0.5 wt % Fe) the high Si type (10 wt % Si, 1 wt % Ni); and the Al/Cu/Ni type.

The mechanical properties of the first type of alloys are near to those of 2*S*.

An introductory investigation of the creep properties of the alloy containing 1 wt % Ni, 0.5 wt % Fe has just been concluded [17]). The creep rate is plotted as a function of stress in fig. 3. The creep strength for the alloy with 10 wt % Si, 1 wt % Ni is also very low.

Many of the conventional aluminium alloys with high strength at elevated temperature contain copper and nickel [18]). The corrosion resistance of Al/Cu/Ni alloys looks promising, but further investigation is needed.

Another way to increase the strength is to add magnesium. Magnesium additions to Al/Ni/Fe alloys will increase the susceptibility to accelerated attack; a maximum of 2 wt % can, however, be tolerated. Additions of Mg to Al/10 wt % Si/1 wt % Ni alloy seem to produce alloys with moderate strength at elevated temperature, but the technological processing of such alloys is difficult.

6. Conclusions

In the last few years various research institutes have studied the corrosion of aluminium in water at elevated temperatures. It has been shown that the grain boundary and the accelerated attack can be prevented by suitable alloying additions. The main difficulty encountered seems to be the high uniform corrosion rate.

Under boiling conditions and at high heat flux, a corrosion rate equal to 0.3 mm/year has been found. Even though this rate appears excessively high, it might, nevertheless, under certain circumstances not be prohibitively so, and it is concluded that the use of aluminium clad fuel elements is a definite possibility for water cooled reactors operating at up to 230° C.

The effect of alloying elements such as nickel and iron is probably due to their formation of cathodic sites. This will lead to an anodic polarization of the matrix, and this is found to prevent grain boundary attack. It is possible that accelerated attack is caused by hydrogen take-up in the cathodic phases. Alloying constituents which reduce the solubility of hydrogen in the second phase should therefore improve the resistance.

In a dynamic system, the corrosion rate of alloys resistant to grain boundary and accelerated attack seems to be determined by a film dissolution process.

With our present knowledge regarding corrosion mechanisms in pure water, it is difficult to propose alloying elements which could be added to obtain a better corrosion resistance. Additions of inhibitors such as H_3PO_4, which modify the corrosion film and decreases the film dissolution rate, appear promising. The effect of inhibitors under heat flux and boiling conditions has to be studied, and the behaviour of other reactor materials, notably steel, under such conditions needs investigation.

The lack of understanding of the corrosion mechanism does not permit us to predict anything regarding corrosion rate etc. under reactor conditions. So far, limited information is available pertaining to the behaviour of aluminium alloys in a reactor. Although the few experiments done indicate that the rate is not significantly affected in a radiation field, there is clearly a substantial amount of work to be done in this sector.

In order to improve our understanding of the basic processes during corrosion, more fundamental research is badly needed.

Acknowledgement

The author wishes to thank Dr. T. J. Barendregt and Mr. S. Aas for discussions and Mr. R. Hansen and H. O. Frosta for assistance with the experiments.

References

[1] J. E. Draley and W. E. Ruther, Argonne (USA) Report, ANL 5430 (1955)

[2] J. E. Draley and W. E. Ruther, International Conference on the Peaceful Uses of Atomic Energy, P/538 (1955)

[3] R. A. V. Huddle and N. J. M. Wilkins, Harwell (UK) Report, AERE 1669A (1956)

[4] N. J. M. Wilkins and C. F. Britton, Harwell (UK) Report, AERE 1669B (1958)

[5] H. Coriou, R. Fornier, L. Grall, J. Hérenguel, J. Hure and P. Lelong, Second International Conference on Peaceful Uses of Atomic Energy, P/1271 (1958)

[6] R. S. Ambartsumian, A. M. Glukhov, V. V. Concharov, A. I. Kovalev and S. A. Skovortzov, Second International Conference on Peaceful Uses of Atomic Energy, P/2196 (1958)

[7] R. L. Dillon, R. E. Wilson and V. H. Troutner, Hanford (USA) Report, HW 37636 (1956)

[8] J. E. Draley, C. R. Breden, W. E. Ruther and N. R. Grant, Second International Conference on the Peaceful Uses of Atomic Energy, P/741 (1958)

[9] J. E. Draley and W. E. Ruther, Argonne (USA) Report, ANL 5658 (1957)

[10] M. D. Ferrier, Chalk River (Canada) Report, CR Met 700 (1957)

[11] R. L. Dillon and V. H. Troutner, Hanford (USA) Report, HW 51849 (1957)

[12] V. H. Troutner, Hanford (USA) Report, HW 53389 (1957)

[13] F. H. Krenz, G. J. Biefer and N. A. Graham, Second International Conference on Peaceful Uses of Atomic Energy, P/194 (1958)

[14] K. Videm, Second International Conference on Peaceful Uses of Atomic Energy, P/767 (1958)

[15] M. S. Hunter and P. Fowle, J. Electrochemical Soc. 103 (1956) 482

[16] K. Videm, Teknisk Ukeblad 105 (1958) 409

[17] N. Christensen and V. Davies, Engineering Research Foundation at the Technical University of Norway, Report SINTEF 688 (1958) (under contract with JENER, unpublished)

[18] American Society for Metals, Metals Handbook (1948)

[19] F. H. Krenz and G. J. Biefer, private communication (1958)

[20] P. G. Anderson, G. J. Biefer, and F. H. Krenz, 6th UK/Canada Technical Conference, UK/C6/126 (1957)

[21] K. Videm, Unpublished data

JOURNAL OF NUCLEAR MATERIALS - 2 (1959) 154–173 - NORTH-HOLLAND PUBLISHING CO., AMSTERDAM

THE CORROSION OF AUSTENITIC STAINLESS STEELS UNDER HEAT TRANSFER IN HIGH TEMPERATURE WATER

J. N. WANKLYN and D. JONES

UKAEA, *Atomic Energy Research Establishment, Harwell, Didcot, Berks., UK*

Received 31 January 1959

The corrosion of two 18/8 austenitic stainless steels under stress and boiling heat transfer in oxygen-free water at *p*H 11 and 280° C has been studied. On plane surfaces, heat transfer does not significantly increase corrosion in times up to 1000 hours. In crevices where heat transfer causes superheating and concentration of solutes, stress-corrosion cracking occurs. This is due to the caustic alkali (60 ppm) required to raise the *p*H to 11: by comparison, a chloride concentration of 0.5 ppm in the bulk water has a negligible effect.

Unlike the previously reported stress-corrosion by caustic alkali, the cracking is wholly intercrystalline. The minimum superheat and caustic concentration required to produce it are about 25–35° C and 40–50 wt % KOH, respectively. The better-known transcrystalline cracking appears to require higher concentrations than this. In the appropriate solutions intercrystalline corrosion is possible in virtually unstressed metal, but mechanical failure is more rapid at stresses of the order of 20 000 psi (1400 kg/cm_2).

La corrosion de deux aciers austénitiques inoxydables 18/8 a été étudié sous tension et sous transfert de chaleur au contact de l'eau exempte d'oxygène, de *p*H 11 et à la température de 280° C. Sur les surfaces planes, le transfert de chaleur n'augmente pas sensiblement la corrosion pour des temps inférieurs à 1000 heures. Dans les crevasses où la transmission de la chaleur provoque une surchauffe et une concentration des solutés, la rupture par corrosion sous tension apparaît. Ceci est dû à la potasse caustique (60 ppm) nécessaire pour élever le *p*H à 11: en comparaison une concentration en chlorure de 0.5 ppm, dans la masse de l'eau est d'un effet négligeable.

A la différence de la corrosion sous tension par la potasse caustique signalée précédemment, la fissuration est complètement intercristalline. La surchauffe et la concentration caustique nécessaires pour produire ce phénomène sont de 25 à 35° C environ et de 40 à 50 % de potasse respectivement. La fissuration transcristalline mieux connue semble demander des concentrations plus élevées que celles-ci. Dans les solutions appropriées, la corrosion intercristalline peut se produire dans un métal à peu près sans tensions, mais pour des tensions de l'ordre de 1400 kg/cm^2 (20 000 psi), la rupture mécanique est plus rapide.

Die Spannungskorrosion von zwei austenitischen Stählen des 18/8-Typs in kochendem sauerstofffreien Wasser bei 280° C und *p*H 11, wurde bei gleichzeitiger Hitzeübertragung studiert. Bei ebenen Oberflächen wird der Korrosionsbetrag bis zu 1000 Stunden nicht merklich durch Hitzeübertragung beeinflusst. Korrosionsrisse bilden sich aber in Spalten wo Überhitzung und darausfolgende Verdichtung der Alkalilösung durch die Hitzeübertragung hervorgerufen werden. Alkali (6×10^{-3} %) wurde zugefügt um das *p*H auf 11 zu bringen; im Vergleich dazu hat eine Chloridkonzentration von 0.5×10^{-4} % einen vernachlässigbar kleinen Einfluss. Die schon bekannte Spannungskorrosion in Alkalilösung ist transkristallin, hier aber ist die Rissbildung interkristallin. Die minimal hierzu benötigte Überhitzung und Alkalikonzentration sind 25–35° C bzw. 40–50 Gew. % KOH. Die transkristalline Rissbildung benötigt scheinbar eine höhere Konzentration. In einer entsprechenden Lösung ist die interkristalline Korrosion des praktisch spannungsfreien Metalls möglich, aber der Bruch erfolgt schneller bei Spannungen in der Gegend von 1400 kg/cm^2 (20 000 psi).

1. Introduction

For some types of pressurised and boiling-water reactors it is possible to consider cladding the fuel with an austenitic stainless steel, an application requiring good corrosion resistance under very high rates of heat transfer. Although these materials have been shown to resist both static and flowing water (at up to 30 ft/sec) at

around 300° C very well, no results have been published for corrosion under heat transfer. Experience in normal steam boilers suggests that even at rates of the order of 50 watt/cm^2, heat transfer can enhance the corrosion of mild steels [2, 3]). The experiments described here and briefly reported elsewhere [1]) were designed to determine what, if any, harmful effects occurred with austenitic stainless steel under the considerably greater heat transfer rates typical of reactor conditions.

While nominal conditions are probably less aggressive in a pressurised-water reactor than in a boiler at similar heat flux, in that no boiling occurs on the steel surface, boiling conditions must nevertheless be considered, because their complete absence in all parts of a reactor core cannot be guaranteed. Furthermore, the boiling-water concept is gaining popularity as an alternative to the pressurised-water system.

Boiling might aggravate corrosion in two ways. First, since heat is removed less rapidly from a surface covered by steam than from one in contact with water, the alternate formation and removal of steam bubbles will cause rapid local fluctuations in the temperature of the oxide film on the metal. These might crack the oxide by thermal shock and reduce its protective properties, leading either to increased general corrosion or to pitting. Secondly, austenitic stainless steels can suffer transcrystalline stress-corrosion cracking when exposed, at around 300° C, to concentrated solutions of chlorides and caustic alkalies [4, 5]). Although the concentrations of these materials in the bulk of the water are low, much higher values could be reached in the "concentrating film" [3]) under each forming bubble, so that, over a long period, all parts of the surface might effectively be exposed to an aggressive solution for an appreciable time. The enhancement of general or pitting corrosion by such a concentrated solution is also a possibility. Further, a fuel element assembly might well contain crevices or other constricted spaces where, under heat transfer, concentrated solutions could accumulate even more readily. Stress corrosion by chloride in such situations has been extensively studied [4, 5, 6]), but less work has been done on the effects of caustic alkalies. Reactor systems whose primary water contained the latter to provide a high pH (e.g. to control the corrosion of mild steel parts) would be particularly vulnerable to such attack. Indeed, while it should be possible to keep the chloride content of primary water below 0.5 ppm, about 20 ppm of KOH are required to raise the pH to 10.5, and about 60 ppm to reach pH 11. In such water, alkali might well prove the greater hazard, especially since the water would be virtually free of oxygen, which is essential for chloride cracking but not for caustic cracking [4, 5]).

In the experiments described below, the corrosion of two stabilised austenitic stainless steels was studied in water at 280° C, pH 11, under heat fluxes up to 200 watt/cm^2, with and without the provision of simulated crevices.

2. Apparatus and Specimens

The experiments were conducted in a simple mild steel "loop" originally designed for heat-transfer studies. No continuous purification was provided, but arrangements for adding solutions intermittently, and for sampling the water, were available. The specimens were in the form of strips about 1 cm wide by 0.12 cm thick, heated by passing a 50 cycles/sec AC current of about 700A through them. They were supported within the test section by nickel bus-bars to which they were welded for good electrical contact (fig. 1). The lower bus-bar passed through an insulating P.T.F.E. O-ring seal in which it was free to move longitudinally, so that, the cross-sectional area of the bar being less than that of the specimen, there was a hydrostatic force tending to drive the bar out through the seal. This was used to apply stress to the specimen, values up to 30 000 psi being attainable by a suitable choice of dimensions. Initially strips of uniform width and simple cylindrical bus-bars were used, but these readily

burned out (i.e. failed in tension under great local overheating) at the joints, due to poor heat transfer in the "corner" between bar and specimen.

A more satisfactory design was eventually evolved, in which the ends of the bars were chamfered off to promote better water flow, and the specimens were given shoulders like normal tensile specimens, to reduce the stress and heat flux near the joint (fig. 2). Specimens *A4*–*A7* were as in fig. 2a, *A8*–*A16*, *A19*–*A20* as in fig. 2b, and fig. 2c gives the dimensions of two specimens (*A17*, *A18*), used to achieve several heat fluxes simultaneously. The earlier specimens were tested either in the cold-rolled condition or emery-polished to 00 paper; but the later ones were electro-polished to give a more reproducible surface and one on which it was easier to observe the effects of corrosion.

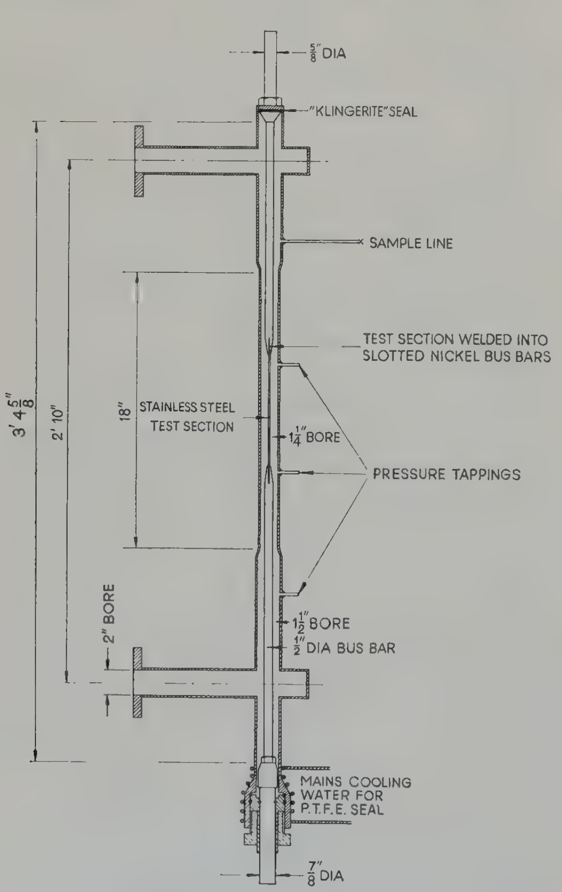

Fig. 1. Arrangement of test section of loop.

At first "plain" specimens, of the forms described and 0.12 cm thick, were tested, but in the later experiments more severe "concentrating conditions" were introduced by making "crevice" specimens. The first of these, *A4*, was a specimen of the usual type slit down the centre so that the two halves, lying edge to edge, formed a crevice 0.12 cm deep. This proved too shallow to produce noticeable results and it was, moreover, difficult to keep the faces in good contact when joining the specimen to its bars. The next specimens were therefore made by placing two strips of the usual dimensions, but half the usual thickness, face to face, so that the crevice depth was equal to the width of the strips. These specimens were easier to make and gave satisfactory results. Any slight difference between the lengths of the two strips after assembly caused the whole tensile load to fall on the shorter strip, which would be enough to make it yield till both strips were of equal length, forming a close-fitting crevice.

The heat-transfer rate was controlled by varying the heating current and using a value of the specimen resistance which was obtained by measuring the latter at room temperature and multiplying by a factor giving the increase up to 300° C. This factor was determined in separate experiments with specimens of steel in a heating bath. The temperature of the specimen in the loop was taken to be about 20° C above that of the water ($\approx$ 280° C). The uncertainty of temperature, and therefore of resistivity, implied an uncertainty of about 2 watt/cm^2 in heat rating. A comparable uncertainty in resistivity arose because the specimen was about 25° C hotter in the centre than at the surface.

Voltage and wattmeter readings were used to measure the heat input to the whole test section, but could not be used for the input to the specimen itself because the resistance of the bars and the various joints was not known.

Two austenitic stainless steels were studied, type FDP (titanium-stabilised) and type FCB (niobium stabilised), several batches of each being used. Details are given in table 1.

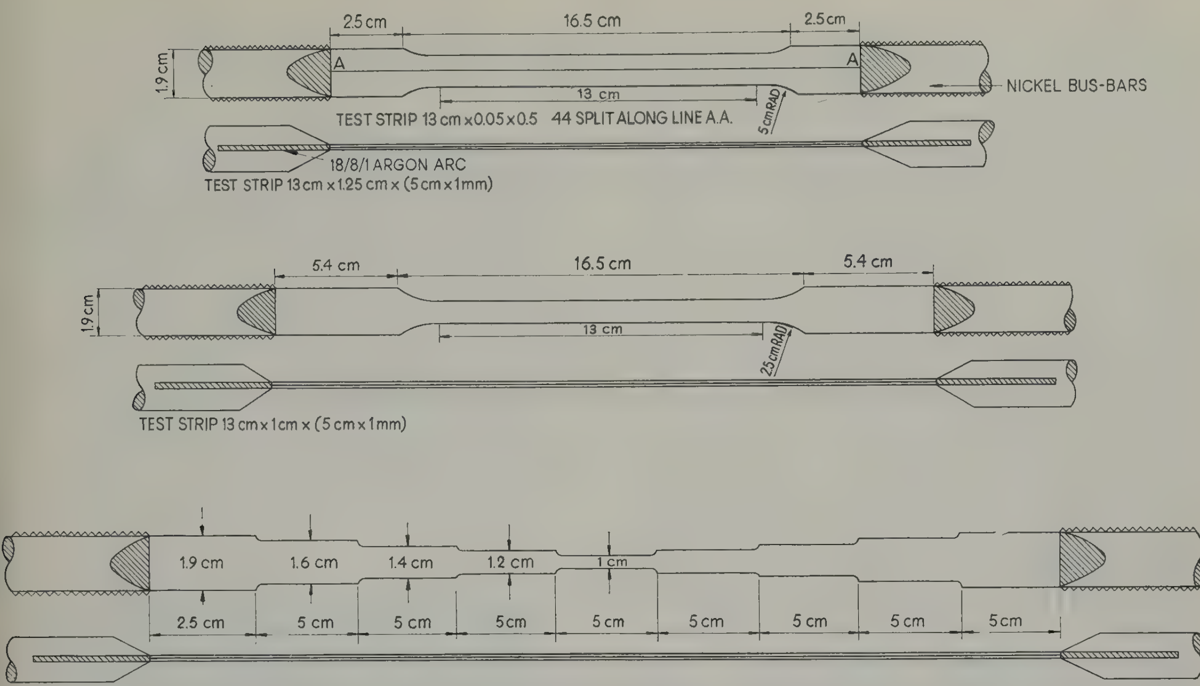

Figs. 2a, b and c. Specimen designs.

Table 1

Analysis of steels studied

Type	Batch	C (%)	Si (%)	Mn (%)	Ni (%)	Cr (%)	Nb (%)	Ti (%)	N (%)	Surface preparation	Specimen number	
											Series *A*	Series *B*
FCB	A	0.07	0.50	0.83	9.65	17.84	0.99			Polished with 00 Emery and degreased	*A1, A2, A3, A4* and *A5*	
FCB	B	0.06	0.50	0.82	9.47	17.83	0.89			As received. Degreased in acetone.	*A6*	
FCB	C	0.06	0.60	0.72	8.53	17.69	0.83		16 ppm	As received and degreased	*A8, A12*	
										Electro-polished and degreased.	*A9, A10, A11, A13*	
FCB	D	0.09	0.56	0.79	9.07	18.04	0.94			As received and degreased	*A7*	*B1, B3*
FDP	E	0.09	1.07	0.83	8.40	17.95		0.64		Electro-polished and degreased.	*A14, A15, A20*	
FCB	F	0.07	0.54	0.83	8.80	17.68	0.91		29 ppm	Electro-polished and degreased.	*A16, A17, A18, A19*	*B2, B4, B5, B6, B7, B8* and *B9*

Note: All steels behaved normally in the Huey (65 % HNO_3) and Strauss (Acid $CuSO_4$) tests and cracked in a transcrystalline manner in $2\frac{1}{2}$–8 hours with the 42 % $MgCl_2$ test.

3. Test Conditions

The experiments were conducted with a bulk water temperature of 280° C and a heat flux (calculated for outer faces only, i.e. assuming no heat removal from within the crevices, where present) of 200 watt/cm^2. Both values are typical of current designs for pressurised-water reactors. No over-pressure being provided in the loop, the water was at its saturation pressure, about 940 psi, so that boiling occurred on the greater part of the specimen. The water was adjusted with additions of KOH to pH 11, a value rather higher than that usually prescribed for a mild steel primary circuit (about 10.5), but chosen to emphasise the aggressive effect of alkali and to avoid an over-optimistic conclusion from the tests. For the same reason the chloride content was, in the earlier tests, kept at 0.5 ppm although in an actual system it should be possible to keep chloride below about 0.2 ppm When it appeared that the effects of chloride were insignificant compared with those of alkali, chloride additions were stopped and the level fell to about 0.1 – 0.2 ppm in most tests. The oxygen content of the water was kept below 0.01 cc/kg by filling under nitrogen with water de-aerated in a column of Potter resin. The nitrogen was blown off at about 100° C during starting up.

Stress corrosion cracking of austenitic stainless steels can occur at stresses as low as 5 000 psi[4, 6]) but to hasten results 20 000 psi or more was applied in these experiments. It was considered that, at such stresses, cracking should occur within a few hundred hours if the appropriate thermal and chemical conditions were present, and most tests were ended at about 500 hours if the specimen had not failed by then. One plain specimen (No. *A7*) was tested for 1 000 hours to see whether there was any significant corrosion of plane surfaces over rather longer times.

At the end of a test the specimen assembly was taken from the loop and the strips sawed from the bus-bars close to the joints. Since this prevented measurements of weight change, only visual examination and measurements of thickness changes were possible. The latter proved negligibly small and were soon abandoned. The assessment of the specimens therefore consisted of examination under low magnification for cracks, pits and other forms of corrosion, and the use of micro-sections to study cracking and changes in the surface condition of the metal. The most informative way of sectioning the specimen was by an oblique cut across the full width of the strip (fig. 3). To assist in revealing cracks some specimens, especially those in which little or no cracking was present, were bent or extended slightly in a tensile machine before examination.

4. Results

The results, set out in table 2, will be described in this section and discussed in more detail in

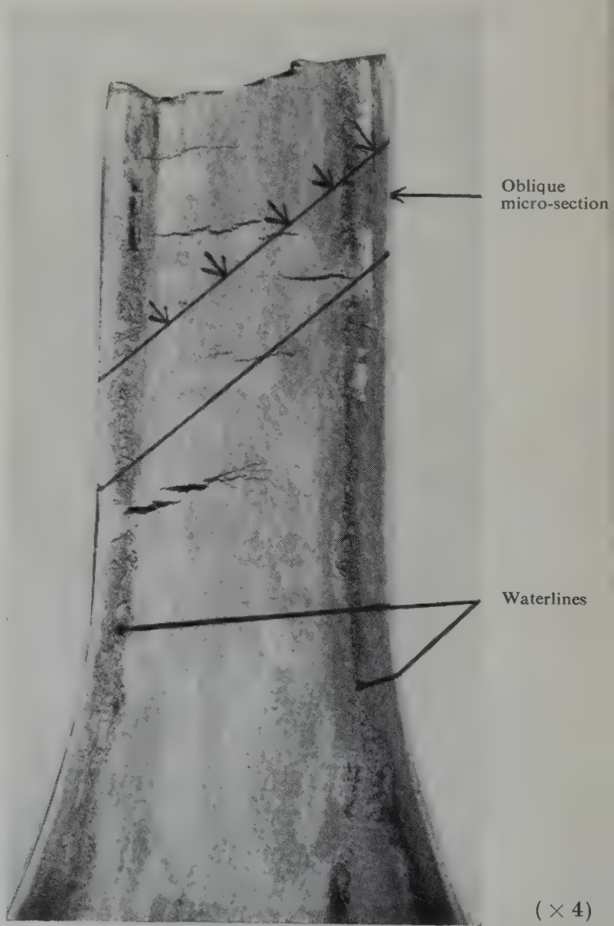

(× 4)

Fig. 3. Method of sectioning specimens (Specimen *A8*).

the next. In addition to those detailed in the table, a further five specimens failed after periods of a few hours due to burn out, faulty welds, or other spurious causes, and will not be further considered.

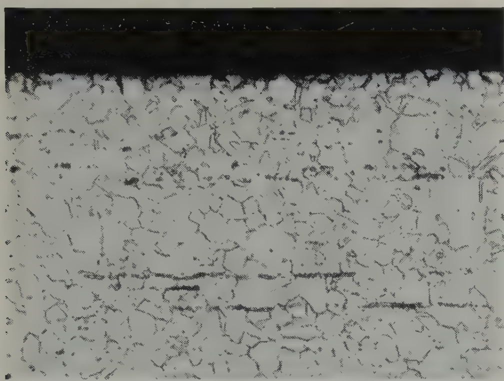

Fig. 4a. Specimen *A3*. As received.

Fig. 4b. Specimen *A3*. After 549 h exposure

Fig. 4c. Specimen *A9* (electropolished). After 196 h exposure.

Fig. 4. Effect of corrosion on surface finish of plain specimens. (All × 330, etched with modified aqua regia.)

Table 2 gives the number of hours for which the specimen was actually exposed to the desired conditions, neglecting time lost in inevitable interruptions. The stresses, heat fluxes and water conditions are those obtaining during the greater part of each test. The high phosphate concentration during the first test was accompanied by a rapidly falling pH. Both were presumably due to the loop having earlier been pickled with phosphoric acid, the iron phosphate coating reacting with alkali to release phosphate. Continued water changes and dosing with KOH solution reduced the phosphate concentration to an insignificant value from specimen *A2* onwards, and from then on a satisfactorily steady pH was maintained.

Specimens *A1*, *2*, *3*, *7* were plain specimens tested for times between about 150 and 1 000 hours. None of these failed by corrosion, but *A2* was accidentally burned out during re-starting after a shut-down. All the specimens had a straw to dark brown oxide film similar to a temper colour, covered by a loose layer of black material, apparently deposited from the water. This deposit was easily removed by rubbing with a damp rag. There were no signs of pitting or other localised attack, and micrometer measurements showed that the changes of thickness were too small to be measured accurately (less than about 0.1×10^{-3} inches). Microscopic examination revealed no signs of cracking in any plain specimen and showed that the surface condition was identical with that of unexposed material (fig. 4).

Specimen *A4*, with the edge type crevice, was similar to the plain specimens. Careful examination of the crevice faces showed no signs of cracking, pitting or other accelerated corrosion. This specimen finally broke within the test length, but the failure was diagnosed as burn-out by the conditions in the loop at the time, and by the melted and extended appearance of the fracture.

Specimens *A5*, *6*, *8–18* were all of the face crevice type, and most of them failed by

TABLE 2. Results

Spec. No.	Specimen type	Length of test (H)	Stress (psi)	Heat flux (watt/cm²)	Wat			
					Temp. (° C)	Pressure (psi)	*p*H	Cl^- (ppm
A1	Parallel strip welded to tapered bus-bar.	439	20 500	200	280	930	10.85–11.0	0.4–0.
A2	–do–	148	21 700	200	280	930	10.85–11.15	0.4–0.
A3	–do– but face welded	549	21 700	200	280	930	10.7–11.0	0.4–0.
A4	Shouldered specimen. Edge type crevice.	538	20 400	200	270	930	10.7–11.1	0.4–0.
A5	Shouldered. Face type crevice.	380	32 800	200	270	940	10.7–10.9	0.4–0.
A6	–do– but face welded	252	22 700	200	270	940	10.7–10.95	0.4–0.
A7	Plain shouldered specimen. No crevice.	1 002	21 600	200	270	940	10.7–11.2	0.4–0.
A8	Shouldered specimen face type crevice.	161	23 300	200	280	940	10.1–11.1	0.2–0.
A9	–do–	196	24 000	200	280	940	11.0	0.45
A10	–do–	373	24 000	50–200	280	940	11.1	0.5
A11	–do–	280	23 500	200	280	940	7.0	0.13
A12	–do–	156	21 600	200	280	940	10.0–11.3	0.6–0.
A13	–do–	88	24 000	200	280	940	10.6–11.0	0.1 ma
A14	–do–	62	24 600	200	280	940	10.4–11.0	0.1 ma
A15	–do–	123	24 400	200	280	940	10.6–11.2	0.1 ma
A16	–do–	493	27 300	200	280	940	6.1–7.5	0.1 ma
A17	Shouldered specimen face type crevice, stepped.	221	12 100–22 500	60–200	280	940	10.6–11.3	0.1–1.
A18	–do–	204	11 800–22 000	60–204	280	940	10.5–11.4	0.1–0.
A19	Shouldered specimen face type crevice.	150	33 900	50	269	860	10.3	0.13
A20	–do–	230	22 200	50	272	900	10.5	0.2

op experiments, series A

Conditions				Result of test
PO_4^{---} (ppm)	SiO_2 (ppm)	O_2 (cc/kg)	Conductivity (μ mho)	
).44–22.0	19.0	< 0.01	131–302	No failure. Light surface oxidation. Black film. No pitting or cracking.
0–1.4	0.8–5.2	< 0.01	165–175	Burn out on restarting loop. Brown-black film. No cracking or pitting.
0–2.6	0.8–7.5	< 0.01	115–262	No failure. Light crud deposit. Brown to black film. No pitting or cracking.
0–2.6	4.3–16.5	< 0.01	102–195	Burn out. Brown-black film. No pitting or cracking.
0.15	1.1	< 0.01	79–144	Failure by intercrystalline cracking in upper joint.
0.17	2.85	< 0.01	82–172	Failure due to "hot shortness" in weld. Pitting and inter-crystalline attack in crevice at "water line" deposits.
).78–1.04	1.85–4.7	< 0.01	136–246	No failure. Dark brown crud deposit. No pitting or cracking.
—	—	< 0.01	71–233	Failure by intercrystalline cracking starting at the crevice face.
0.57	8.0	< 0.01	160	Failure by intercrystalline cracking.
—	3.8	< 0.01	164	Failure by intercrystalline cracking (specimen examined after 230 h at 50 watt/cm², no visible cracking).
—	—	< 0.01	1.5	No failure. No cracking, pitting or even surface roughening.
1.24	2.0	< 0.01	75–247	Failure by intercrystalline cracking.
< 1.0	1.0	< 0.01	80	Failure by intercrystalline cracking.
< 1.0	1.0	< 0.01	85	Failure by intercrystalline cracking.
1.4	0.22	< 0.01	102	Failure by intercrystalline cracking.
0.07	0.35	< 0.01	1.2–7.4	No failure. No cracking, pitting or even surface roughening.
—	—	< 0.01–0.4	69–246	Failure in central length by intercrystalline cracking gradually diminishing as the section width increases.
—	—	< 0.01	64–225	Similar to *A17*.
—	—	< 0.01	62	No failure, pitting or cracking.
—	—	< 0.01	49	No failure, identical to A19.

cracking. Their outer faces, after exposure, were similar in all respects to those of the plain specimens, and gave additional evidence of the very slight attack on plane surfaces, even under boiling conditions. The outer faces of the specimens will not be further described.

The inner, or crevice faces of the specimens were altogether different in appearance. As fig. 5 shows, the outermost $1-3$ mm had only the yellow-brown temper colour typical of outer surfaces, but within these regions lay two lines of dark brown to black deposit presumably thrown down by water entering the crevice. Between these two "water lines" the metal had a thick black oxide film and, generally, pitting or cracking. Micro-sections of this region of *A5* and *A6* showed considerable pitting together with intergranular penetration about one grain deep. This attack was most marked at or just within the water lines and was absent outside the latter. Neither of these specimens failed within the test length. *A5* broke within the double crevice where the specimen entered the slot in its bus-bar, and micro-examination revealed extensive intercrystalline cracking here. The intercrystalline nature of the cracking was difficult to understand at the time, because all previous work indicated that stress corrosion due to chloride or caustic should be transcrystalline. There is, however, little doubt that this cracking was of the same origin as that produced with many later specimens and discussed below. Specimen *A6* also broke at the upper joint, but this was shown to be due to a faulty weld. An attempt had been made with this specimen to seal the crevice within the bus-bar by welding across the face of the specimen as well as along the sides. This weld suffered from micro-fissuring and hot-shortness aggravated by dilution of the austenitic filler rod by the pure nickel bus-bars. Cracking was present in the weld deposit even before testing. No further specimens were therefore welded in this way and the risk of failure at the joints was diminished by reducing the stress and heat flux there by further widening of the end portions of the specimen (fig. 2b). The first specimen of this type was *A8*, which failed by extensive cracking within the crevice after 161 hours. Micro-examination showed that contrary to expectation, the cracking was entirely intercrystalline (fig. 6). This surprising result was repeated with specimens *A9* and *A10*. The latter was tested for the first 230 hours at 50 watt/cm^2, after which no cracking was visible to the naked eye. It was then replaced in the loop and tested at 200 watt/cm^2, whereupon it broke after a further 153 hours.

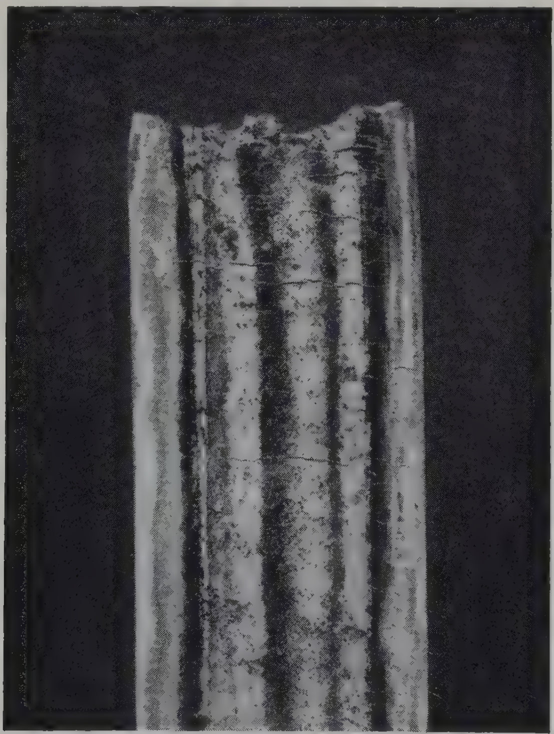

Fig. 5. Crevice face of specimen, showing cracking and water-line deposits ($\times$ 4).

The steel used for the above specimens was examined to see whether it was abnormal in any way which might account for the cracking taking an intercrystalline rather than a transcrystalline form. Its analysis and micro-structure were however quite typical, and it behaved normally in the 65 % nitric acid test (weight loss 0.001 $g \cdot cm^{-2} \cdot d^{-1}$) and in the Strauss copper sulphate test (no intercrystalline attack in 72 hours). U-bend specimens exposed to 42 % $MgCl_2$ solution cracked in a few hours in the usual transcrystalline manner.

crevice face →

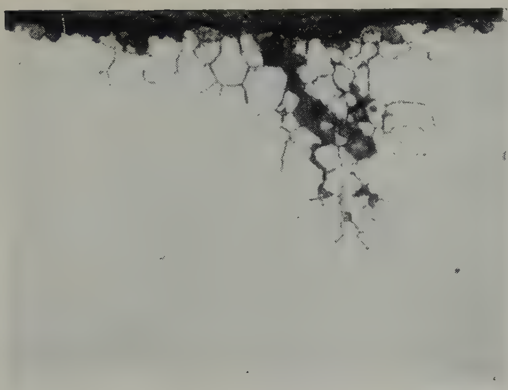

Fig. 6a. (× 330)

crevice →

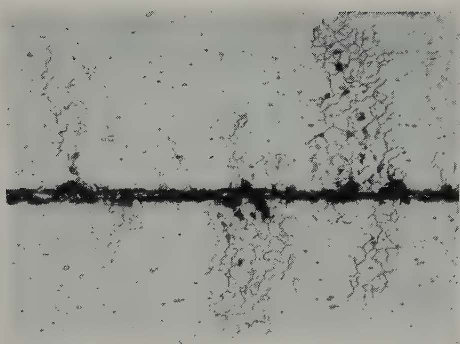

Fig. 6b. (× 100)

Fig. 6. Inter-crystalline cracking in crevice face of specimen A8.

To verify that electropolishing, which leaves the metal with a particularly protective oxide film, was having no effect on the results, specimen *A12* was exposed, as received, in the cold-rolled condition in alkaline water. It failed, after 156 hours, in an identical manner to *A8*, *9* and *10*.

It was by now suspected that the small amount of chloride present in the water had no influence on the corrosion, and to check this the next three specimens, *A13*, *14* and *15* were exposed in alkaline water containing not more than 0.1 ppm chloride. With specimens *A14* and *A15* a change of steel was also made, from type FCB to type FDP. Cracking wholly similar to that already described was found in all three specimens. In all specimens which failed by cracking the latter was fairly uniformly distributed along the test length. Specimens *A11* and *A16*, exposed in neutral water without failure or any sign of cracking after 280 and 500 hours, respectively, confirmed that caustic alkali was essential for intercrystalline corrosion.

At this stage the method of estimating the concentration of alkali reached in the crevice, discussed in the next section, had been developed and it was desired to carry out experiments at a variety of heat fluxes, to estimate the minimum heat flux and alkali concentration required to produce cracking. For this purpose specimens *A17* and *A18* were prepared to the design shown in fig. 2c.

The individual sections of these stepped specimens were arranged to be about five times as long as they were wide, so that conditions within them should be reasonably free from end effects. The resistance of the central section was calculated in the usual way and the dimensions of the other sections were used to calculate their resistances from that of the central one.

The results for the two specimens were very similar: those for *A18* are given in table 3. Owing to the introduction of contamination during repairs, the chloride values in these and subsequent experiments occasionally rose to 0.5 or 1 ppm In view of earlier findings it is unlikely that these changes of chloride content had any significant influence. The *p*H was also rather lower than in earlier tests, but since, as discussed later, concentration by a factor of about 10^4 must occur in the crevice, the change of KOH concentration there, as between *p*H 11 and *p*H 10.5, was probably insignificant.

Both stepped specimens failed after about 200 hours in the central section, and oblique microsections were taken from the central 1 cm of this and the other sections. As table 3 and fig. 7 show, sections with progressively smaller heat flux showed progressively less extensive cracking, until this was reduced to intercrystalline attack about one half to one grain deep, generally at the base of pits. At lower heat fluxes still, only the pitting remained, and this finally became imperceptible at a heat flux of about 60 watt/cm^2.

These tests indicated that there should be

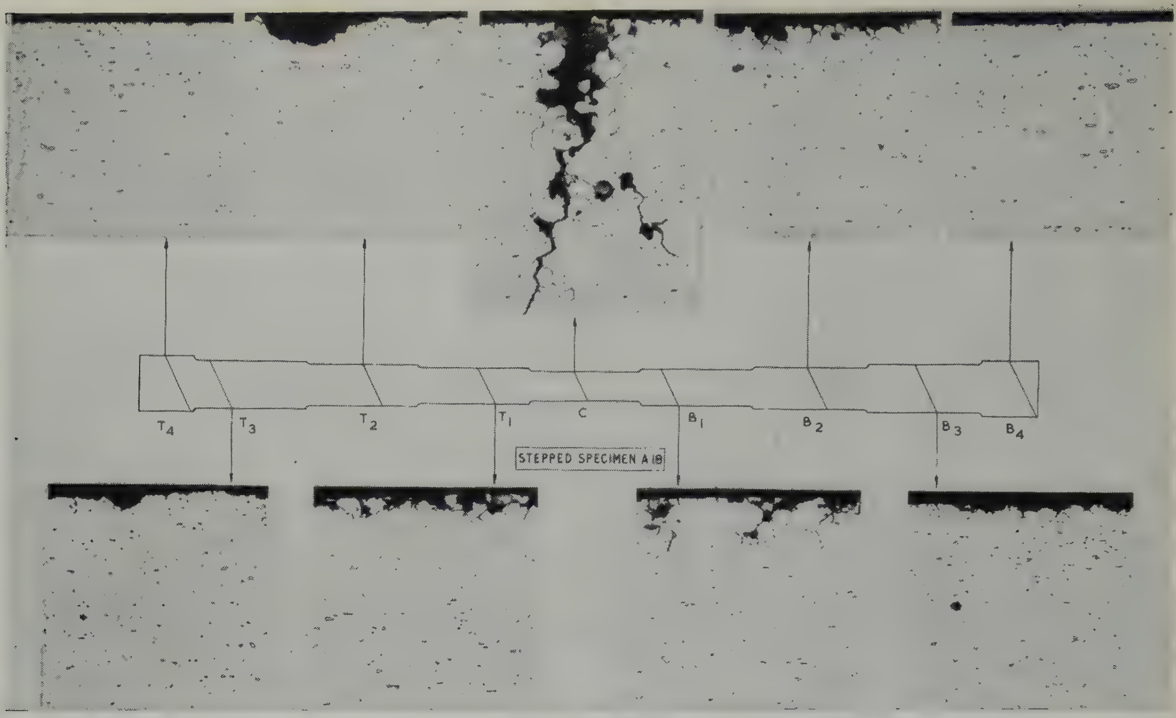

Fig. 7. Stepped specimen *A18* (crevice face). Magnification × 220, etch. NaCN electrolytic.

negligible attack at 50 watt/cm², a conclusion which was confirmed by specimens *A19* and *A20* (table 2) which after 150 and 230 hours respectively were uncracked and showed neither pitting nor even surface roughening.

It is convenient to anticipate the interpretation given in the next section and to record here some supplementary experiments which arose from consideration of the results. The latter posed two main problems:

1. To decide whether the intercrystalline form of the attack was due to some particular property of the apparatus and materials used.
2. To estimate the degree of super-heating and crevice-concentration required to produce the attack.

To answer the first point, specimens of stainless steel were exposed to concentrated KOH solutions in entirely different apparatus in which, in particular, large electrical heating currents were absent. This was done by weighing the quantities of solid KOH to make solutions of 10–50 wt % into short lengths of type FDP tube, adding water and sealing by welding. These tubes were then placed in a furnace at 325° C for various times. Two types of "capsule" were used, one of 1.3 cm o.d., and 0.060 cm wall thickness in which the steam pressure itself produced a stress of 10 000 to 20 000 psi, the other 1.3 cm o.d. and 0.32 cm wall thickness in which small U-bend specimens of stainless steel sheet were placed. Both sets of capsules were water quenched from ~1050° C and descaled with nitric/hydrofluoric acid before use. The thin ones were closed by squeezing their ends flat and welding the edges together; cylindrical plugs were welded into the ends of the thick ones. Fig. 8 shows the design of closure eventually developed to minimise welding stresses. However, many of the tests were partly vitiated by premature leaking of the capsules, generally due to cracking. The resulting loss of steam caused stresses and KOH concentrations to vary in an unknown way. Nevertheless, both inter- and trans-crystalline cracking, in varying amounts, (fig. 9) were found in both capsules and U-bends, confirming that the intercrystalline

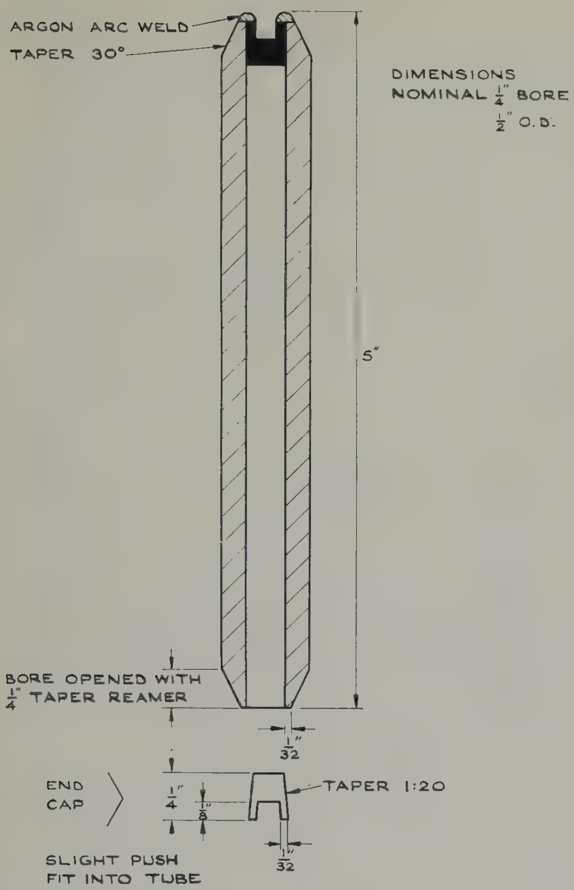

Fig. 8. Cross-section of thick-walled capsule, showing method of closure.

form could be produced otherwise than in the loop. Results for the capsules which did not leak led to the tentative conclusion that intercrystalline corrosion begins at concentrations between about 25 wt % and 60 wt % KOH. On the other hand significant amounts of transcrystalline cracking were only seen in capsules containing more concentrated solutions or those in which leaking allowed higher concentrations to be reached.

Significant amounts of intercrystalline attack were seen in relatively unstressed metal e.g. in the sides, and even the inner faces of U-bends, and in the walls of the thick capsules. In contrast, where transcrystalline cracking was found, it was generally in regions were high stresses could be assumed, e.g. the main failure at the apex of a U-bend, or near welds in the capsules.

Experiments with capsules containing NaOH suggested that this produced less severe cracking than KOH at the same concentrations, although this was not firmly established.

As explained in the discussion, an estimate could be made from heat-transfer data of the minimum degree of superheating and, thus of KOH concentration, necessary to produce intercrystalline attack, and the latter value was roughly confirmed by the capsule experiments. However, as discussed below, there was some

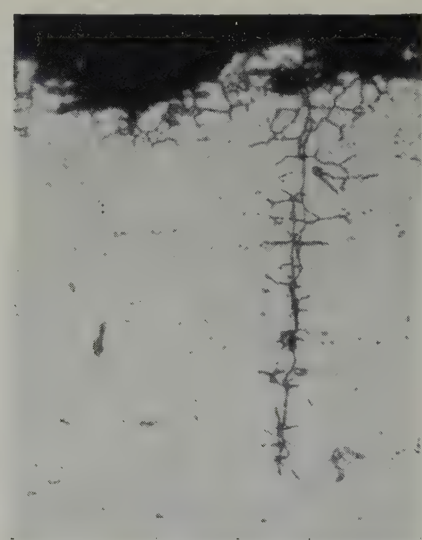

Fig. 9a.

Fig. 9b.

Fig. 9. Cracking in U-bend specimens exposed in capsules. 50 % KOH-etch NaCN Electrolytic. ($\times$ 350)

TABLE 3. Results for stepped specimen. *A18*

Average current — 759 A
Average water temp. — ≈ 280° C

Average pressure — 932 psi
Average spec. thickness — 0.057 cm

pH 10.5 — 11.4

Section No.	Width (cm)	Resistance † (ohm/cm × 10^{-3})	Watt/cm²	ΔT_m †† (° C)	ΔT_s †† (° C)	Total ΔT †† (°C)	Observations	Stress (p.s.i.)	Estimated wt.% KOH
T_4	1.89	0.42	60	10	8	18	Very slight roughening.	11 800	33
T_3	1.59	0.50	84	14	8	22	Slight pitting.	14 000	39
T_2	1.39	0.58	111	18	9	27	Pitting and slight local attack.	16 000	43
T_1	1.20	0.67	147	25	10	35	Some intercrystalline cracking.	18 500	51
C	1.01	0.79	204	34	11	45	Much intercrystalline cracking, failure	22 000	60
B_1	1.20	0.67	147	25	10	35	Some intercrystalline cracking.	18 500	51
B_2	1.40	0.57	109	18	9	27	Pitting and slight local attack.	15 900	43
B_3	1.60	0.50	84	14	8	22	Slight pitting.	13 900	39
B_4	1.87	0.43	62	10	8	18	Very slight pitting.	11 900	33

† Calculated from measured value for section C.
†† ΔT_m = temperature drop within strip; ΔT_s = temperature drop between outer surface of specimen and bulk water; $\Delta T = \Delta T_m + \Delta T$.

TABLE 4. Results for loop experiments. Series *B*

Spec. No.	Specimen type	Length of test (H)	Stress (psi)	Heat flux (watt/cm²)	Water conditions: Temp. (° C)	Press (psi)	pH	Cl^- (ppm)	PO_4^{---} (ppm)	SiO_2 (ppm)	O_2 (cc/kg)	Cond. μ mho	Result of test
B1	Plain shouldered spec. No crevice.	250	17 500	200	280	1 500	10.7	< 0.1	< 0.01	≈ 1	< 0.01	60	No failure. Light deposit of crud. Brown to black film. No cracking, pitting or surface roughening.
B2	Shouldered face type crevice.	44	17 500	200	280	1 500	10.9	< 0.1	< 0.01	≈ 1	< 0.01	93	Failure by intercryst. cracking.
B3	Plain shouldered spec. No crevice.	1 087	17 500	200	280	1 500	10.7	< 0.1	< 0.01	≈ 1	< 0.01	70	No failure. Light deposit of crud. Brown to black film. No cracking, pitting or surface roughening.
B4	Shouldered face type crevice.	58	17 500	200	280	1 500	10.6	< 0.1	< 0.01	≈ 1	< 0.01	50	Failure by intercryst. cracking.
B5	–do–	125	17 500	200	265	1 500	10.3	< 0.1	< 0.01	≈ 1	< 0.01	65	Localized intercrystalline cracking at failure. Rest of specimen pitted with traces of intercrystalline attack ½ to one grain deep.
B6	–do–	25	17 500	200	265	1 500	—	< 0.1	< 0.2	≈ 0.5	< 0.01	—	Failure by intercryst. cracking.
B7	–do–	41	17 500	200	265	1 500	10.5	< 0.1	< 0.2	≈ 0.5	< 0.01	75	Failure by intercryst. cracking.
B8	–do–	20	17 500	200	270	1 500	—	< 0.1	< 0.2	≈ 0.5	< 0.01	—	Failure by intercryst. cracking.

doubt about the calculation of superheating in the loop experiments, and to check these, further experiments were carried out in another loop. The latter was a more elaborate stainless-steel loop in which an ion-exchange by-pass provided better control of water purity. The loop also had a separate pressuriser enabling the water temperature and pressure to be varied independently. Thus, while the earlier experiments had been conducted at constant pressure and temperature but varying heat flux, it was possible in the second loop to keep pressure and heat flux constant and vary the water temperature. The implications of this difference, illustrated in fig. 10, are discussed in the next section.

The arrangement of the test section was very similar to that of the mild steel loop except for the provision of a baffle to reduce the area of water flow around the specimen. The resulting high velocity of flow prevented boiling on the specimen surface. Crevice specimens of the usual type, with slightly modified dimensions, were tested in this loop. Results are given in table 4. Several specimens failed prematurely at the joints while a suitable design was being evolved, and are not included in the table.

Specimens *B1 – B4* served to confirm the earlier findings, i.e. a negligible attack on plain specimens and outer faces and, at an appropriate degree of superheating, intercrystalline cracking within crevices. Fig. 11 shows a section from the crevice face of specimens *B2* and *B4*, very similar in appearance to those of the *A* series of specimens.

Specimens *B5 – B8* were exposed at the same heat flux, 200 watt/cm², as their predecessors,

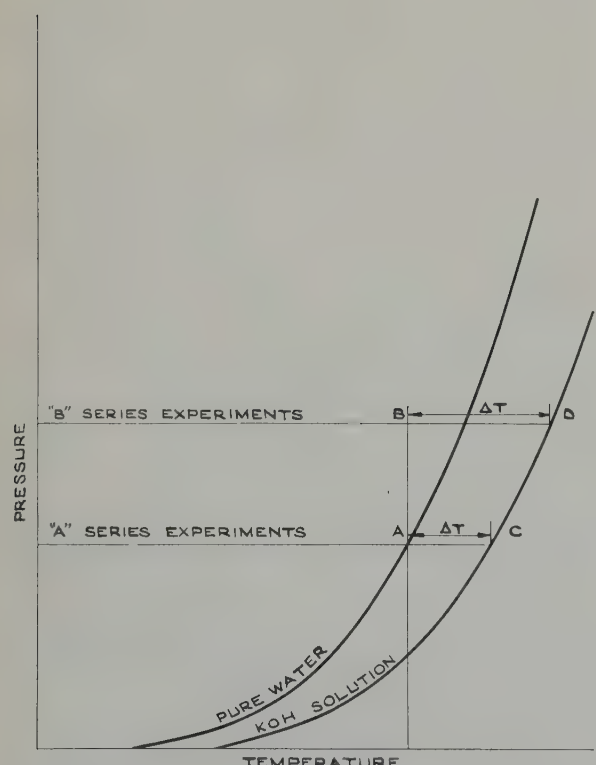

Fig. 10. Vapour pressure/temperature curves for pure water and a concentrated KOH solution, showing the relation between degree of superheat and concentration of caustic.

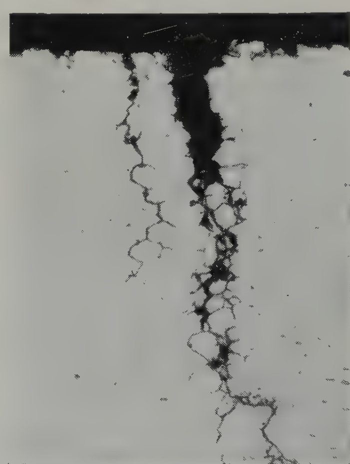

Fig. 11a. Specimen B 2.

Fig. 11b. Specimen B 4.

Fig. 11. Typical intercrystalline attack in crevices, series B. Etch NaCN electrolytic. (× 125).

but the bulk water temperature was varied from 265° C to 270° C. Specimens *B5*, *B6* and *B7* tested at the lower temperature, failed by intercrystalline cracking, but the latter was confined to the immediate vicinity of the break, suggesting that for some reason, conditions were locally more severe at this point. The remainder of the crevice faces showed only pitting, with slight signs of intercrystalline penetration about one grain deep.

Specimen *B8*, tested at 270° C, showed considerable intercrystalline attack near the fracture, and the beginnings of similar attack elsewhere in the crevice region.

5. Discussion

The observations of the plain specimens and of the outer surfaces of the crevice ones show that, at least up to 1000 hours, boiling heat transfer caused no great increase in the general corrosion of the two austenitic steels examined. There was, moreover, no sign of pitting or cracking in spite of the effective concentration of solutes on the surface by the Hall [3]) "concentrating film" mechanism †. Use for fuel cladding would require a much longer life, of the order of 10 000 or 20 000 hours, and while one cannot certainly predict such a life from shorter tests, it seems unlikely that, after satisfactory resistance for 1000 hours, any greatly accelerated form of corrosion would begin after longer times. Moreover the occurrence of boiling almost certainly made the test more stringent than the conditions to which most of the cladding would be exposed.

In the crevice specimens, on the other hand, a much higher concentration of solutes must have been reached. As shown by the experiments at low chloride concentration, and by those in neutral water, the cracking and other forms of attack were due to potassium hydroxide.

However, since all reported stress corrosion by chloride and caustic alkali has been transcrystalline in form, it was first thought that the intercrystalline cracking found in the loop experiments might result from some feature of the apparatus, in particular the use of electrical heating. Edeleanu and Snowden [4]) have shown that chloride contamination can decrease the creep-rupture life of austenitic stainless steel at 600° C, the failure being by intercrystalline cracking. It seemed likely that caustic alkali might behave similarly, provided the metal temperature were at least 600° C. A possible means of reaching such temperatures locally might be the "bunching" of the lines of current flow at the base of small pits and incipient cracks, with consequent increase in heat production there. Drs. J. Greenwood and B. Williamson [7]) kindly examined this question and concluded that, even starting with a number of cracks 0.01 cm deep and 0.02 cm apart the temperature rise would only be of the order of 10° C, i.e. far too small to initiate creep failure.

It also seemed possible that, since the voltages present were high by electrochemical standards ($\approx 10-20$ volts r.m.s.), polarisation effects might, in spite of the use of alternating current, occur within the crevice in such a way as to cause preferential attack at grain boundaries. To check such effects the capsule experiments were performed. The concentrations of potassium hydroxide used in these were decided by estimating the concentration reached in the centre of the crevice in the loop specimens. Two assumptions were made in this calculation.

1. That there was no significant removal of heat from the centre of the crevice.
2. That the pressure in the centre of the crevice was virtually the same as in the bulk of the water.

By the first assumption the temperature in the crevice was the same as that in a solid specimen, twice as thick as the individual strips and transferring heat at the same rate from its outer faces. At 200 watt/cm^2 and with a thermal conductivity of 0.041 cgs units the temperature drop from centre to surface in a strip 0.12 cm thick is about 30° C. To this must be added the drop between the metal surface and the bulk

† This is consistent with the fact that the metal surface was only about 10° C hotter than the bulk water (pp 168–169) and that this amount of superheating is insufficient to produce cracking (pp 169–170).

water. At 200 watt/cm^2 and 940 psi, Jens and Lottes † relation for boiling heat transfer gives about 10° C. Thus the crevice centre was about 40° C hotter than the bulk water and, by assumption (2), at the same pressure. These conditions are reprsented by point C in fig. 10, in which the vapour pressure of pure water and of a concentrated potassium hydroxide solution are plotted against temperature. Point A represents the bulk water conditions. The curve through C represents a concentrated potassium hydroxide solution in which the dissolved alkali depresses the vapour pressure below that of water at the same temperature. Water in a crevice, superheated by say ΔT°C, will initially exert a higher pressure than the bulk of the water and will therefore evaporate and concentrate till it reaches equilibrium at point C on the "KOH curve". By plotting vapour pressure/temperature curves for various potassium hydroxide solutions and drawing a horizontal line corresponding to the system pressure through them, the concentration corresponding to any given degree of superheat, ΔT, may be determined. Unfortunately, data for potassium hydroxide in the required range of temperature were not available and an approximation was based on values for sodium hydroxide, which do cover the required temperatures [8]). These figures, together with those for potassium hydroxide, show that, at the highest temperature available for the latter (100° C), the vapour pressure depression by potassium hydroxide is about 10 % greater than for an equimolar sodium hydroxide solution. Assuming that this is true at higher temperatures and that vapour pressure depression is proportional to concentration, the concentration of potassium hydroxide equivalent to x wt % sodium hydroxide is approximately $0.9 \times 56/40\ x = 1.3\ x$ wt %. The form of the curves for sodium hydroxide is such that, within the accuracy of the experiments, the concentration/superheat relation is independent of the exact pressure, at the pressures involved, and the curve given by Hecht *et al.*[9]) was used in the calculations. These showed 40° C superheat to correspond to about 55 wt % potassium hydroxide.

The capsule experiments nominally ranged from 10 wt % to 100 wt % potassium hydroxide. Although premature leaking largely prevented quantitative conclusions, these experiments did definitely confirm that intercrystalline attack can, in the absence of complicating factors, take place when altogether normal stabilised, austenitic steels are exposed to concentrated caustic solutions. It is somewhat surprising, in view of the ease with which such attack may be produced, that there is so little systematic reference to it in the literature, although it has been very briefly mentioned by several workers [10, 11, 12]). Those capsules which did not leak showed cracking at 60 wt % potassium hydroxide, but only pitting and slight intercrystalline attack at 25 %, suggesting that the minimum concentration for intercrystalline cracking was probably about 50–60 %. The concentration required for transcrystalline cracking was apparently higher than this.

The possible difference between sodium and potassium hydroxide at similar concentrations is interesting, but awaits further confirmation. No reason for such a difference is at present apparent. However, if real, it might in part explain the lack of reference to intercrystalline cracking, for most workers have used sodium rather than potassium hydroxide, and it is possible that, at concentrations below that required for the better known transcrystalline cracking, their solutions were less prone to produce the intercrystalline form than the potassium solutions studied here.

The experiments with the stepped specimens (table 2, *A17* and *A18*; table 3) represent an attempt to estimate more accurately the superheat and concentration required for intercrystalline cracking. The results show that about 35° C superheat, corresponding to about 50 wt %

† $\Delta T_S = \dfrac{33\,(Q/10^6)^{\frac{1}{4}}}{\exp\,(P/900)}$ where ΔT_S = Temperature drop in ° C; Q = Heat flux in B.t.u./ft$^2\cdot$h; P = Pressure in psi. From W. H. Jens and P. A. Lottes, Argonne National Laboratory Report ANL.4627, (1951).

potassium hydroxide is required for definite cracking, and that no perceptible attack occurs below about 18° C superheat, or about 30 wt % potassium hydroxide. The former figures agree reasonably with the estimate given by the capsule experiments, while the lower limits are rather higher than those suggested by these experiments. The range of superheat between significant pitting and definite cracking was from 25° C to 35° C, i.e. about 10°.

In the stepped specimens the stress varied from one section to the next, but this is unlikely to have had a large influence compared with the variations of heat flux. As figs. 6, 9 and 11 show, the cracks typically form a broad network of intercrystalline attack in which a significant amount of cracking takes place in a direction parallel to the stress and can thus be little influenced by the latter. The capsule experiments, moreover, showed much cracking in virtually unstressed metal. It seems likely therefore that the extent of intercrystalline attack is much more dependent on the concentration of caustic than on the stress level, and that the latter, if high enough, merely serves to open up the cracks and hasten mechanical failure.

The complete absence of transcrystalline cracking in all the loop specimens, in spite of stresses sufficient for this form of attack [4, 6]), suggests that the latter requires a caustic concentration in excess of 60 wt % potassium hydroxide. This agrees approximately with observations of two of the capsules which did not leak: at 60 % some transcrystalline attack was found in the U-bend specimen and at 80 % there was as much trans- as intercrystalline cracking.

The estimates of caustic concentration reached in the loop depend on the assumptions used in calculating the temperature within the crevice, and these should be examined more closely. As regards the pressure, it is difficult to imagine any great difference existing between the centre of the crevice and the exterior. Such a pressure drop could be caused only by surface tension effects, or by the net outward flow of steam and water as the latter evaporates. Even if the crevice were as narrow as 2.5 μ (10^{-4} in), the surface tension effect would only be of the order of 10 psi; and, in view of the small amount of steam and water flowing outwards, the frictional pressure drop seems unlikely to be any greater. Such a pressure difference would (see fig. 10) reduce the effective superheat by only about 1° C, implying an error in concentration of less than 1 wt % potassium hydroxide.

With regard to the assumption that no heat is removed from the centre of the crevice, the appearance of the inner faces of the strips, with their well formed "water lines" of deposit (fig. 5) indicates that little water passes these lines into the central region. However, since alkali accumulates there, some liquid must penetrate. Presumably from time to time small amounts of liquid, already partly concentrated in the outer parts of the crevice, seep into the central region and are further evaporated to the concentration calculated above. There is thus no question of heat removal by a continuous flow of liquid through the crevice, but some might be removed as latent heat in the steam. It is impossible to assess this accurately but an approximate calculation shows the magnitudes involved. For example, if 10 % of the 200 watt/cm^2 supplied by the strips were removed inside the crevice, the evaporation there would have to be about 2 cc of water per minute for each centimetre length of specimen (assuming a latent heat of 400 cal/g and a density of 0.7 g/cc, which neglects solutes). Under these conditions the temperature drop through the strips and the caustic concentration would be lower, by about 7° C and 5 wt % KOH, than those calculated above.

The evaporation ($\approx$ 2 cm^3/min·cm length) required to cause these errors seems rather large, particularly when it is realised that it would occur after considerable concentration in the outer parts of the crevice at the water lines, and therefore implies a much larger volume of water entering the mouth of the crevice. It therefore seems reasonable to consider that the errors are no worse than these figures suggest,

and to assume that at 200 watt/cm² the calculated superheats are possibly 5° C and certainly not more than 10° C too high.

The temperatures discussed here are those at the surface of the metal within the crevice. In view of the fall of temperature through the strips, it is desirable to see that, once cracks have advanced appreciably into the metal, conditions are still suitable for cracking. In a strip heated by an electric current and cooled at the outer faces, the temperature variation from centre to outside is not linear, but parabolic. In the present case, the temperatures one third and one half of the way through individual strips of the specimen would be only 3° C and 8° C, respectively, below the temperature in the crevice itself. The calculations referred to above (page 170) suggest that electric current "bunching" at the base of such cracks should give a temperature rise sufficient to offset these reductions.

The *B* series of loop experiments, besides confirming the earlier qualitative findings in alternative apparatus and in rather purer water, give some reinforcement to the quantitative assessments. This arises from the following consideration. Due to this loop being pressurised, bulk-water conditions were as at point B (fig. 10) and there was no boiling on the specimen surface. The temperature drop from surface to bulk water (from the Colburn equation †) was about 33° C, higher than in the *A* series so that, although point B lies to the left of the vapour pressure curve for water, point D, representing conditions in the crevice, lay on about the same "%-KOH" curve as the earlier experiments. By keeping the heat flux constant (200 watt/cm²) so that the temperature drop between crevice and bulk water (ΔT) was unchanged, but lowering the bulk water temperature, it was possible to move points B and D simultaneously

† $\Delta T_S = Q/h$ where ΔT_S = temperature drop; Q = Heat flux; h = Heat transfer coefficient and h is given by $hD/K = 0.023\ \mathrm{Re}^{0.8}\ \mathrm{Pr}^{\frac{1}{3}}$, where D = Hydraulic mean diameter of section; K = Thermal conductivity of water; Re = Reynolds No.; Pr = Prandtl No.

to the left. This provided an estimate of the difference in superheat values corresponding to the first onset of pitting and the start of definite cracking, independent of the actual value of ΔT. Table 4 shows that this difference was about 15° C, which is of the same order as that derived from the A series experiments. Now, if the ΔT values in the latter were too large, by some factor, the difference in values as between the start of pitting and the appearance of definite cracking would also be too large. Putting the argument another way, if the ΔT values of table 3 were too high it would be expected that, in the *B* series experiments, all signs of attack would have vanished when the water temperature (point B, fig. 10) was reduced to 265° C. That is, the *B* specimens would have resembled the outermost sections of the specimens of table 3 (T_4, B_4) rather than sections T_2 and B_2 which they did in fact resemble over the majority of their surface. Thus the estimates of superheat and concentration derived from table 3 must be of the right order.

Obviously, in view of the limited accuracy of the measurements and the variability of corrosion phenomena, the above rather indirect approach gives only tentative confirmation of the earlier estimates. A more direct assessment of the caustic concentrations and stresses required for intercrystalline attack could be obtained by studying specimens in the form of hollow cylinders which could be filled with the desired solution and stressed at the appropriate temperature. Such experiments are in progress elsewhere [13]).

Turning to the more metallurgical aspects of the results, present knowledge of stainless steels offers no explanation of the intercyrstalline form of the attack. It is unlikely that abnormal properties of the material used were responsible, for several batches of steel (table 1) all behaved similarly and were all normal in analysis, microstructure and in their response to the usual tests for inter- and transcrystalline susceptibility. There was, moreover, no sign of grain boundary carbide networks in any of the material.

It has been suggested [14]) that the attack may be related to that found in strongly oxidising acid media in which chromium dissolves as chromate and which can take an intercrystalline form. Under strongly alkaline conditions which favour the formation of chromate, considerably less oxidising conditions might suffice for this type of corrosion. If this is correct, intercrystalline corrosion might occur at lower caustic concentrations than those calculated above if the solutions contained dissolved oxygen, and were therefore more oxidising. However, the more fundamental question as to why the attack is intercrystalline must await further experiments.

The practical implications of the results, briefly stated, are that under the conditions outlined in the introduction, heat transfer should not significantly enhance the corrosion of plane surfaces of the two steels studied. However, crevices in which heat transfer produces superheating of more than about 25° C are likely to suffer intercrystalline attack, even if the metal is virtually unstressed. More rapid cracking may be expected at stresses of the order of 20 000 psi.

Behaviour in less alkaline water, say at pH 9 or 10, might be of practical interest. This work shows that, when cracking is produced, the caustic concentration is increased from about 50 ppm to 50 % by weight, i.e. by about 10^4. A reduction in pH to 10, involving only a tenfold reduction in bulk caustic concentration, seems unlikely to have much effect on the ultimate result, although it might make the attack slower. The same is probably true of a further reduction to pH 9, though it is impossible to say at what pH the life would be equal to that in neutral water. A more speculative suggestion is that, in systems involving the risk of crevice effects and also requiring a pH of $10-11$, this might safely be provided by the use of alkaline phosphates, as is done in normal boilers to prevent intercrystalline attack on mild steel by excessive caustic at points where the water becomes concentrated. There is no information on the effects of alkaline phosphates in systems such as those described here, but they seem worth investigation.

6. Conclusions

1. The corrosion of plane surfaces of two stabilised 18/8 stainless steels in oxygen-free water at 280° C, pH 11 (by KOH) and containing ≈ 0.5 ppm chloride, is not seriously increased by boiling heat transfer at up to 200 watt/cm^2.
2. In crevices where, under heat transfer, higher temperatures and solute concentrations can be reached, intercrystalline corrosion can occur.
3. Of the solutes, the influence of chloride, at 0.5 ppm is insignificant compared with that of potassium hydroxide. The minimum concentration of the latter required to produce intercrystalline cracking is about $40-50$ % by weight KOH.
4. This concentration of potassium hydroxide corresponds to a superheat, above the saturation temperature of the water, of $25-35°$ C; that is, crevices superheated by this amount are in danger of attack.
5. Variations of stress are unlikely to influence the rate of attack greatly, though mechanical failure will be more rapid at higher stresses. Under appropriate thermal conditions intercrystalline corrosion of virtually unstressed metal seems possible.
6. The better-known transcrystalline stress corrosion cracking is not observed under the above conditions. It appears to require higher concentrations of caustic alkali.
7. The method used to establish the above temperatures and concentrations is liable to several uncertainties and a more direct assessment in simpler apparatus is desirable.
8. There is slight evidence that potassium hydroxide is more aggressive than sodium hydroxide at comparable concentrations, but this requires further confirmation.
9. Further work is required to explain why, at similar temperature and stresses, the attack is inter- or transcrystalline according to the concentration of caustic.

Acknowledgements

The authors acknowledge the assistance of many colleagues in the Metallurgy, Reactor and Chemical Engineering Divisions, AERE, in carrying out these experiments. In particular they wish to thank Mr. W. Broome and Mr. R. Aldred for metallurgical work and Mr. G. W. Williams, Mr. F. Jenks and Mr. D. Walmsley for operation of the two loops. They are indebted to Dr. J. Greenwood and Dr. B. Williamson for the calculations described on page 170, and to Dr. C. Edeleanu, Mr. P. P. Snowden and Mr. R. B. Bowring for valuable discussions.

References

1) J. N. Wanklyn and D. Jones, Chemistry and Industry (1958) 888

2) E. C. Potter, Research **8** (1955) 450

3) R. E. Hall, Trans. ASME **66** (1944) 457

4) C. Edeleanu and P. P. Snowden, J. Iron Steel Inst. **186** (1957) 406

5) W. L. Williams, Corrosion **13** (1957) 539t

6) W. L. Williams and J. F. Eckel, J. Amer. Soc. Naval Engrs. **68** (1956) 93

7) J. Greenwood and B. Williamson (Private Communication)

8) International Critical Tables Vol. **3**. pp. 370, 373

9) M. Hecht, W. C. Schroeder, E. P. Partridge and S. F. Whirl, Corrosion Handbook, Ed. H. H. Uhlig (1948) p. 530

10) F. Adcock and A. J. Cook, J. Iron Steel Inst. **143** (1941) 119P

11) F. G. Straub, University of Illinois Engineering Experimental Station Bulletin, No. 216 (1930)

12) C. D. Weir, Chemistry and Industry (1953) 1077

13) P. P. Snowden, Chemistry and Industry (1958) 1692

14) C. Edeleanu, Private communication

JOURNAL OF NUCLEAR MATERIALS - 2 (1959) 174–181 - NORTH-HOLLAND PUBLISHING CO., AMSTERDAM

HIGH TEMPERATURE CREEP AND ANELASTIC PHENOMENA IN POLYCRYSTALLINE REFRACTORY OXIDES

ROGER CHANG

Atomics International, A Division of North American Aviation, Inc., Canoga Park, California, USA

Received 12 February 1959

High temperature creep and anelastic phenomena in polycrystalline Al_2O_3 and BeO were studied. The activation energies for both "steady-state" creep and grain boundary relaxation are approximately 2.0×10^5 calories per mole for Al_2O_3 and 1.2×10^5 calories per mole for BeO. Addition of small amounts of Cr_2O_3 or La_2O_3 to Al_2O_3 and of MgO to BeO introduces additional grain boundary relaxation peaks at lower temperatures and reduces grain boundary viscosity. The beneficial effects of these additives in improving the high temperature ductility of refractory oxides are briefly discussed.

A correlation between the experimentally observed "steady-state" creep rates and those calculated according to the Nabarro–Herring mechanism from self-diffusion data for BeO suggests that the Nabarro–Herring mechanism may predominate in the creep of polycrystalline BeO and possibly other oxides at high temperatures and low stresses. Further verification of the observation is needed.

Le fluage à haute température et les phénomènes anélastiques dans les oxydes polycristallins Al_2O_3 et BeO ont été étudiés. Les énergies d'activation, pour le fluage secondaire et pour la relaxation aux joints de grains, sont approximativement: 2.0×10^5 cal/mol pour Al_2O_3 et 1.2×10^5 cal/mol pour BeO. L'addition de petites quantités de Cr_2O_3 ou La_2O_3 à Al_2O_3 et de MgO à BeO introduit des pics additionnels de relaxation aux joints de grains à des températures plus faibles et réduit la viscosité des joints de grains. Les effects bénéfiques de ces additions, utilisées pour améliorer la ductilité des oxydes réfractaires à haute température, sont brièvement discutés. Une corrélation entre les vitesses de fluage secondaire, observées expérimentalement et calculées selon le mécanisme de Nabarro–Herring, à partir des données d'auto diffusion pour l'oxyde de béryllium, laisse supposer que le mécanisme de Nabarro–Herring peut être prédominant dans le fluage de l'oxyde de béryllium polycristallin et probablement d'autres oxydes à température élevée et sous faible tension. Il est nécessaire de vérifier à nouveau cette observation.

An polykristallinem Al_2O_3 und BeO wurden das Kriechverhalten bei hohen Temperaturen und anelastische Effekte untersucht. Die Aktivierungsenergieen sowohl für das "steady-state" Kriechen als auch für das Korngrenzengleiten betragen etwa 2.0×10^5 cal/Mol für Al_2O_3 und 1.2×10^5 cal/Mol für BeO. Zusätze kleiner Mengen von Cr_2O_3 oder La_2O_3 zu Al_2O_3 und MgO zu BeO haben zusätzliche Maxima bei niederen Temperaturen zur Folge und verringern die Korngrenzenviskosität. Die günstigen Effekte dieser Zusätze, die die Verformbarkeit der hitzebeständigen Oxyde bei hohen Temperaturen verbessern, werden diskutiert.

Es wurde eine Übereinstimmung der experimentell beobachteten "steady-state" Kriechgeschwindigkeiten mit denen gefunden, die nach dem Nabarro–Herring Mechanismus under Verwendung der Selbstdiffusionswerte von BeO errechnet wurden. Dies lässt darauf schliessen, dass beim Kriechen des polykristallinen BeO und möglicherweise anderer Oxyde bei hohen Temperaturen und geringen Belastungen der Nabarro–Herring Mechanismus vorherrschend ist. Weitere Bestätigungen dieser Beobachtungen sind notwendig.

1. Introduction

Two concepts of high-temperature, low-stress creep of polycrystalline solids have been suggested. Nabarro [1]) has initiated, and Herring [2]) has expanded, a concept of stress-directed, diffusional migration of vacancies. Mott [3]) has initiated, and Weertman [4]) has expanded, a concept of dislocation-climb. Past research presents a complex picture [5, 6]). Many problems continue to exist in the study of creep in polycrystalline solids.

The mechanism of grain boundary relaxation

in polycrystalline solids is also not well understood. Although Ke [7]) has shown that grain boundaries in metal behave viscously at high temperatures, the actual mechanism by which viscous gliding occurs along the grain boundaries is not yet well-defined. Mott [8]) postulates that the elementary act which allows slip to occur along a grain boundary is the disordering of atoms within each island of good fit separated by lines of poor fit. On the other hand, Crussard [9]) suggests that it can be described by a movement of dislocations or dislocation networks along the grain boundary.

Attention is today directed to the plastic deformation of ceramic oxides by the requirements for high temperature load-bearing materials is nuclear reactor applications. Materials to be used at high temperatures and stresses, and for considerable periods of time, must not undergo excessive creep, although a certain amount of ductility might be desirable.

The present paper describes the high temperature creep and anelastic behavior of two polycrystalline oxides, BeO and Al_2O_3. The data are discussed in terms of the various mechanisms outlined above.

Specimens used in this study were prepared in the Fabrication Laboratory at Atomics International. Highest purity powders were used as a starting material (+99.95 percent pure). The Al_2O_3 specimens were cold-pressed and sintered while the BeO specimens were hot-pressed. Grain sizes of the finished products were of the order of 25 to 30 microns. Densities varied between the limits 95 to 97 percent of theoretical for Al_2O_3 and 97 to 99 percent of theoretical for BeO. Metallographic examination of the specimens indicated a homogeneous single-phase polycrystalline solid and the absence of any second phase material along the grain boundaries or inside the grains.

2. Tensile Creep

A schematic diagram of the tensile creep apparatus is shown in fig. 1. Specimens 13 mm in gauge length were machined from sintered stock. The tests were carried out in air in a

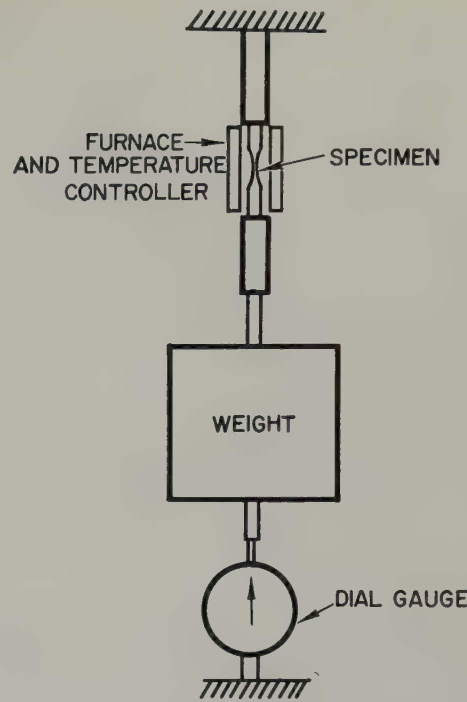

Fig. 1. Schematic diagram of the tensile creep apparatus.

molybdenum-wound furnace. A recording thermocouple was placed near the center of the specimen. Temperature difference over the 13 mm gauge length was determined to be less than 10° C. Specimen temperature was maintained within 2 to 3° of the mean temperature over the gauge length by means of a Leeds and Northrop Speedomax recorder with dual action proportional control. During a test the specimen was heated to the desired temperature under its own weight and the lower specimen grip (~ 10 psi); stress was then applied to the specimen by means of dead-weight loading, care being taken to avoid impact. Dial gauge readings, indicating elongation of the specimen under applied stress, were taken at constant time intervals immediately after the stress was applied. The equipment was believed to be sensitive to strains of about 1×10^{-5}. Since only "steady-state" creep rates are involved, possible sliding of grips at the beginning of a creep test is of no concern. No further sliding of grips is expected during a creep run because the grips

are located outside the hot zone of the furnace. Some plastic deformation is expected near the necked regions of the test specimen; such deformation however, was shown to be small compared with that associated with the gauge length portion of the specimen by the fact that the actual increase in length of the gauge length portion and corresponding reduction in cross-sectional area measured after a creep run agreed quite well with that calculated from the dial gauge movement during a creep run.

Typical creep curves for BeO and Al_2O_3 are shown respectively in fig. 2 and fig. 3. A plot of the "steady-state" creep rate versus applied tensile stress (temperature constant) for BeO is shown in fig. 4. Typical data needed to evaluate

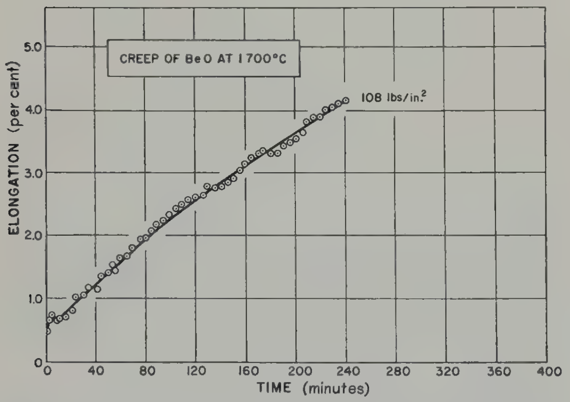

Fig. 2. Typical creep curve of a polycrystalline BeO body at 1700° C.

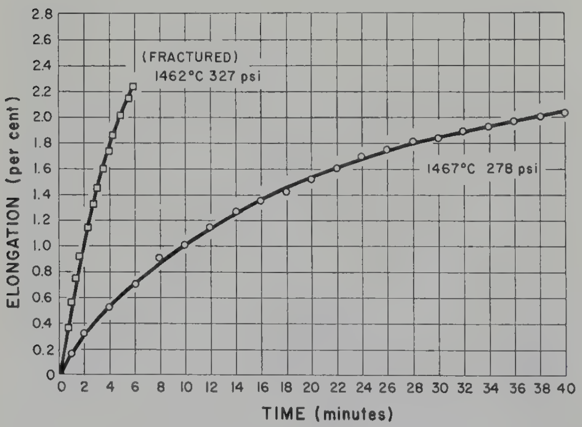

Fig. 3. Typical creep curves of polycrystalline Al_2O_3 bodies.

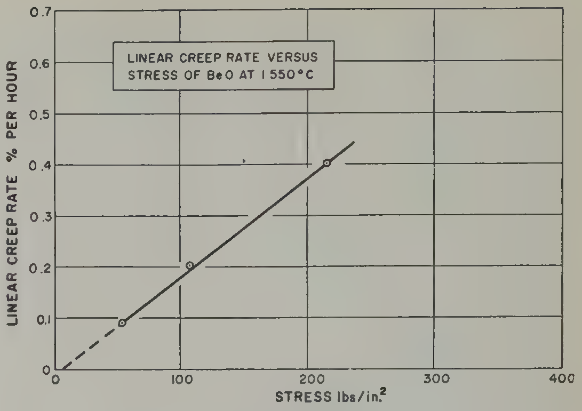

Fig. 4. "Steady-state" creep rate versus stress, polycrystalline BeO, at 1550° C.

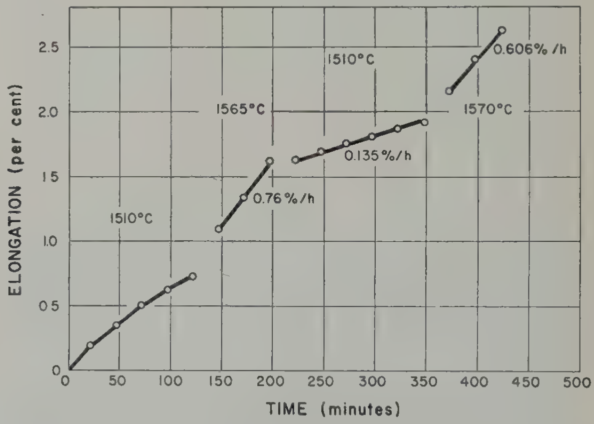

Fig. 5. Typical data to evaluate activation energy "Steady-state" creep.

activation energy during "steady-state" creep are shown in fig. 5 for Al_2O_3. Pure BeO, BeO containing one weight percent MgO, pure Al_2O_3, and Al_2O_3 containing, respectively, one weight percent Cr_2O_3 and 0.25 weight percent La_2O_3 were studied. The experimental data † yield the following activation energies for "steady-state" creep: 1.2×10^5 calories per mole for BeO and 2.0×10^5 calories per mole for Al_2O_3, regardless of chemical composition.

3. Anelastic Studies

A low frequency, direct recording, internal friction apparatus has been constructed for the study of various relaxation processes in ceramic

† Not shown here for sake of space.

materials. A full description of the technique appeared in an article by Chang and Gensamer [10]). The present work was limited to an investigation of the mechanism of grain boundary relaxation in polycrystalline ceramic oxides. The internal friction spectra of a polycrystalline and single crystal Al_2O_3 are compared in fig. 6, where the grain boundary relaxation of polycrystalline Al_2O_3 is clearly indicated by a sharp rise in internal friction at about 1100° C. Our internal friction data for polycrystalline Al_2O_3 are combined with Wachtman's data [11]) of a duplicate specimen in the kilocycle range in fig. 7. Assuming a single relaxation mechanism, the peak shift yields an activation energy of about 2.0×10^5 calories per mole for the grain boundary relaxation of Al_2O_3.

When additives are present in polycrystalline Al_2O_3 in solution, new internal friction peaks were found in the temperature region 800 to 900° C. Typical internal friction spectra of polycrystalline Al_2O_3 containing Cr_2O_3 and La_2O_3 are shown, respectively, in fig. 8, and fig. 9. Since the internal friction spectrum of a ruby single crystal (Al_2O_3 containing approximately 2 weight percent Cr_2O_3) failed to show similar peaks in the temperature region 800 to 900° C, the new internal friction peaks must be also associated with grain boundary relaxation. Comparisons of fig. 8 (or fig. 9) and fig. 7 show

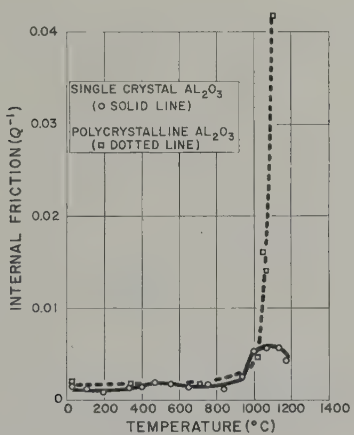

Fig. 6. Internal friction spectra of polycrystalline and single crystal Al_2O_3.

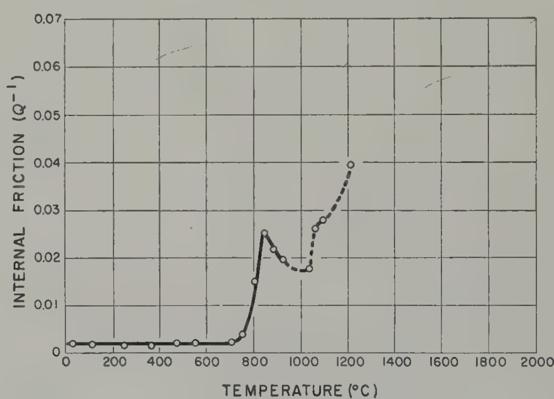

Fig. 8. Internal friction spectrum of polycrystalline Al_2O_3 containing one weight percent Cr_2O_3 (frequency $\approx$ 7 cps).

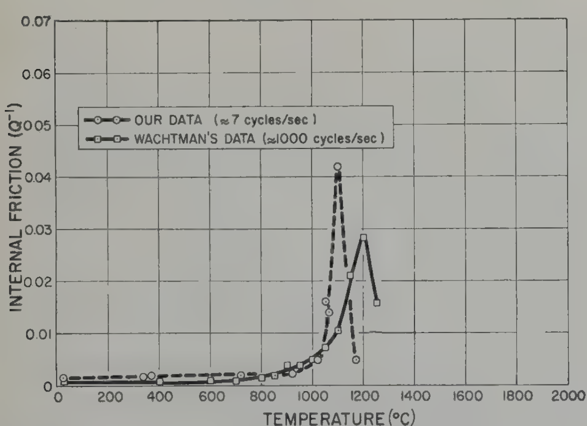

Fig. 7. Internal friction spectra of a polycrystalline Al_2O_3 body at two frequencies.

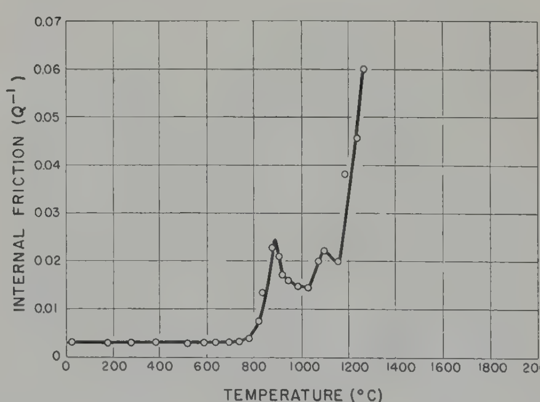

Fig. 9. Internal friction spectrum of polycrystalline Al_2O_3 containing 0.25 weight percent La_2O_3 (frequency $\approx$ 15 cps).

that the internal friction spectra of polycrystalline Al_2O_3 containing Cr_2O_3 (or La_2O_3) consist of the following:

(a) a weakened or suppressed main grain boundary peak at about 1100° C.
(b) a new solute peak at 800 to 900° C, and
(c) a background internal friction increasing very rapidly with rising temperature.

Fig. 10 shows the shift of solute internal friction peak of a Cr_2O_3-containing specimen measured at two frequencies, from which an activation energy of 47 000 calories per mole was obtained. Fig. 11 shows similar solute peak shifts of a La_2O_3 containing specimen †.

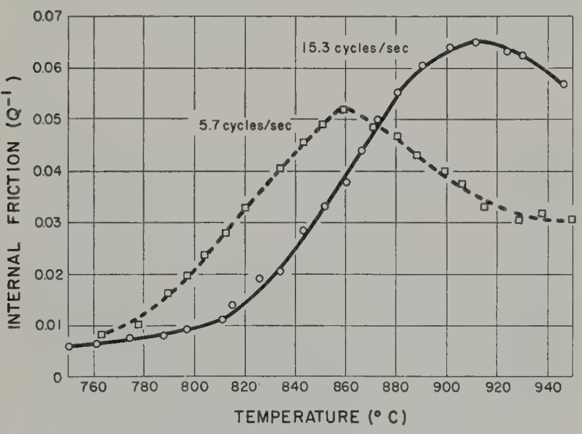

Fig. 10. Internal friction spectra of polycrystalline Al_2O_3 (one weight percent Cr_2O_3) at two frequencies.

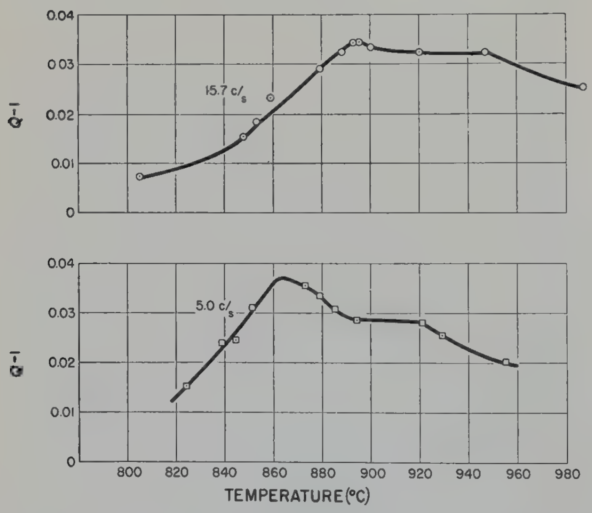

Fig. 11. Internal friction spectra of polycrystalline Al_2O_3 (0.25 weight percent La_2O_3) at two frequencies.

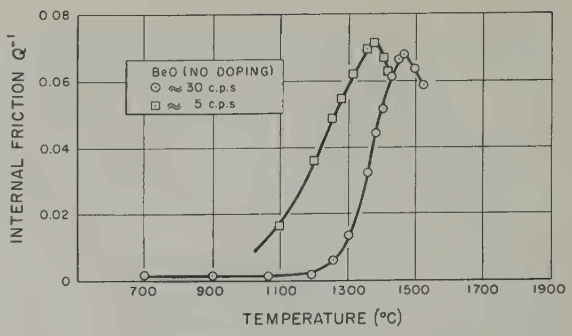

Fig. 12. Internal friction spectra of polycrystalline BeO at two frequencies.

Further measurements of solute internal friction peaks show that the peak temperature increases with increasing Cr_2O_3 concentration but decreases with increasing La_2O_3 concentration. The observed solute peak temperatures of specimens containing various amounts of Cr_2O_3 or La_2O_3 are shown, together with the observed grain sizes of these specimens, in table 1.

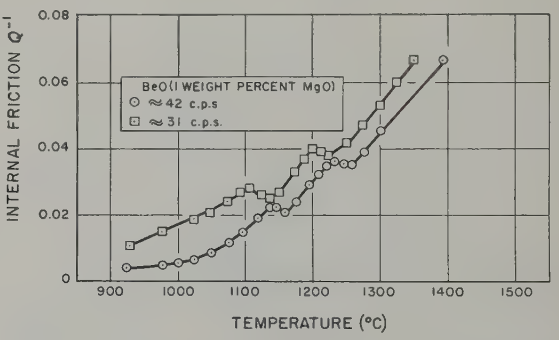

Fig. 13. Internal friction spectra of polycrystalline BeO (one weight percent MgO) at two frequencies.

The internal friction spectra of polycrystalline BeO with and without MgO addition at two frequencies of vibration are shown respectively in fig. 12 and fig. 13. The peak shift for pure BeO

† This solute peak shift is not sufficiently well-defined for a reliable estimate of the activation energy.

yields an activation energy of about 115 000 calories per mole. Addition of one weight percent MgO introduces additional relaxation peaks with activation energies of 35 000 to 40 000 calories per mole.

TABLE 1

Change of solute peak temperature with chemical composition of Al_2O_3

(Frequency $\approx$ 16 cycles/sec)

Solute	Solute concentration (weight percent)	Solute peak temperature (°C)	Average grain size (microns)
Cr_2O_3	0.5	823	30
Cr_2O_3	1.0	895	25
Cr_2O_3	3.0	911	15
La_2O_3	0.25	895	20
La_2O_3	0.5	830	30
La_2O_3	1.0	790	30

4. Discussion

The present work on polycrystalline BeO and Al_2O_3 shows that the activation energy associated with grain boundary relaxation and with "steady-state" creep is approximately equal to that for self-diffusion †, in agreement with similar work of Ke [7]) on metals. However, Rotherham and Pearson [12]) found that the activation energy for grain boundary relaxation in copper is 33 000 calories per mole while alloying elements (Zn, Ga, Ge, As, Si) increase the activation energy for grain boundary relaxation to approximately 44 000 calories per mole (the activation energy for self-diffusion in Cu is 44 000 to 49 000 calories per mole). Similarly, the effect of alloying elements (Cd, In, Sn) is to increase the activation energy for grain boundary relaxation from 22 000 calories per mole for spectroscopically pure silver to 43 000 calories per mole for the solid solution (the activation energy for self-diffusion in Ag is 44 000 to 46 000 calories per mole). We find the opposite effect in oxides. While the effect of adding solute atoms to copper and silver is to increase the grain boundary viscosity as would be expected if grain boundary slip were due to the movement of dislocations, the effect of adding solute atoms to BeO and Al_2O_3 is to decrease the grain boundary viscosity and to enhance grain boundary mobility. Although the reason for this difference is not yet well understood, the phenomenon may have a far reaching effect on the high temperature strength, ductility, and fracture behavior of polycrystalline oxides. The plastic deformation of grains and grain boundaries cannot be considered as isolated processes. The conditions of geometrical consistency introduce an interaction between the deformation sustained by the grains and by the boundaries. The interaction between crystalline slip and viscous gliding at the boundaries is an important factor determining the high temperature fracture behavior of polycrystalline solids. The question of intergranular porosity and intergranular cracking is a timely subject under careful study by many investigators [13]). The concensus of opinion is as follows: Grain boundaries act as vacancy sinks. Vacancies are attracted towards the tips of embryonic microcracks near the grain boundary, causing lateral crack growth. On the other hand, the surface tension tends to round out the cracks by atomic migration on the internal surfaces of these cavities. Thus additives, which decrease grain boundary viscosity, may have beneficial effects of delaying crack growth, hence permitting more crystalline slip. This appears to be a fruitful field for further experimental verification.

The "steady-state" creep data for polycrystalline BeO seem to fit very nicely the vacancy-diffusion mechanism of Nabarro and Herring. Under conditions of complete grain-boundary relaxation, Herring has shown that

† The activation energy for self-diffusion in BeO is 1.15×10^5 calories per mole from Be^7 diffusion data by Austermann [14]); and that in Al_2O_3 is approximately 1.8×10^5 calories per mole from sintering data by Coble [15]).

the "steady-state" tensile-creep rate $\dot{\varepsilon}$ is related to the tensile stress, σ, by: [2])

$$\dot{\varepsilon} = (\tfrac{10}{3})\,(4\pi/3V)^{\frac{2}{3}}\, N D\, \Omega\sigma/RT \tag{1}$$

$$D = D_0 \exp\,(-Q/RT) \tag{2}$$

where V is the mean volume of a grain, Ω † the volume of a vacancy, σ the applied tensile stress, R the gas constant, T the absolute temperature, D_0 the diffusivity constant for self-diffusion, and Q the activation energy for self-diffusion. The diffusion of Be^7 in polycrystalline BeO is being studied in our laboratory. Preliminary measurements yielded the following diffusion coefficient in the temperature range 1600–1750° C [14])

$$D \cong 10^4 \exp\,(-115\,000/RT). \tag{3}$$

It is interesting to find that the activation energy for the diffusion of Be^7 in polycrystalline BeO is, within experimental error, equal to that for creep. Presumably the diffusion of Be ions is the rate-limiting process in BeO self-diffusion. Since the only unknown quantity in eq. (1) is D, the "steady-state" creep rate at any given temperature and stress can be calculated directly from eq. (1) if D is known. Assuming that D in eq. (1) is given by eq. (3), the calculated "steady-state" creep rates are compared with experimental linear creep rates in table 2.

TABLE 2

Comparison of observed and calculated creep rates of polycrystalline BeO according to the vacancy-diffusion model

(Average grain size ≈ 25 microns, stress 108 lbs/in.^{2})

Temperature °C	"Steady-State" creep rates, percent per hour	
	Experimental	Calculated
1650	0.33	0.26
1700	0.72, 0.77	0.54
1745	1.49	1.02

The agreement between the observed and calculated creep rates according to the vacancy-diffusion model suggests that the stress-directed vacancy-diffusion mechanism may predominate in the creep of BeO at the temperatures and stresses indicated. According to the concepts of dislocation theory, slip will occur if a sufficiently high stress is applied to nucleate Frank–Read sources. Dislocations released from these sources might pile up against various types of barriers. For creep to continue at high temperatures, the piled-up dislocations at the barriers might escape by a dislocation-climb process. If the stress is lower than that necessary to nucleate the longest Frank–Read source, slip would not occur. Since the activation energy to nucleate the understressed Frank–Read source is extremely high, the probability of creep by movement of dislocations becomes negligibly small, and creep in these low stress ranges could only take place by the stress-directed diffusion of vacancies. If the above analysis is true, the dislocation-climb process might predominate at stresses sufficiently high to cause yielding, while at stresses below the yield strength, creep should occur exclusively by the vacancy-diffusion mechanism. In fact, actual creep runs at higher stresses indicate that the "steady-state" creep rate increases much more rapidly with stress than is demanded by linear proportionality according to the vacancy diffusion mechanism. In order to study the problem without complications due to grain boundaries, the use of single crystals is essential. Such studies are outside the scope of the present paper and will be reported separately.

Our "steady-state" creep data indicate that addition of Cr_2O_3 or La_2O_3 increases slightly the creep rate of polycrystalline Al_2O_3, in contrast to the observed fact that addition of Cr_2O_3 decreases the creep rate of single crystal Al_2O_3 (unpublished data). This would be understandable if the high temperature creep of polycrystalline Al_2O_3 follows the vacancy-diffusion mechanism while that of single crystal Al_2O_3 requires the activation and propagation of slip bands. Without self-diffusion data, it is not possible at present to state which creep mechanism prevails. Further studies are needed.

† It is assumed to be equal to the volume of a BeO "molecule" in the present calculation.

References

1) F. R. N. Nabarro, Report of a Conference on Strength of Solids, The Physical Society, London, **75** (1948)
2) C. Herring, J. Appl. Phys. **21** (1950) 437
3) N. F. Mott, Proc. Roy. Soc. A **220** (1953) 1
4) J. Weertman, J. Appl. Phys. **26** (1955) 1213
5) J. E. Dorn, J. Mech. Phys. Solids **3** (1954) 85
6) J. Harper and J. E. Dorn, Acta Met. **5** (1957) 654
7) T. S. Ke, Phys. Rev. **71** (1947) 533
8) N. F. Mott, Proc. Phys. Soc. **60** (1948) 391
9) C. Crussard and R. Tamhankar, Trans. AIME **212** (1958) 718
10) L. C. Chang and M. Gensamer, Acta Met. **1** (1953) 483
11) J. B. Wachtman, Jr., U.S. Air Force, Wright Air Development Center, Report WADC–TR–57–526 (1957)
12) S. Pearson and L. Rotherham, Trans. AIME **206** (1956) 894; L. Rotherham and S. Pearson, Trans. AIME **206** (1956) 881
13) See, for example, Symposium and Creep and Fracture of Metals at High Temperatures, Teddington, Great Britain (1954), (H.M. Stationery Office, London, 1956)
14) Private Communication by S. Austerman
15) R. L. Coble, J. Am. Cer. Soc. **41** (1958) 55

JOURNAL OF NUCLEAR MATERIALS - 2 (1959) 182–190 - NORTH-HOLLAND PUBLISHING CO., AMSTERDAM

EFFECT OF FISSION RATE AND LAMELLA SPACING UPON THE IRRADIATION-INDUCED PHASE TRANSFORMATION OF U-9 wt % Mo ALLOY

M. L. BLEIBERG

Westinghouse Electric Corporation, Bettis Plant, Pittsburgh, Pa., USA

Received 18 February 1959

Samples of U-9 wt % Mo alloy of various U^{235} enrichments and interlamellar spacings were neutron irradiated at low temperatures, and the kinetics of the neutron-induced phase transformation determined by electrical resistivity measurements. The kinetics of this reaction may be described in terms of macroscopic diffusion occurring within a "displacement" or a "thermal spike". The diffusion coefficient was determined to be $1.4 \times 10^{-18} \pm 0.6 \times 10^{-18}$ cm²/sec for a fission rate of 5.25×10^{12} fissions per cm³/sec. The diffusion coefficient was found to be directly proportional to the fission rate, but independent of sample temperature between —90° C and +200° C and of neutron flux intensity.

Des échantillons d'uranium à 9 % en poids de Mo à différents taux d'enrichissement en U^{235} et d'espacements interlamellaires différents ont été irradiés à basse température. La cinétique de transformation de phase induite par les neutrons a été déterminée par des mesures de résistivité électrique. La cinétique de cette réaction peut être décrite par une diffusion macroscopique se produisant à l'intérieur d'un "déplacement" ou d'une "pointe de feu". Le coefficient de diffusion déterminé est de 1.4×10^{-18} cm²/sec $\pm$ 0.6×10^{-18} pour un taux de fission de 5.25×10^{12} fissions par cm³/sec. Le coefficient de diffusion trouvé était directement proportionnel au taux de fission et à l'intensité du flux de neutrons, mais indépendant de la température de l'échantillon entre —90° et + 200° C.

U-9 Gew. % Mo Legierungsproben mit verschiedener U^{235}-Anreicherung und verschiedenem Lamellenabstand wurden bei niedrigen Temperaturen mit Neutronen bestrahlt und die Kinetik der durch die Bestrahlung hervorgerufenen Phasenumwandlung wurde mittels Widerstandsmessungen bestimmt. Die Kinetik dieser Reaktion kann mit Hilfe einer makroskopischen Diffusion innerhalb eines "displacement spike" oder "thermal spike" beschrieben werden. Der Diffusionskoeffizient wurde als $1.4 \times 10^{-18} \pm (0.6 \times 10^{-18})$ cm²/Sek bestimmt. Der Diffusionskoeffizient war direkt proportional der Spaltungshäufigkeit, aber temperaturunabhängig zwischen —90° C und +200° C und auch unabhängig von der Intensität des Neutronenflusses.

1. Introduction

The mechanism of the phase reversal of U-Mo alloys due to neutron bombardment was attributed to spontaneous diffusion within a displacement spike by Bleiberg, Jones, and Lustman, and to a similar mechanism within a thermal spike by Konobeevsky [1, 2]. Bleiberg has shown that the kinetics of this reaction may be studied by continuous measurements of electrical resistivity of a U-9 wt % Mo sample while under pile-irradiation and at low temperatures. The special irradiation facility for performing these measurements and preliminary results on samples irradiated in this facility have been given elsewhere [3, 4]).

The equation describing the spontaneous diffusion of uranium and molybdenum atoms within a displacement or thermal spike predicts that the kinetics of the reaction are directly proportional to the fission rate of the samples (i.e., the number of fission events per unit time-unit volume) and are inversely proportional to the square of the interlamellar spacing (the diffusion path). The present test was performed

to verify this, and consisted of irradiating samples of U-9 wt % Mo alloy with various interlamellar spacings and U^{235} enrichments.

2. Experimental Technique

Foil samples of U-9 wt % Mo alloy 0.025 cm thick × 0.125 cm wide × 3.80 cm long enriched with 10 %, 15 %, and 20 % U^{235} were homogenized and gamma quenched by heat treatment in evacuated Vycor tubes at 900° C for 24 hours and water quenched. Some samples were left in this condition while others were isothermally transformed by re-sealing in evacuated Vycor bulbs and heat treated at 500° C or 475° C for 2 weeks to transform the gamma phase to the alpha plus epsilon phases. The chemical composition and heat treatments of the samples are shown in table 1. Also shown in table 1 for comparison, is the alpha plus epsilon sample irradiated in the previous in-pile test and herein called sample *1* [3]).

Table 1

Sample composition and heat treatment

Sample No.	Composition: wt % Mo	wt % U^{235}	Heat treatment
1	8.8	13.7	900° C for 24 h plus 525° C for 2 weeks
2	8.8	10.9	900° C for 24 h plus 475° C for 2 weeks
3	8.8	15.0	900° C for 24 h plus 500° C for 2 weeks
4	8.8	10.9	900° C for 24 h plus 500° C for 2 weeks
5	9.1	21.9	900° C for 24 h

Electrical connections were made by spot welding 0.025 cm diameter molybdenum wires 2.5 cm apart around the center of the specimens. The specimens were then placed on lavite slabs 0.150 cm thick with holes and grooves machined into the lavite to allow the lead wires to be insulated and also to hold the specimen firmly in place. Copper-constantan thermocouples were attached to two of the specimens by forcing the thermocouple bead between the specimen and lavite slab. Eight of these specimen "packets" were then glued onto an aluminum spring collet as shown in fig. 1. After wrapping the resulting specimen assembly with 0.025 mm thick mica sheet, the assembly was slipped into an aluminum specimen housing. The specimens were forced against the housing by a stainless steel expansion collet driven into the aluminum specimen collet. The resulting assembly was bolted into place. In this manner good thermal contact was established between the specimens and the specimen housing, yet the specimens were individually insulated electrically. These components are shown in fig. 1.

The potential leads of each specimen consisted of molybdenum wire from the sample to the face of the reactor where they were brazed to copper wire which extended to a recorder. In this manner, spurious e.m.f. drops due to temperature differentials were avoided. The electrical resistances of the samples were measured by the current-potential method in which the polarities of the current and potential leads were automatically reversed on every other reading by a specially modified recorder. Each specimen constituted an independent electrical circuit. The electrical resistivity values, which were calculated from the resistance measurements, were accurate to about ± 0.5 %, and the specimen temperature was known to about ± 1° C.

The outer diameter of the specimen housing was carefully machined to fit the non-holding taper of the heat exchanger in the in-pile unit. This is described in detail elsewhere and consisted of a recirculating helium gas loop wherein the helium gas was cooled in a liquid nitrogen refrigerator and circulated through a cryostat installed in the reactor [4]).

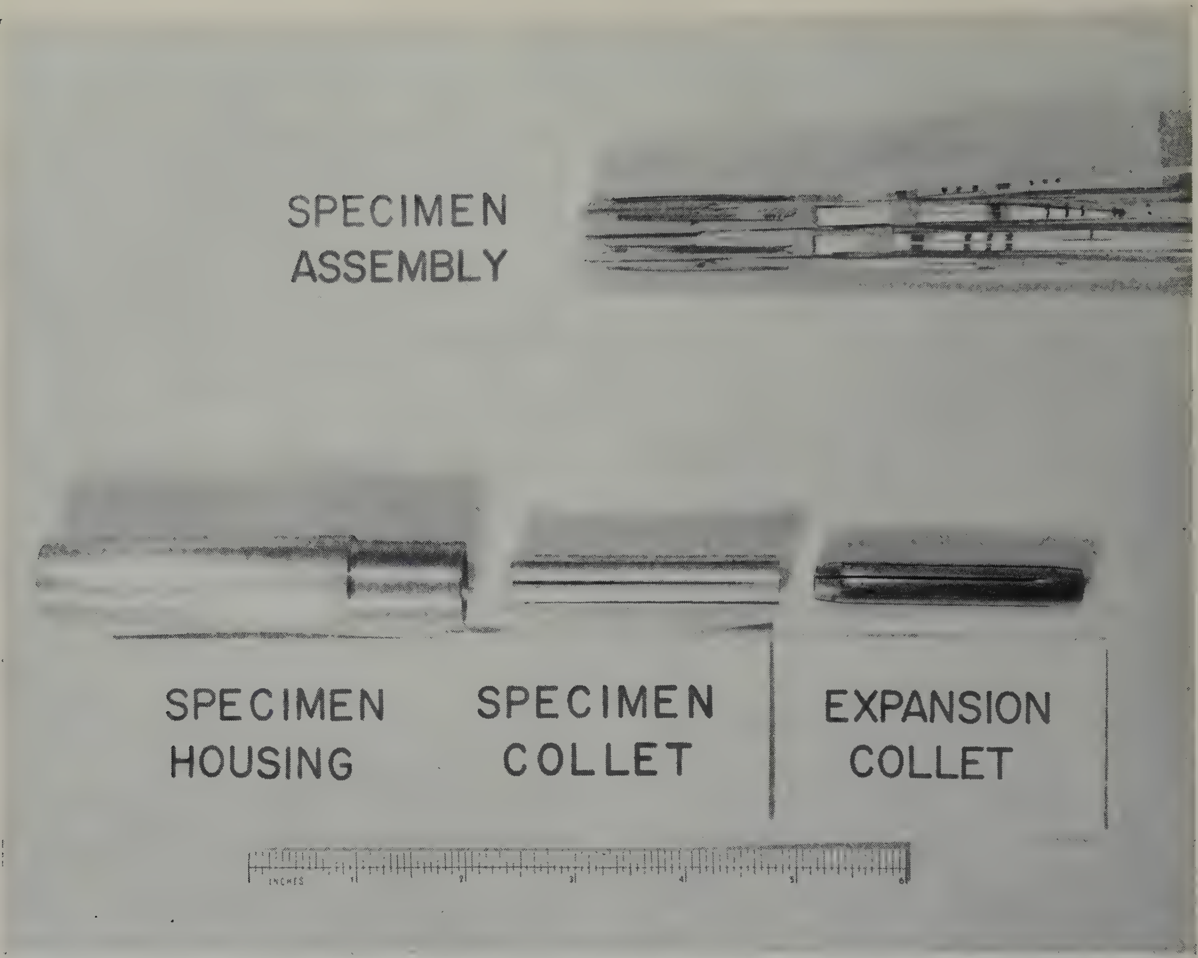

Fig. 1.

In addition to recording the changes in electrical resistivity of the samples during irradiation, the temperature coefficients of electrical resistivity were obtained during each reactor shutdown by slowly allowing the samples to warm up. Of the eight samples irradiated, the four listed in table 1 are of interest in this test, the remaining four samples being of different alloy composition. During the test period the Brookhaven National Laboratory reactor underwent a fuel reloading which resulted in an increase in the thermal neutron flux in the low-temperature facility. This resulted in an increase in the heat load of the facility due to the increased fission heat of the samples and caused the sample temperatures to change from the original temperature of $-40°$ C to about $+20°$ C at the end of the test. Assuming that the temperature differential of the samples was directly proportional to the increased flux, the flux was calculated to be as follows during the test:

Cycles 1 and 2 — 2 $\times 10^{12}$ neutrons/cm$^2\cdot$sec
Cycle 3 — 3.1 $\times 10^{12}$ neutrons/cm$^2\cdot$sec
Cycle 4 — 4.25 $\times 10^{12}$ neutrons/cm$^2\cdot$sec
Cycles 5, 6, 7 — 5.8 $\times 10^{12}$ neutrons/cm$^2\cdot$sec.

The calculated flux during cycle 5 agrees with the value of flux experimentally determined by Brookhaven reactor personnel during this time.

3. Results

The changes in electrical resistivity of the U-9 wt % Mo alloy samples during the pile irradiation are shown in fig. 2. Also shown are

the data obtained on sample *1* in the previous test. The rapid increase in the electrical resistivity of the "alpha-transformed" samples and the simultaneous rapid decrease in the gamma-quenched sample during the initial stages of the test are similar to the preliminary results reported previously on sample *1* and were attributed to an order-disorder reaction in this alloy [3]). The gamma-quenched sample exhibited no further change in electrical resistivity throughout the test up to about 2.9×10^{19} neutron/cm² exposure. Examination of fig. 2 shows a qualitative relationship between the four "alpha-transformed" samples. The interlamellar spacing decreases with decreasing heat-treatment temperature and this should cause a more rapid transformation to the gamma phase. It may be seen that sample *2* (475° C transformation) does indeed exhibit the most rapid increase in electrical resistivity even though samples *1*, *3*, and *4* have the same or a greater enrichment of U^{235}. A comparison between sample *3* and *4* shows the effects of enrichment upon the kinetics of the reaction. Both samples have the same interlamellar spacing (500° C transformation) but sample *3* was enriched to 15 % U^{235} as compared to 10 % for sample *4*. It is obvious that sample *3* transformed more rapidly although unfortunately a lead wire brooke on this sample after an exposure of about 6.4×10^{18} neutrons/cm². These qualitative relationships are also shown

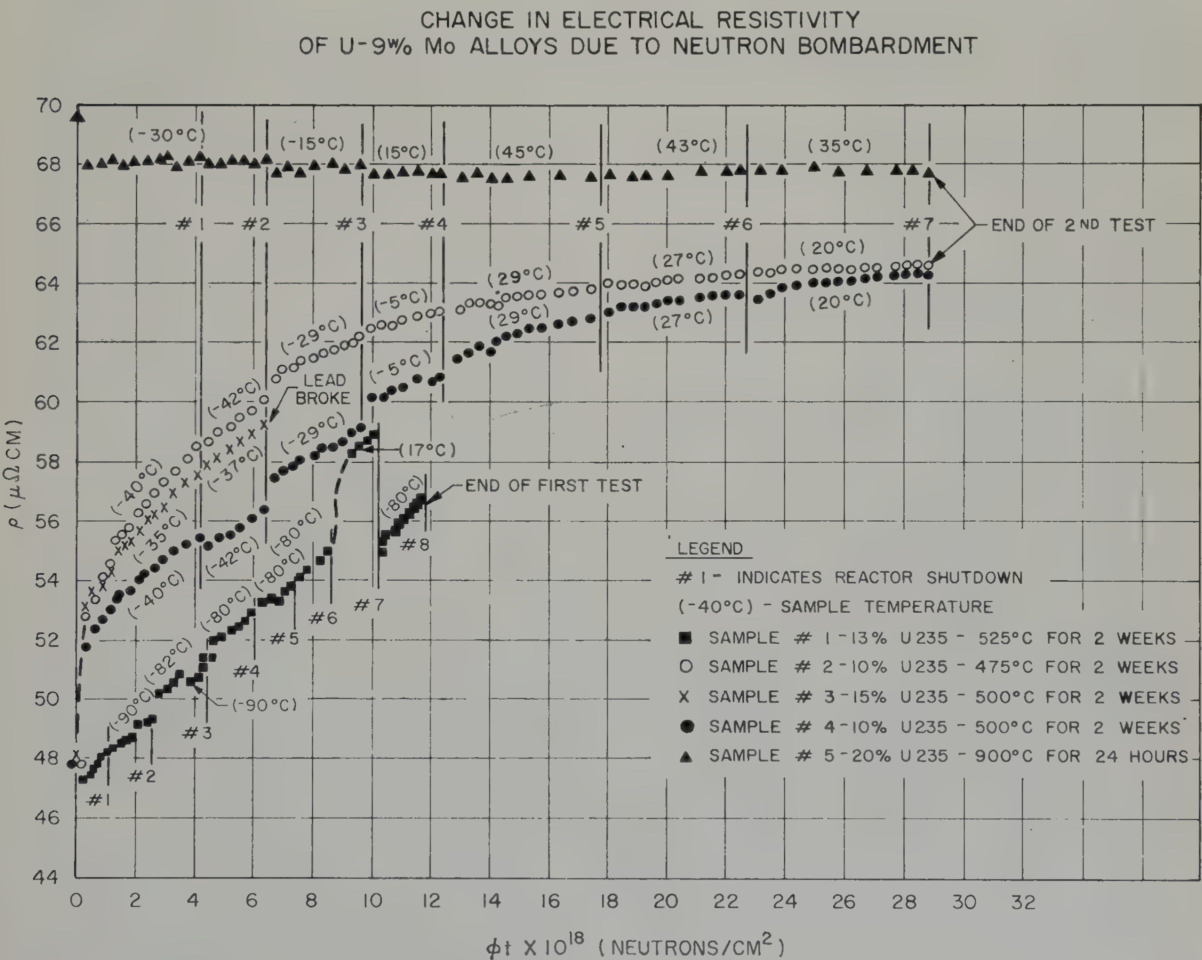

Fig. 2.

in the electrical resistivity-temperature data obtained during the reactor shutdowns in fig. 3. It may be seen that sample *2*, with the smallest interlamellar spacing has completely reversed from a positive to a negative temperature coefficient of electrical resistivity at the end of the test. Sample *4* is significantly less transformed than sample *2*, and sample *3* shows a kinetic behavior between these two samples.

The change in concentration of molybdenum as a function of time in the reactor is described by:

$$C(x,t) = A_0 + \sum_{n=1}^{\infty} A_n \cos\frac{2n\pi x}{L} \exp\left(-\frac{4Dn^2\pi^2 t}{L^2}\right) \quad (1)$$

where L = interlamellar spacing, $x=0$ is the center of an alpha uranium lamella and $x=\frac{1}{2}L$ is the center of the adjoining epsilon lamella. Eq. (1) was solved in terms of the dimensionless parameters x/L and Dt/L^2. Using the known

LOG σ VERSUS X/L FOR VARIOUS VALUES OF Dt/L².

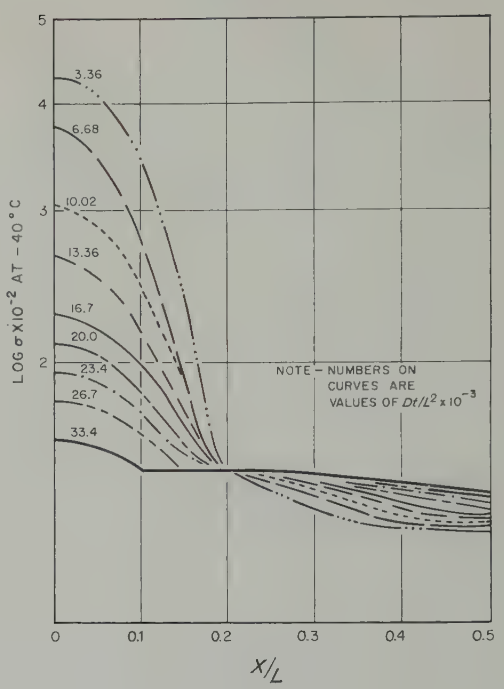

Fig. 4.

CHANGE IN TEMPERATURE DEPENDENCE OF ELECTRICAL RESISTIVITY OF U–9 w/o Mo ALLOY DUE TO NEUTRON BOMBARDMENT

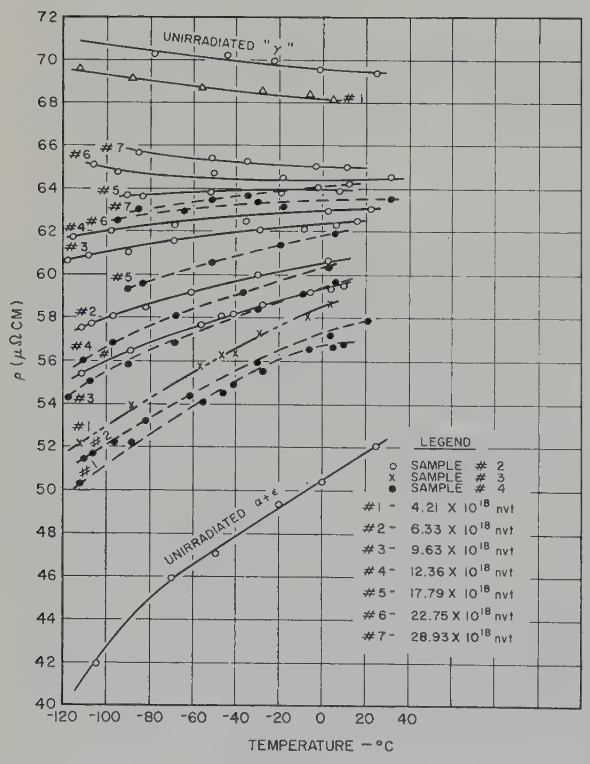

Fig. 3.

experimental data of the electrical conductivity of U-Mo alloys from 0 to 15 wt % Mo, the solution to eq. (1) was then graphically translated to plots of electrical conductivity as a function of the dimensionless parameters. These graphs represented the change in electrical conductivity through the cross section of one interlamellar spacing of the alloy for various in-pile exposure times. In order to determine the value of electrical resistivity after any time in-pile it was necessary to obtain the average value of electrical conductivity from these plots. Several methods of averaging were tried and it was found that the logarithmic average gave the best fit with the experimental data, although the reason for this is not clear. This is expressed by:

$$\log\bar{\sigma} = \sum_i \theta_i \log \sigma_i \quad (2)$$

where θ_i is the volume fraction of each phase and σ_i its respective electrical conductivity. The plot of log σ at $-40°$ C versus X/L for various values of Dt/L^2 is shown in fig. 4. The

average value of electrical conductivity was determined for each time unit by graphical integration of the curves of fig. 4 and the resultant electrical resistivity values obtained are shown in fig. 5.

Since the time of irradiation was known, the experimental data of fig. 2 and 3 could be matched to the calculated values by assuming the appropriate value of D/L^2 as is shown for each of the four samples in fig. 5, for the data obtained during reaction shutdowns. Excellent agreement is shown between the calculated and experimental values up to about 20×10^{-3} Dt/L^2 units where the alloys are about 90 % or greater transformed from the stable to the metastable phase (63 microhm·cm as compared to the equilibrium value of 68 microhm·cm). A possible explanation for this divergence during the latter part of the homogenization process may be the observation made by Bleiberg, Jones and Lustman on the metallography of the transformed alloy [1]). It was shown that the microstructure of the initially transformed alloy did not change after irradiation even though the material was completely homogenized to the gamma phase. This was attributed to the presence of impurities precipitated during transformation which were not redissolved by the displacement or thermal spikes and hence outlined the former lamella boundaries, giving a lamellar appearance to the structure. It may be postulated that these impurities cause the slightly lower values of electrical resistivity observed during the latter part of the homogenization process.

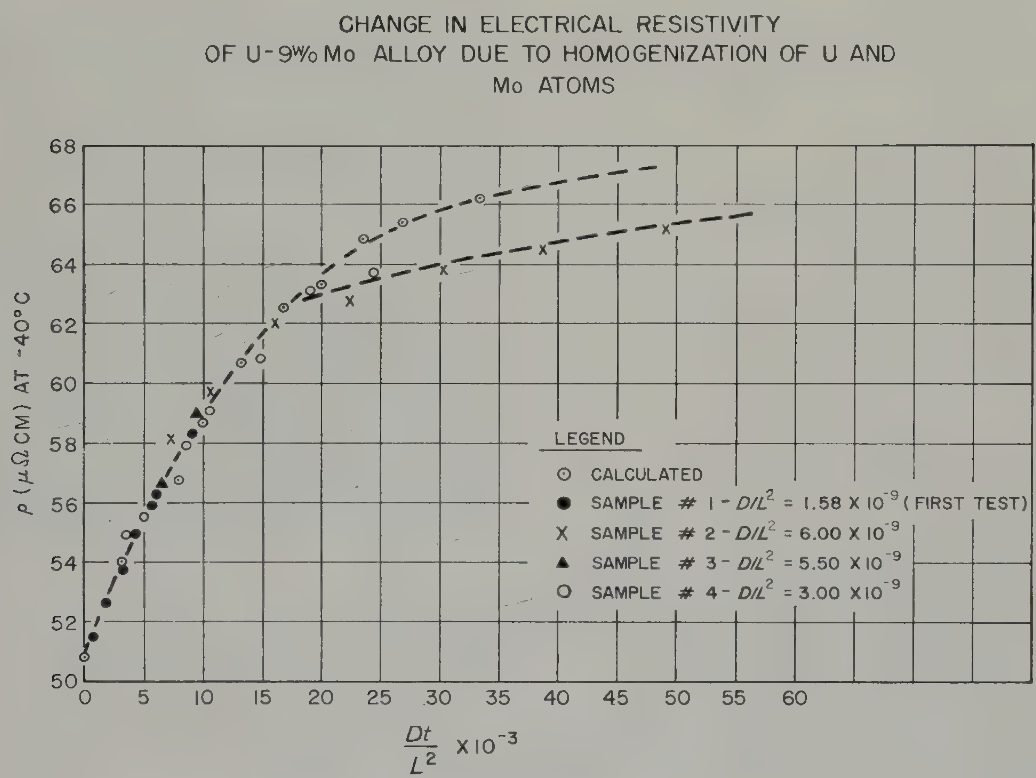

Fig. 5.

In order to obtain the values of the diffusion coefficients of each of the four samples it was necessary to obtain the best possible value of the interlamellar spacing of each heat-treated condition. This was done by using the statistical treatment of Covert from examination of 36 electron micrographs of each sample [3]). Typical

electron micrographs are shown in fig. 6 for this alloy. The interlamellar spacings determined are shown in table 2 along with the calculated values of the diffusion coefficients corrected to a single fission rate of 5.25×10^{12} fissions/cm^3·sec (D_{fr}) which is equivalent to a U-9 wt % Mo alloy specimen enriched 10 % with U^{235} and irradiated in a neutron flux of 2×10^{12} neutrons/cm^2·sec. Also shown in table 2 are the two samples irradiated in a pre-post test in the Materials Testing Reactor (A-8, A-9) to a value of Dt/L^2 of about 65 units as estimated from fig. 5 [1]). An average value of D_{fr} equal to $1.4 \times 10^{-18} \pm 0.6 \times 10^{-18}$ cm^2/sec was obtained from these six samples.

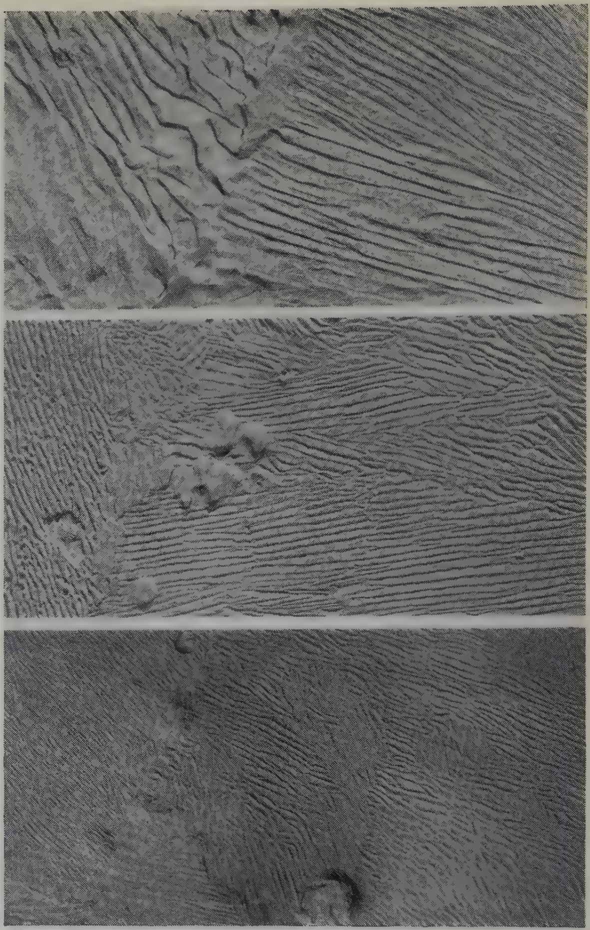

Fig. 6. Typical electron micrographs of U-9 wt % Mo alloy heat-treated to alpha plus epsilon phases. *Top*, 525° C for 2 weeks, *middle*, 500° C for 2 weeks, *bottom*, 475° C for 2 weeks. Original magnification 10 000 ×. Reduced about 2:1 for reproduction.

4. Discussion of Results

The agreement shown in table 2 between the absolute values of the diffusion coefficients (D_{fr}) for the neutron-induced homogenization of six samples of U-9 wt % Mo alloy, of varying enrichments and interlamellar spacings, and irradiated under widely divergent conditions enables the following observations to be made:

1. Eq. (1), which was independently derived by Bleiberg, Jones, and Lustman using the displacement-spike model, and Konobeevsky using the thermal-spike model, predicts the kinetics of the phase reversal. This is particularly evidenced by the influence of various interlamellar spacings of the alloy.

2. The "diffusion coefficient" is independent of temperature in the range of −90° C to +200° C, which were the limits of the irradiation temperatures experienced by the six samples.

Table 2

Diffusion coefficients for homogenization of U-9 wt % Mo alloy

Sample No.	Sample enrichment	Interlamellar spacing $\times 10^{-5}$ cm	Av. neutron flux (neutrons/cm^2/sec)	D_{fr} (cm^2/sec) corrected for $E = 10\ \%\ \phi = 2 \times 10^{12}$
1	13.7 %	3.0	2×10^{12}	1.4×10^{-18}
2	10.9 %	1.4	3.53×10^{12}	0.6×10^{-18}
3	15.0 %	2.5	3.53×10^{12}	1.3×10^{-18}
4	10.9 %	2.5	3.53×10^{12}	1.0×10^{-18}
A-8, A-9	0.7 %	3.0	2.0×10^{14}	2.9×10^{-18}

$D_{fr} = 1.4 \times 10^{-18} \pm 0.6 \times 10^{-18}$ cm^2/sec for a fission rate $= 5.25 \times 10^{12}$ fissions/cm^3·sec.

3. The "diffusion coefficient" is independent of neutron flux intensity, which varied 100 fold, from 2×10^{12} to 2×10^{14} neutrons/cm$^2\cdot$sec in these tests, but is directly proportional to the fission rate of the specimens.

Bleiberg *et al.*, and also Dienes and Vineyard, have shown that the diffusion coefficient may be expressed by [1, 5])

$$D=\frac{1}{12}\, N_0 X^5 \qquad (3)$$

where N_0 is the number of spikes/cm$^3\cdot$sec and X^3 is the volume of the spike. Letting $N_0 = 5.25\times10^{12}$ fissions/cm$^3\cdot$sec and $D = 1.4\times10^{-18}$ cm^2/sec, then substitution into eq. (3) shows that the volume of material affected during each fission event is 2.01×10^{-18} cm^3. Assuming a b.c.c. lattice and an interatomic distance of 3.4×10^{-8} cm, it can be shown that about 1.05×10^5 atoms are affected during each fission event which produces homogenization in the alloy. Using Brinkman's treatment, there are approximately 8×10^4 atoms in each displacement spike, which would indicate that 1 to 2 displacement spikes are created during each fission event [6]). This is reasonably good agreement with the mechanism proposed by Bleiberg, Jones and Lustman, although they assumed that about six displacement spikes were produced per fission event [1]). Examination of eq. (3) shows that the denominator (12) is based on the assumption that the shape of the concentration-distance curve within the volume affected by a displacement spike is linear although this may not be the case. If the homogenization within each individual spike were less efficient than was assumed, then the denominator would be larger (i.e., less mass transfer) and the above analysis would indicate a greater number of displacement spikes per fission. The results of this test cannot resolve this question but the analysis shows that the data are of the right magnitude for agreement with the displacement spike model.

Konobeevsky reasoned that the displacement-spike model was unable to explain the phase-reversal phenomenon. According to Seitz, approximately 5 MeV is liberated in thermal spikes in each fission event in uranium (about 3 % of the kinetic energy of the fission fragments [7]). Since the displacement spike model does not permit the accumulation of a large number of defects with large potential energy (in the above calculation only about 0.1 MeV is dissipated per fission assuming 1 eV per atom as Brinkman suggests), Konobeevsky assumed that the energy was released in the form of a thermal pulse. The energy was considered released at a point source in a sphere whose radius was specified by a maximum temperature of 2000° C. The distribution of the excess temperature was described by:

$$T = \frac{q}{\varrho c}\cdot\frac{1}{(4\pi kt)^{3/2}}\cdot \exp\left(-r^2/4kt\right)$$

where

$$\left(\frac{\partial T}{\partial t}\right)_{t=t_{\max}} = 0 \quad \text{and} \quad t_{\max} = \frac{r^2}{6k}. \qquad (4)$$

Therefore

$$r = \left[\frac{q}{T_{\max}\,\varrho c}\right]^{1/3}\left[\frac{3}{2\pi e}\right]^{1/2}$$

where r is the radius of the sphere, q the energy released in calories, ϱ the density, and c the specific heat of the material. Konobeevsky defined the diffusion coefficient as:

$$D = \frac{1}{27}\, N_0 \pi r^5. \qquad (5)$$

Substituting the above value of D and N_0 into eq. (5), the radius of a spike was found to be 118 Å and from eq. (4) the ratio of $q/T_{\max}$ was determined as 2.76×10^{-4} MeV/°C. Using Konobeevsky's assumption of a maximum temperature of 2000° C, then the energy released within each thermal spike is about 0.6 MeV. This is roughly a factor of ten lower than the value assumed by Konobeevsky. It would appear from these results that the thermal-spike mechanism must be modified so that only about one-tenth of the total energy dissipated as thermal spikes is effective in causing homogenization of the alloy.

5. Conclusions

The phase reversal in U-9 wt % Mo alloy due to neutron bombardment can be explained equally well by assuming that a "displacement" or "thermal" spike is operative in homogenizing the uranium and molybdenum alloys. In the case of the displacement spike it must be assumed that one to two such spikes are produced per fission event, each spike containing about 8×10^4 atoms. The experimental data is also satisfied, if it is assumed that the effective temperature at the radius of a thermal spike is 2000° C, and the total thermal energy released available for homogenization of the alloy is 0.6 MeV. Both of these models are consistent with the experimental observations of this test and can be used to derive the diffusion equation which describes the kinetics of the phase reversal.

The "diffusion coefficient" for the process was determined to be $1.4 \times 10^{-18} \pm 0.6 \times 10^{-18}$ cm^2/sec for a fission rate of 5.25×10^{12} fission/cm^3·sec from six samples which were irradiated under widely divergent conditions. These data show that the "diffusion coefficient" is independent of sample temperature in-pile between $-90°$ C and $+200°$ C, and that it is directly proportional to the fission rate but independent of the neutron flux intensity.

Acknowledgments

The author wishes to express his deep appreciation to Dr. B. Lustman, Manager, PWR Metallurgy Subdivision, Westinghouse Electric Corporation, for his many helpful suggestions and his encouragement throughout the course of these tests. The author wishes to thank Messrs. J. A. Weissburg and C. A. Johnson, of Bettis Plant, for their aid and cooperation in the design of the specimen assembly. Drs. E. K. Halteman, E. R. Boyko, and J. Markowitz of the PWR Metallurgy Subdivision were very helpful in their discussions of the test data. The specimen assemblies were fabricated by Mr. R. Gray and the in-pile facility operated by Mr. L. R. Lynam. The electron micrographs were obtained by Mr. P. Schnizler. The author wishes to express his appreciation to the US Atomic Energy Commission and to the Westinghouse Electric Corporation for permission to publish this work.

This work was performed under AEC Contract No. AT-11-1-GEN-14.

References

1) M. L. Bleiberg, L. J. Jones and B. Lustman, J. Appl. Phys. 21 (1956) 1270
2) S. T. Konobeevsky, J. Nuclear Energy **1** (1956) 356
3) M. L. Bleiberg, 2nd At. Conf. Geneva (1954) P/619
4) M. L. Bleiberg, AEC (USA) Report WAPD-T-767, to be published in Nuclear Science and Engineering
5) G. J. Dienes and G. H. Vineyard, Radiation Effects in Solids (Interscience Publishers, Inc., New York, 1957) p. 45
6) J. A. Brinkman, J. Appl. Phys. **25** (1954) 961
7) F. Seitz, Discussions of the Faraday Society **5** (1949) 271

THE PREPARATION OF A LARGE PLUTONIUM-BERYLLIUM NEUTRON SOURCE

K. L. WAUCHOPE and J. BAIRD

Chemistry and Metallurgy Division, Atomic Energy of Canada Ltd., Chalk River, Ontario, Canada

Received 2 March 1959

A plutonium-beryllium alloy neutron source, containing 100 g of plutonium and 68 g of beryllium, was prepared by the reduction of plutonium dioxide with beryllium followed by vacuum sintering at 1450° C to form a mechanically strong, non-friable compact. The compact was sealed in a double aluminum container. Neutron output from the source is $1.01 \pm 0.03 \times 10^7$ neutrons/second.

In preparation of the source, tongs with 25 cm handles were used in all operations after mixing of the original ingredients, to prevent serious overexposure of personnel.

The source is now in use for the calibration of neutron-counting instruments and for the irradiation of small experimental samples.

On a préparé une source de neutrons avec un alliage plutonium-béryllium, contenant 100 g de plutonium et 68 g de béryllium, de la facon suivante: réduction du dioxyde de plutonium par le béryllium, puis frittage sous vide à 1450° C pour former un compact mécaniquement fort et non friable. Le compact a été scellé dans une gaine double en aluminium. Cette source émet $1.01 \pm 0.03 \times 10^7$ neutrons par seconde.

Une fois les produits originaux mélangés, on a utilisé des pinces avec des bras de 25 cm dans toutes les manipulations au cours de cette préparation pour éviter les dangers d'irradiation sérieux du personnel.

La source est maintenant utilisée pour l'étalonnage des instruments de comptage de neutrons et l'irradiation de petits échantillons expérimentaux.

Eine Neutronenquelle aus einer Plutonium-berylliumlegierung (100 g Plutonium und 68 g Beryllium) wurde durch Reduktion von Plutoniumdioxyd mit Beryllium hergestellt; durch nachfolgendes Sintern bei 1450° C im Vakuum erhielten wir einen mechanisch festen und nicht-zerreissbaren Block aus diesem Material. Dieser Block wurde in einen doppelten Behälter aus Aluminium fest eingeschlossen. Die Anzahl der aus dieser Quelle kommenden Neutronen beträgt $1.01 \pm 0.03 \times 10^7$ sec.

Während der Herstellung der Quelle wurden bei sämtlichen Arbeitsgängen Zangen benutzt, deren Grifflänge 25 cm betrug, um schwere Strahlenschädigungen des Personals zu vermeiden.

Die Quelle wird zur Zeit zur Eichung von Neutronenzählern und Bestrahlung kleiner Versuchsproben benutzt.

1. Introduction

Pressed mechanical mixtures of salts of Ra^{226} or Po^{210} with beryllium have, in the past, been used as neutron sources where outputs exceeding 10^6 neutrons/second have been required.

Radium-beryllium and polonium-beryllium sources have a high neutron output per unit weight, but also have certain disadvantages, notably the high γ field associated with radium-beryllium and the relatively short life of polonium-beryllium due to the 138-day half-life of Po^{210}.

Although the neutron output per unit weight is lower from plutonium-beryllium alloy neutron sources, it does not decrease appreciably with time, due to the 24 360-y half-life of Pu^{239}. In addition, only a small amount of low-energy γ radiation is emitted.

Thus, when a requirement arose for a neutron source with a minimum yield of 10^7 neutrons/second for the calibration of neutron-counting instruments under development by Atomic Energy of Canada Ltd., it was decided that a plutonium-beryllium alloy source should be

used. The methods used in the preparation of such a source, containing approximately 100 g of plutonium, are described below.

2. Methods of Preparation

Plutonium-beryllium alloy neutron sources were prepared at Los Alamos [1]) by melting the two metals together under an inert atmosphere. At Chalk River, Runnalls and Boucher [2]) prepared sources by the reduction of plutonium trifluoride with beryllium in vacuo. The beryllium fluoride product distilled, leaving a fluoride-free source which could then be melted. Both these methods produce solid alloy sources having neutron outputs approaching the theoretical yield.

Michaud and Boucher [3]) have recently prepared sources by the reduction of plutonium dioxide with beryllium in vacuo, followed by sintering at 1450° C to form a compact. The product has been shown metallographically to consist of $PuBe_{13}$ in a porous matrix of beryllium. The presence of beryllium oxide has been demonstrated by X-ray diffraction, but appears to have little effect on neutron yield, the outputs being comparable to those obtained from solid alloy sources. X-ray diffraction of the residue from hydrochloric acid leaching of the compacts has failed to show plutonium dioxide, indicating that reduction is essentially complete.

The latter technique is attractive since it directly utilizes plutonium dioxide which is easily prepared and handled and thus avoids the fluorination step and the preparation and handling of metallic plutonium.

Since no work on the scale required had been done, a preliminary experimental program using uranium dioxide as a stand-in for plutonium dioxide was undertaken. Mixtures of uranium-dioxide and beryllium were heated to 1450° C in an induction heated, quartz-tube-type vacuum furnace, using a graphite tube as a susceptor.

The chief results of the investigation are summarized below:

I. The mixtures showed a marked tendency to outgas at approximately 120° C and again at approximately 420° C. Outgassing was sufficiently violent to cause some material to be blown out of the crucible. Loss of material could be minimized by holding the mixtures at the temperatures indicated until furnace pressure returned to normal.

II. Early compacts were very porous and mushroom shaped at the top. The latter effects could be minimized by placing a weight on the material in the crucible before sintering.

III. If the precautions noted above were taken, mechanically strong, non-friable compacts with densities of 2.0 to 2.5 g/cm^3, approximately 60 % of theoretical, could be prepared.

The large plutonium-beryllium alloy source was therefore prepared by this technique.

3. Beryllium-Plutonium Ratio

High neutron yields per gram of plutonium are obtained from plutonium-beryllium alloy sources at a Be:Pu atom ratio of approximately 200 [2]). At Be:Pu = 200, the yield from a source containing 100 g of plutonium of specific activity approximately 1.6×10^8 dpm/mg would be approximately 1.5×10^7 neutrons/second.

However, the volume of such a source, even assuming close approach to theoretical density on sintering would exceed 500 cm^3. This was considered to be much too large and cumbersome for the intended use.

Optimum neutron yields per unit weight of source are obtained at Be:Pu ratios of approximately 13,[1,4]) at which essentially the entire source consists of the intermetallic compound $PuBe_{13}$. At a Be:Pu ratio of 13, the yield from a source containing 100 g of plutonium of specific activity 1.6×10^8 dpm/mg would be 1.0×10^7 neutrons/second, while the volume, even if only 60 % of theoretical density were achieved in sintering, would not exceed 60 cm^3. However, Michaud and Boucher [3]) have recently found that sources prepared at the above ratio did not sinter well at 1400° C, presumably due to the high melting point of $PuBe_{13}$. This condition was corrected by the addition of a small excess of beryllium.

At a Be:Pu atom ratio of 18, a source containing 100 g of plutonium should have a

neutron output of slightly over 1.0×10^7 neutrons/second. The volume of such a source, 60 % dense and allowing for the beryllium oxide present and the excess beryllium, would not exceed 90 cm^3. The Be:Pu atom ratio of 18 was, therefore, chosen for the large source as representing an acceptable compromise between high neutron yield and reasonable size of the finished source. The two extra atoms of beryllium per atom of plutonium required for the reduction are included in the ratio.

4. Health Precautions

Before work on the source was started, all the planned operations following the mixing of the original ingredients were carried out in mock up using 25 cm tongs for handling, to determine the time required for each step. Calculations of the maximum neutron fields expected to be encountered and maximum allowable exposure times at these levels indicated that use of such tongs would be sufficient protection against overexposure of personnel.

As the work progressed, constant neutron field measurements were made and the exposure time of each operator was closely checked. The measured neutron fields were found to be consistently somewhat lower than the calculated values, but exposure times based on the latter were retained as a safety measure.

The maximum exposure suffered by any of the four operators concerned with preparation of the source was approximately 3 millirad total body and 45 millirad to the hands during a three-day period. While this is not an overexposure, the dose to the hands is high enough to indicate that if routine production of high-output neutron sources were contemplated remote-handling facilities should be provided.

5. Materials

Plutonium dioxide was prepared by precipitation of plutonium from nitric acid solution by oxalic acid crystals, followed by drying and calcination of the oxalate at 650° C for 3 h to form the oxide. The purity of the product was estimated at 99.5 %. Mass-spectrometer analysis showed 5.96 % wt Pu^{240} and 0.49 % wt Pu^{241}. The calculated specific activity of the plutonium was 1.62×10^8 dpm/mg. The oxide powder was ground to −200 mesh.

Commercial beryllium powder, −200 mesh, 99.8 % wt pure was used.

6. Preparation

The materials, in the atomic ratio Be:Pu = 18, i.e. 68 g of beryllium and 114 g of plutonium dioxide, were mixed in a household blender with variable speed control. The neutron emission rate was followed on a neutron counter set up in front of the glove box. After two minutes, no further increase in neutron yield was noted, indicating that substantial mixing had been achieved.

The mixture was transferred to a high purity recrystallized alumina crucible, packed down lightly by tapping the crucible and placed in a vacuum furnace. To prevent loss of material, the furnace was evacuated very slowly to 10^{-4} mm Hg.

The mixture was heated at 10° C/min to 120° C and held at this temperature for 60 min to permit outgassing. Heating was continued at 10° C/min to 420° C where another 60 min were allowed for outgassing. The furnace was then cooled to room temperature under vacuum.

During the above heating cycle, the neutron output from the source was recorded on a neutron counter set up outside the furnace box. Only a very slight increase in neutron yield was noted.

The mixture was removed from the furnace. The presence of a light film of the mixture on the furnace wall and head indicated that a small amount of material had been lost from the crucible. An alumina disc was placed on top of the mixture, followed by a graphite slug weighing 150 g. The mixture was returned to the furnace which was evacuated to 10^{-4} mm Hg, heated at 15° C/min to 1450° C, held at this temperature for 30 min and allowed to cool to room temperature under vacuum.

The neutron output was observed during the heating cycle. Little change was noted until about 700° C had been reached. Between 700° C

and 900° C a rapid increase in neutron output occurred, rising to approximately 1.8 times the original value, indicating that reduction of the plutonium dioxide and formation of the compound $PuBe_{13}$ had taken place. The neutron output remained steady during the remainder of the heating cycle.

A mechanically strong, non-friable compact approximately 4.6 cm in diameter and 5.3 cm in height was produced. The compact weighed 178.2 g indicating a loss of 3.8 g by dusting, loss from the crucible and distillation of beryllium during sintering. The density of the compact as estimated from its dimensions and weight, was 2 g/cm³, approximately 60 % of theoretical. The cylindrical source had necked in slightly in the centre and mushroomed at the top, making it somewhat irregular in shape.

The source was placed in a thin-walled aluminum capsule machined to provide an interference fit. Aluminum foil pads were used bottom and top to prevent possible movement of the source within the container. The capsule was sealed by a screw-in cap, decontaminated, removed from the glove-box line and slip fitted into a heavier aluminum container having a ring at one end to permit easier handling. A sketch of a cross section of the source and containers is shown in fig. 1.

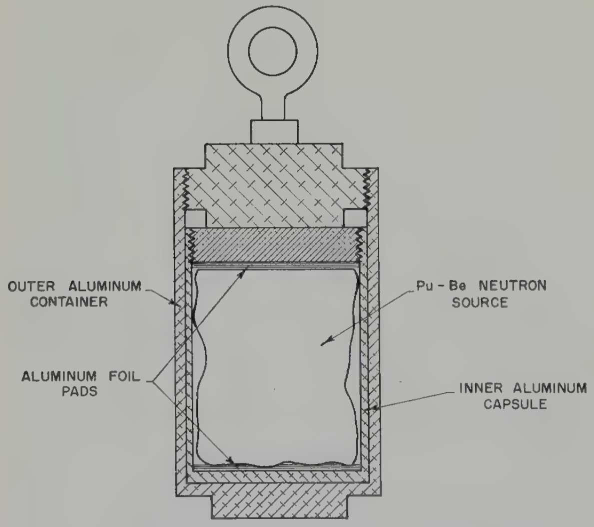

Fig. 1. Cross section of plutonium-beryllium neutron source and containers

7. Calibration

The neutron yield from the source was determined by a direct comparison of its neutron output with that from a standard Chalk River Pu-α-Be source, using the paraffin-block counter described by Runnals and Hanna [5]).

The calibration indicated a neutron yield of $1.01 \pm 0.3 \times 10^7$ neutrons/second. Assuming a final atom ratio Be:Pu = 18 in the source, this is approximately 92 % of the theoretical maximum yield [2, 3]).

8. Discussion of Methods of Preparation

While a quite satisfactory neutron source was prepared by the methods described, it is felt that there is considerable scope for improvement.

Since the preparation of the large source, it has been shown in small-scale work that compacting of the mixed ingredients under 20 000 psi pressure prior to sintering has the following beneficial effects:

I. The density of the finished compact is slightly higher.

II. Change of size and shape of the compact during sintering is very slight.

III. The outgassing step described above is not necessary, the pressed compacts apparently being strong enough to withstand the internal pressures built up during outgassing.

Any such sources prepared in future will therefore be compacted before sintering.

If only occasional sources of this size were required, exposure of personnel to neutron irradiation could be kept sufficiently low by the use of a vacuum furnace designed for easy loading and unloading and by provision of jigs and fixtures for handling of the source during canning. However, if routine production of such sources were contemplated, the provision of remote-handling facilities for all operations might be justified.

References

[1]) R. E. Tate and A. S. Coffinberry, Second International Conference on the Peaceful Uses of Atomic Energy (1958) Paper P/700

[2]) O. J. C. Runnalls and R. R. Boucher, Can. J. of Phys. 34 (1956) 949–58

[3]) G. G. Michaud and R. R. Boucher, Atomic Energy of Canada Ltd Report, CRFD 819. To be published

[4]) S. T. Konobeevsky, Proceedings of a Session of the Academy of Sciences of the USSR on the Peaceful Use of Atomic Energy, Vol. 3 (1955) 362–74

[5]) O. J. C. Runnalls and G. C. Hanna, Can. J. of Phys. 34 (1956) 959–67

JOURNAL OF NUCLEAR MATERIALS - 2 (1959) 196–202 - NORTH-HOLLAND PUBLISHING CO., AMSTERDAM

AN EVALUATION OF THE BERYLLIA-WATER VAPOR REACTION IN AN OPEN-CYCLE AIR-COOLED REACTOR †

R. L. McKISSON

Atomics International, A Division of North American Aviation, Inc., Canoga Park, California, USA

Received 11 March 1959

An expression describing the corrosion rate of a beryllia surface in moist, flowing air has been developed and verified by experiment. The data supports the hypothesis that the rate-controlling step in the corrosion process is the diffusion of the gaseous beryllium hydroxide product through the laminar boundary layer at the beryllia surface. The corrosion rate r is

$$r = 3.19\times 10^7 \frac{D}{T_f t} (Kp_w - p_b) \text{ mm/y}$$

where D is the diffusion coefficient of beryllium hydroxide through air, cm²/sec; T_f is the average temperature of the boundary layer, °K; t is the boundary layer thickness, cm; K is the equilibrium constant; p_w is the partial pressure of water vapor, atm; and p_b is the partial pressure of beryllium hydroxide product in the bulk gas stream, atm. This equation, when used to predict the corrosion rates expected in the operation of an open-cycle, air-cooled, beryllia moderated power reactor, indicates that the corrosion reaction will not limit the feasibility of operation at beryllia surface temperatures below 860° C.

Une formule exprimant la vitesse de corrosion superficielle de l'oxyde de béryllium sous un courant d'air humide a été développée et vérifiée expérimentalement. Les résultats permettent d'avancer l'hypothèse que le phénomène dont dépend la vitesse de corrosion est la diffusion de l'hydroxyde de béryllium gazeux à travers les couches limites laminaires à la surface de l'oxyde de béryllium. La vitesse de corrosion r est donnée par l'expression suivante:

$$r = 3.19\times 10^7 \frac{D}{T_f t} (Kp_w - p_b) \text{ mm/an}$$

où D est le coefficient de diffusion de l'hydroxyde de béryllium à travers l'air en cm²/sec; T_f la température moyenne entre les couches limites en °K; t l'épaisseur des couches limites en cm; K la constante d'équilibre; p_w la pression partielle de la vapeur d'eau en atmosphères; p_b la pression partielle de l'hydroxyde de béryllium produit dans le courant gazeux en atmosphères. Utilisée pour prévoir les vitesses de corrosion dans un réacteur en marche, en cycle ouvert, refroidi à l'air et modéré avec de l'oxyde de béryllium, cette équation indique que la réaction de corrosion n'empêchera pas l'opération pour une température inférieure à 860° C à la surface de l'oxyde de béryllium.

Eine Gleichung, die die Korrosionsgeschwindigkeit einer Berylliumoxydoberfläche in strömender, feuchter Luft beschreibt, wurde aufgestellt und durch Versuche bestätigt. Die Ergebnisse unterstützen die Hypothese, dass die Diffusion des entstehenden gasförmigen Berylliumhydroxydes durch die laminare Grenzschicht an der Berylliumoxydoberfläche der die Korrosionsgeschwindigkeit bestimmende Vorgang ist. Die Korrosionsgeschwindigkeit beträgt:

$$r = 3.19\times 10^7 \frac{D}{T_f t} (Kp_w - p_b) \text{ mm/Jahr}$$

wobei D der Diffusionskoeffizient von Berylliumhydroxyd in Luft ist (cm²/sec); T_f bedeutet die durchschnittliche Temperatur der Grenzschicht (in °K), t die Dicke der Grenzschicht (in cm) und K die Gleichgewichtskonstante; p_w is der Dampfdruck des Wassers und p_b der des Berylliumhydroxydes in der gesamten Gasströmung (beide in atm). Wenn die Gleichung für die Berechnung der Korrosionsgeschwindigkeit beim Betrieb eines luftgekühlten, mit Berylliumoxyd moderierten Kraftreaktors mit offenem Kreislauf angewandt wird, zeigt sich, dass die Korrosion die Betriebsfähigkeit nicht einschränkt, vorausgesetzt die Oberflächentemperatur des Berylliumoxydes bleibt unter 860° C.

†) This work was done under the auspices of the US Atomic Energy Commission under Contract AT–11–1–GEN–8.

A major objective in the design of power reactors is that heat be delivered at the highest practical temperature because of the higher potential efficiency of the conversion to power. Exit temperatures of the primary coolants of pressurized water and boiling water power reactors are in the 200° to 300° C range, and coolants of gas-cooled graphite-moderated power reactors operate to 340° C. The polyphenyl moderator-coolant of the organic moderated reactors is available at 370° C; and primary coolant exit temperatures in liquid metal cooled reactors are in the range 480°–570° C. In these power reactor systems, the heat is used to generate electrical power through a steam cycle, and their efficiencies approach those of conventional steam plants. If exit gas temperatures of 700° C (1300° F) or higher could be attained, an efficient gas turbine cycle can be visualized [1]). One such system which might prove feasible for small scale applications is an open-cycle air-cooled beryllia-moderated reactor.

Although there are many problems associated with demonstrating the feasibility of such a reactor system, this paper will concern itself only with the corrosion of the beryllia moderator through reaction with the water vapor in the air. The chemical reaction produces a gaseous product [2, 3, 4]) so that in an open cycle system, beryllia is continually lost from the surface during operation. This paper will examine the extent of this corrosion and establish allowable surface temperature levels for the beryllia moderator.

Consider a reactor consisting of an assembly of alternating moderator and fuel plates separated by air passages as shown in fig. 1. The air is heated primarily by the fuel plates, and to a much lesser extent by the moderator. The air flow rates would be rather high so that the flow would be turbulent. The corrosion process can then be visualized as the sequence: (1) transfer of water vapor to the surface, (2) the reaction with the BeO, and (3) the transfer of the product $Be(OH)_2$ into the gas stream. In a turbulently flowing gas stream, two well-defined regions of flow are present. Most of the gas flows in the

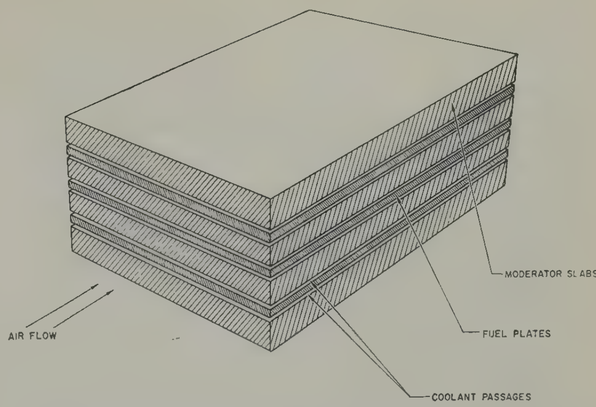

Fig. 1. Schematic diagram, flat plate reactor.

"turbulent core", that is, in the region away from the wall. Lateral movement of gaseous species in the core is effected by eddy diffusion, a rapid process relative to molecular diffusion. Because of this, concentration gradients are relatively low, and can frequently be neglected. However, the gas adjacent to the wall moves in laminar flow, and very little lateral mixing occurs. Lateral transfer of material can take place by molecular diffusion, however, since steady state concentration gradients can be developed in this boundary layer. Using these concepts, process (1) above can be considered primarily as the diffusion of water vapor from the turbulent core through the laminar boundary layer to the surface; and process (3) becomes the diffusion of $Be(OH)_2$ across the boundary layer to the bulk stream in which it is rapidly mixed.

The rate-controlling step in this sequence would appear to be step (3). Step (1), the diffusion of water vapor, should not be a factor because of the relatively high concentration level of the water vapor (0.08–0.4 atm). A gradient in the water vapor concentration undoubtedly exists across the boundary layer, but it is so small that the $H_2O(g)$ concentration at the surface is essentially equal to that in the bulk phase. On the other hand, step (3), the diffusion of $Be(OH)_2$, will be important to the kinetics because of the very low concentration of $Be(OH)_2(g)$ at the surface. Therefore, even a small concentration gradient with its low

diffusion rate markedly reduces the concentration of $Be(OH)_2(g)$ at the surface, and causes the reaction to proceed as the $Be(OH)_2(g)$ is removed. Step (2) cannot be entirely discounted as rate-controlling, but it does not seem likely that the chemical reaction rate would be slow enough at the temperatures involved to be the controlling factor. Therefore, the most likely rate-controlling step is the diffusion of the $Be(OH)_2$ gaseous product away from the surface.

On this assumption, then, one can derive an expression for the rate of corrosion by assuming a system consisting of the steady state diffusion of $Be(OH)_2$ through a layer of non-diffusing gas. Even though the air in the boundary layer is moving along the tube, a well-defined concentration gradient of $Be(OH)_2$ is established at every point y during steady state operation. For this case, the rate of transfer of $Be(OH)_2$ through the boundary layer is given by Sherwood [5])

$$N = \frac{DP}{RT_f t} \ln \left[\frac{P - p_b}{P - p_s}\right], \qquad (1)$$

where N is the transfer rate, g mol/sec·cm² of surface; D is the diffusion coefficient, cm²/sec; P is the total pressure, atm; R is the gas constant, 82.1 cm³·atm/g mol·°K; T_f is the film temperature, °K; t is the boundary layer thickness, cm; p_b is the partial pressure of $Be(OH)_2$ in the bulk gas, atm; and p_s is the partial pressure of $Be(OH)_2$ at the surface, atm. The geometry of the system is shown in fig. 2.

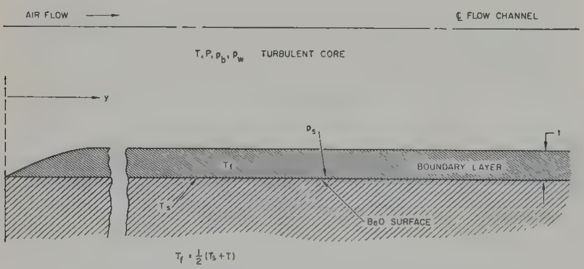

Fig. 2. Diffusion system geometry.

If equilibrium is assumed at the surface, the equilibrium constant K relates p_w to p_s,

$$p_s = K p_w. \qquad (2)$$

Further, if p_b and p_s are small relative to P, the following substitution can be made,

$$\ln \left[\frac{P - p_b}{P - p_s}\right] \cong \frac{1}{P}(p_s - p_b). \qquad (3)$$

Now, combining (1), (2), and (3), one finds,

$$N = \frac{D}{RT_f t}(K p_w - p_b) \text{ g mol/sec·cm}^2. \qquad (4)$$

In eq. (4), D, the diffusion coefficient for $Be(OH)_2$ through air, can be estimated using a relation given by Sherwood,

$$D = \frac{0.0043\, T^{3/2}}{P(V_A^{1/3} + V_B^{1/3})^2} \sqrt{\frac{1}{M_A} + \frac{1}{M_B}} \text{ cm}^2/\text{sec}, \qquad (5)$$

where the V's are measures of the molecular volumes, the M's are the molecular weights and T is measured in °K. Using the value for air given by Sherwood, $V_A = 29.9$, and assuming $V_B = 27.2$ for $Be(OH)_2$, eq. (5) reduces to

$$DP = 2.76 \times 10^{-5} T_f^{3/2} \text{ atm·cm}^2/\text{sec}. \qquad (6)$$

The boundary layer thickness t can be estimated by an expression given by Jakob [6])

$$t = 25.25\, d(\mathrm{Re})^{-3/4} \text{ cm}, \qquad (7)$$

where d is the hydraulic diameter of the flow channel, cm, and Re is the Reynold's number for the flow. The equilibrium constant for the reaction

$$BeO(s) + H_2O(g) = Be(OH)_2(g) \qquad (8)$$

is given by Grossweiner and Seifert [2]),

$$\log_{10} K = 1.63–9060/T_s. \qquad (9)$$

The partial pressure of water vapor, p_w, is related to the humidity, H (g water/g dry air),

$$p_w = P \left[\frac{1.6\, H}{1.6\, H + 1}\right]. \qquad (10)$$

The average rate of loss of a corroding surface is given by

$$r = (8760)(10)(3600)(N M_s/\varrho_s) \text{mm/y}. \qquad (11)$$

For a dense beryllia surface, $M_s = 25$ g/g mol and $\varrho_s = 3$ g/cm³. The combination of (4) and (11),

with the substitution of the numerical value of R, reduces to

$$r = 3.19 \times 10^7 \frac{D}{T_f t} (Kp_w - p_b) \text{ mm/y.} \quad (12)$$

Eq. (12), together with (6), (7), (9), and (10), describes the local rate of corrosion of a BeO surface in humid air when the rate-controlling step is the diffusion of the $Be(OH)_2$ product away from the surface. Although (12) can be used in a step-wise procedure to find the values of p_b as a function of y along the length of the passage, a preliminary study such as this need only be concerned with the maximum corrosion rate. For this purpose, (12) can be evaluated for the maximum BeO wall temperature, and for $p_b = 0$.

It is of interest to investigate experimentally the validity of eq. (12). To this end, the apparatus shown in fig. 3 was built. Briefly, its

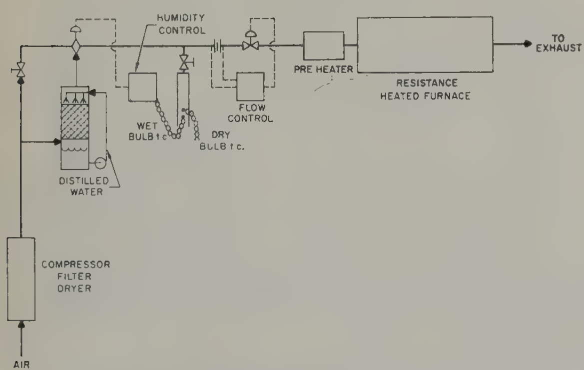

Fig. 3. Schematic diagram of test apparatus.

operation is as follows: A dried, compressed air stream is divided so that one part passes through a counter-current flow pebble bed humidifier and thence to a mixing valve. The remaining air passes through a needle valve to the mixing valve. The mixing valve controls the amount of humid air which is added to the dry air stream in response to a wet bulb thermocouple temperature controller. The wet bulb temperature corresponding to the desired humidity and dry bulb temperature is set into the controller as the control point.

The controlled humidity air stream passes through a flow control system comprising a

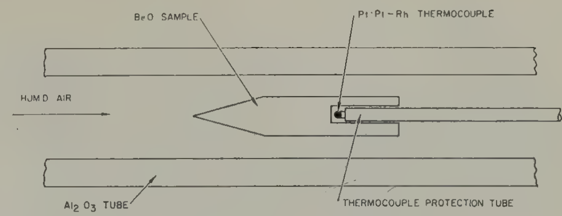

Fig. 4. Assembly of BeO sample.

modified venturi, a Minneapolis Honeywell Tel-O-Set control system, and a control valve. The air is then heated by passing through the pre-heater and finally through the heated alumina furnace tube. The hot humid air passes over a BeO probe supported on a thermocouple inside the furnace tube as shown in fig. 4. Weight losses from the probe are measured and compared with the corresponding values from eq. (12). Because of the extremely low weight loss rates obtaining at the temperatures of interest for an open cycle reactor, the experiments were performed at higher temperatures at which loss rates permit the measurements to be taken in a few hours.

Table 1 is a summary of the observed data. The calculated corrosion rates are found to range from a lower extreme of 0.35 of the observed rate to the higher extreme of 2.50 of the observed rate, neglecting Runs 1–1 and 3–3, for which no losses were observed. Of the eighteen remaining observations, fourteen show overall agreement within a factor of two. The reproducibility of the data is shown in the first set of data in table 2. Although the test conditions are nearly constant, the observed loss rates vary from 2.0 mm/y to 6.7 mm/y. These data show that while the average of several equivalent determinations may be within 20 % of the value predicted by eq. (12), any single value may deviate by ± 50 %. This observation is also demonstrated by an examination of the ratio column of table 1.

The temperature dependence of the observed loss rates is also illustrated in table 2. Eq. (12) predicts a 2.15-fold increase in loss rate over the temperature interval 1580° to 1675° K, and a 2.2-fold increase in the average values is observed. Although the high degree of agreement

TABLE 1

Summary of Data

No.	Temp.	Flow Rate	Humidity	Duration	Total Pressure	Corrosion Rate, r		Ratio
	T_s (°K)	Q (liters/min)	H (g H_2O/g air)	(h)	P (atm)	obs (mm/y)	calc (mm/y)	calc/obs
1–1	1595	101	0.0031	2	1.35	0.0	1.1	∞
1–2	1590	88	0.0315	2	1.30	21.0	9.4	0.45
1–3	1585	89	0.0145	4	1.35	6.1	4.3	0.71
1–4	1580	210	0.0157	4	2.00	5.6	5.3	0.95
2–1	1580	210	0.0137	4	1.95	3.2	4.7	1.48
2–2	1680	92	0.0149	3	1.35	16.9	5.9	0.35
2–3	1680	88	0.0300	3	1.30	19.8	11.2	0.56
2–4	1580	208	0.0147	4	1.85	6.7	4.7	0.70
2–5	1580	208	0.0147	4	1.85	2.0	5.0	2.50
3–1	1580	202	0.0148	4	1.80	5.6	4.7	0.84
3–2	1580	206	0.0145	4	1.80	2.4	4.7	1.96
3–3	1680	162	0.0017	4	1.70	0.0	1.1	∞
3–4	1680	322	0.0019	3.6	2.35	1.8	2.0	1.11
4–1	1675	202	0.0150	3	1.90	9.5	10.3	1.08
4–2	1675	149	0.0150	4	1.25	9.2	8.0	0.87
4–3	1720	63	0.0100	3	1.10	15.1	6.0	0.40
4–4	1705	58	0.0260	2	1.10	26.1	13.0	0.50
4–5	1675	117	0.0150	4	1.15	6.7	6.7	1.00
4–6	1675	118	0.0150	4	1.15	8.3	6.7	0.81
5–1	1680	211	0.0150	4	1.45	9.5	11.0	1.16

TABLE 2

Temperature-Dependence Data

No.	Temp.	Flow Rate	Humidity	Total Pressure	Corrosion Rate	
	T_s (°K)	Q (liters/min)	H (g H_2O/g air)	P (atm)	Obs (mm/y)	Calc (mm/y)
1–4	1580	210	0.0157	2.00	5.6	5.3
2–1	1580	210	0.0137	1.95	3.2	4.7
2–4	1580	208	0.0147	1.85	6.7	4.7
2–5	1580	208	0.0147	1.85	2.0	5.0
3–1	1580	202	0.0148	1.80	5.6	4.7
3–2	1580	206	0.0145	1.80	2.4	4.7
Avg.	1580	206	0.0147	1.9	4.3	4.9
4–1	1675	202	0.0150	1.90	9.5	10.3
5–1	1680	211	0.0150	1.45	9.5	11.0
Avg.	1680	206	0.0150	1.70	9.5	10.7

here is undoubtedly fortuitous in view of the spread in individual values, a close relation is indicated.

The dependence of the loss rate on flow rate, Q, is illustrated in table 3. An analysis of eq. (12) shows that the loss rate, $\bar{r}$, should have a $^3/_4$ power dependence upon Q. Neglecting 2–2, one sees that the observed losses rise with increasing Q, and generally follow the trend of the calculated values.

The effect of humidity upon the loss rate is shown by examination of the data of table 4. The expected dependence is linear for small values of H. The table shows four sets of data having various ratios of H from 2 to 10, and the observed loss rates are in general agreement with a linear relation.

Although close agreement between the observed corrosion rates and the calculated rates is not found, it is felt that variances of the order of a factor of two are not unreasonable in view of the nature of the measurement and the assumptions involved. The greatest uncertainty is the evaluation of t by eq. (7). This relation applies to well-developed flow in which t is constant with y, while the experimental condition is similar to an entry-condition in which the boundary layer is building up. The result of this is that the effective t is smaller than the calculated t so that the calculated results should tend to be low. Uncertainties in the corrosion rate ranging up to $\pm$ 5 percent are predicted by the uncertainties in the values of flow rate and humidity. The effect on r of $\pm$ 10° C uncertainty

TABLE 3
Flow Rate Dependence Data

No.	Temp.	Flow Rate		Humidity	Total Pressure	Corrosion Rate, r	
	T_s (°K)	Q (liters/min)	$Q^{3/4}$ (liter/min)$^{3/4}$	H (g H_2O/g air)	P (atm)	Obs (mm/y)	Calc (mm/y)
2–2	1680	92	30.	0.0149	1.35	16.9	5.9
4–5	1675	117	35.5	0.0150	1.15	6.7	6.7
4–6	1675	118	36.	0.0150	1.15	8.3	6.7
4–2	1675	149	42.5	0.0150	1.25	9.2	8.0
4–1	1675	202	52.	0.0150	1.90	9.5	10.3
5–1	1680	211	53.	0.0150	1.45	9.5	11.0

TABLE 4
Humidity Dependence Data

No.	Temp.	Flow Rate	Humidity	Total Pressure	Corrosion Rate, r	
	T_s (°K)	Q (liters/min)	H (g H_2O/g air)	P (atm)	Obs (mm/y)	Calc (mm/y)
1–2	1590	88	0.0315	1.30	21.0	9.4
1–3	1585	89	0.0145	1.35	6.1	4.3
1–1	1595	101	0.0031	1.35	0.0	1.1
2–3	1680	88	0.0300	1.30	19.8	11.2
2–2	1680	92	0.0149	1.35	16.9	5.9
5–1	1680	211	0.0150	1.45	9.5	11.0
3–3	1680	162	0.0017	1.70	0.0	1.1
3–4	1680	322	0.0019	2.35	1.8	2.0
4–4	1705	58	0.0260	1.10	26.3	13.0
4–3	1720	63	0.0100	1.10	15.1	6.0

in temperature is of the order of $\pm$ 10 %. In view of this, then, the degree of agreement of the observed and calculated values of r is adequate, and eq. (12) describes the loss of BeO in a humid air stream.

Further, the assumption that the reaction at the interface is not a controlling factor is verified by the temperature and flow dependence observations. It is not likely that the temperature dependencies of the chemical reaction and of the diffusion process would be the same; and essentially no flow-dependence would be expected if the chemical reaction were controlling. Therefore, it must be concluded that the process is diffusion controlled.

Eq. (12) has been evaluated for a set of typical flow conditions for a small open-cycle reactor [1]). These corrosion rates are summarized in Curve B of fig. 5. In addition, the effect of variation in humidity is shown in Curves A and C; and the effect of flow rate, in Curve D.

A reactor of the type under discussion should have a nominal life of 10 to 20 years. During this time, a loss of 1 % of the BeO moderator should be tolerable. Therefore, the maximum allowable penetration rate for 20-year service would be about 0.00635 mm/y for a reactor having a moderator plate thickness of 2.54 cm[7].

Examination of fig. 5 shows that for a nominal 2 % humidity (curve B, dew point of 25° C or 77° F at 1 atm pressure), a corrosion rate of 0.00635 mm/y would be expected at $T_s = 1135°$ K or 860° C †. This wall temperature could produce an output gas temperature of about 830° C. If the air were usable at 975° K (700° C or 1300° F) for which $T_s = 1000°$ K, the expected nominal corrosion rate for 2 % humidity would be 7×10^{-4} mm/y for the lower flow rate of 63 liters/min · cm², and about 2.4×10^{-3} mm/y for the higher flow rate of 315 liters/min · cm².

It is therefore concluded that the BeO–H_2O interaction will not limit the feasibility of operating an open cycle, BeO moderated power reactor at passage surface temperatures up to 860° C.

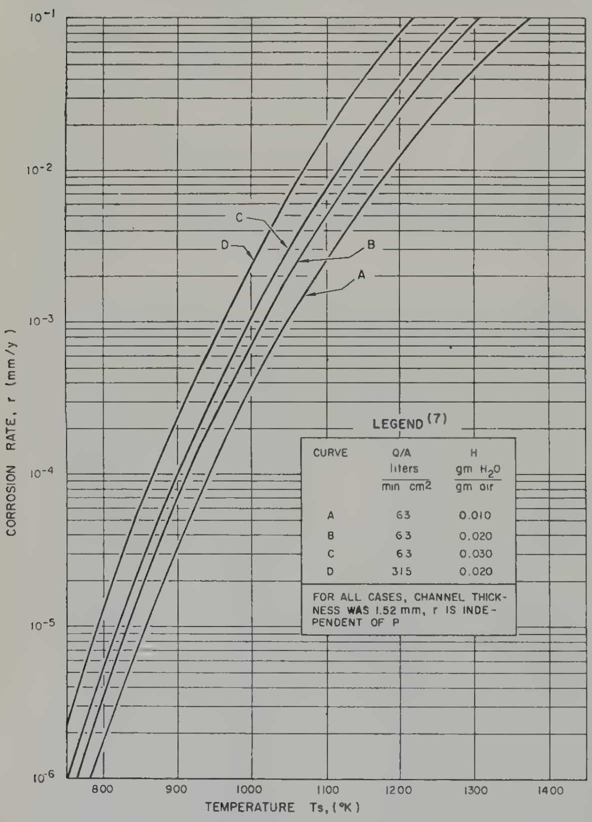

Fig. 5. BeO corrosion rates calculated by eq. (12).

References

1) S. T. Robinson, C. H. Fox, J. G. Gallagher and T. Jarvis, "Nuclear Gas Turbines", (a Symposium), Mechanical Engineering **78** (1956) 606

2) L. I. Grossweiner and R. L. Seifert, J. Am. Chem. Soc. **74** (1952) 2701

3) C. A. Hutchison, Jr. and J. G. Malm, J. Am. Chem. Soc. **71** (1949) 1338

4) G. R. B. Elliott, "Gaseous Hydrated Oxides, Hydroxides, and Other Hydrated Molecules", University of California Radiation Laboratory (USA) Report, UCRL 1831 (June 1952)

5) T. K. Sherwood, "Absorption and Extraction" (McGraw–Hill Co. Inc., New York, 1937)

6) M. Jakob, "Heat Transfer", Vol. I (John Wiley & Sons, Inc., New York, 1949) p. 437

† These calculations were originally made in English units and converted to metric units for this report. The allowable corrosion rate corresponds to 0.25 mil/y, and is expected at 1560° F from curve B of fig. 5. This curve was based upon a flow rate of 40 standard cubic feet per minute in an 0.005 ft × 4 ft channel. The corrosion rate expected for 1300° F air (T_s = 1340° F = 1800° R) is 0.026 mil/y for 40 standard cubic feet per minute flow and 2 % humidity, and 0.09 mil/y for 200 standard cubic feet per minute (315 liter/min · cm²) flow and 2 % humidity.

JOURNAL OF NUCLEAR MATERIALS - 2 (1959) 203–209 - NORTH-HOLLAND PUBLISHING CO., AMSTERDAM

EVALUATION DU VOLUME D'UNE POINTE DE FISSION DANS L'URANIUM

Y. QUÉRÉ et F. NAKACHE

Centre d'Etudes Nucléaires de Saclay, Gif-sur-Yvette (S & O), France

Reçu le 20 mars 1959

Le nombre des défauts de réseau créés dans l'uranium par irradiation aux neutrons présente une rapide saturation qui peut être mise en évidence par des mesures de conductibilité électrique. Cette saturation est due à l'existence, pour chaque fission, d'un domaine d'intense agitation thermique, la "pointe de fission", dans lequel les défauts déjà existants sont annihilés. A ce phénomène se superpose une évolution des défauts à la température d'irradiation (température ambiante). On peut dégager ces deux effets l'un de l'autre et évaluer le volume de la pointe de fission à 2.10×10^{-16} cm^3 $\pm$ 0.20×10^{-16} cm^3.

The number of lattice defects formed in uranium by neutron irradiation shows a rapid saturation which can be demonstrated by electrical conductivity measurements. This saturation arises from the existence of a region of intense thermal agitation, the "fission spike", associated with each fission. In this region pre-existing defects are annihilated. A diminution of defects at the temperature of irradiation (room temperature) is superimposed on this effect. It is possible to disentangle these two effects and determine that the volume of the "fission spike" is 2.10×10^{-16} cm^3 $\pm$ 0.20×10^{-16} cm^3.

Die Zahl der durch Neutronenbestrahlung in Uran erzeugten Gitterstörungen erreicht rasch einen Sättigungswert, der durch Messungen der elektrischen Leitfähigkeit festgestellt werden kann. Diese Sättigung ist veranlasst durch das Entstehen einer Zone intensiver Wärmebewegung für jede Spaltung. In dieser "fission peak" genannten Zone werden bestehende Gitterstörungen eliminiert. Diese Erscheinung ist überlagert durch Störungen, die bei der Temperatur der Bestrahlung (atmosphärische Temperatur) entstehen. Beide Erscheinungen können approximativ getrennt analysiert werden. Das Volumen des "fission spike" wird zu 2.10×10^{-16} cm^3 $\pm$ 0.2×10^{-16} cm^3 geschätzt.

1. Introduction

L'irradiation aux neutrons d'un cristal crée des défauts *transitoires* (défauts électroniques, phonons) et des défauts *permanents* – défauts de réseau (défauts ponctuels, tels que lacunes et intersticiels, mais aussi des dislocations ou même des macles).

L'évolution de ces défauts au cours de l'irradiation, donc finalement le nombre de défauts créés, est essentiellement différente suivant que le matériau est fissile ou non.

Dans le cas d'un matériau non fissile, ce sont surtout les chocs élastiques neutron-atome qui perturbent le réseau. Ces chocs produisent des déplacements d'atomes et la densité des défauts ainsi créés est alors une fonction assez régulièrement croissante du flux intégré de neutrons.

Pour un matériau fissile, l'évènement important – en termes de défauts créés – est moins l'arrivée du neutron dans le réseau que la fission qu'il est susceptible de produire.

En effet, l'énergie du neutron incident est par exemple de 0.025 eV (neutron thermique) alors que, après fission, deux particules (atomes de fission) d'un diamètre bien supérieur sont projetées dans le réseau avec une énergie d'environ 83 MeV chacune. Ces atomes de fission sont les vrais responsables des perturbations créées dans le réseau.

Leur énergie se dissipe au cours de leur ralentissement suivant deux processus:

Ionisation des atomes (phénomène prépondérant au début du ralentissement, de 83 à 2 MeV environ);

Déplacements d'atomes en cascade et mise en vibration du réseau.

L'évolution, pour une fission, des défauts permanents est alors régie par le schéma suivant:

1) Création par chocs d'un nombre important de défauts permanents dans une zone allongée suivant la trajectoire de la particule de fission (le long de sa trajectoire, la particule de fission heurte et chasse de leur site des atomes du réseau qui, à leur tour, en chassent d'autres, etc.) avec en fin de trajectoire, une région sans doute plus dense en défauts.

2) Vibration du réseau (phonons) dans un domaine de taille bien supérieure à celle des zones précédentes, domaine où l'agitation thermique est intense. Ce domaine subit sans doute une trempe brutale qui laisse subsister les défauts qui pouvaient s'y être créés. Mais l'effet primordial de l'agitation dans un tel domaine est, au contraire, la disparition des défauts "permanents" qui s'y trouvaient précédemment.

Cette double action de la fission est schématisée sur la figure 1.

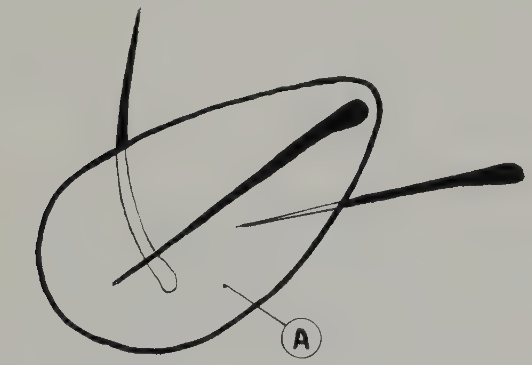

Fig. 1. Schéma simplifié d'une pointe de fission.

Nous appellerons désormais "pointe de fission", le domaine où précisément tous les défauts antérieurs se trouvent annihilés par recuit. ("A" sur la figure).

N.B. Cette action N⁰ 2 est bien mise en évidence pour les faibles irradiations d'uranium écroui par la diminution de microdureté et l'affinement des raies de diffraction des rayons X. Elle joue sans doute aussi un rôle dans l'homogénisation par irradiation des eutectoïdes U/Mo à 9 pds % ($U_\alpha + U_2Mo$).

Il est alors naturel de s'attendre à une saturation assez rapide du nombre de défauts créés par irradiation dans les métaux fissiles. Des mesures de conductibilité électrique à faibles taux d'irradiation mettent en évidence cette saturation.

La rapidité avec laquelle on l'atteint doit permettre d'évaluer le volume de la pointe de fission.

2. Dispositions Experimentales

Nous avons mesuré la résistance électrique de fils d'uranium avant et après irradiation aux neutrons thermiques.

2.1. Echantillon de mesure

L'uranium utilisé est de l'uranium naturel. Il contient comme impuretés principales:
Si = 90 ppm Cu = 20 ppm Fe = 20 ppm
(le carbone n'est pas dosé).

Les fils ont un diamètre de 0.2 mm. Après un recuit de 3 h à 850° C avec refroidissement lent et palier en haut de la phase α, ils sont formés de grains plus gros que le diamètre.

Après polissage électrolytique, un fil est introduit en épingle à cheveux dans deux canaux d'un tube d'alumine à 4 canaux. En accolant deux de ces tubes et en utilisant les autres canaux pour les arrivées de courant et les prises de potentiel, on obtient un échantillon

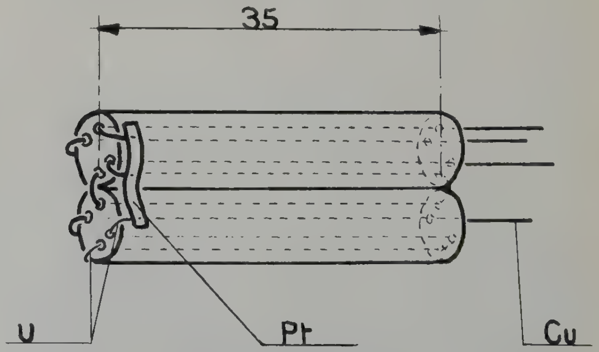

Fig. 2. Enchantillon de mesure. 35 mm.

rigide où l'uranium est bien protégé contre les chocs (fig. 2).

La liaison entre uranium et cuivre est réalisée par des plaquettes de platine soudées par points.

2.2. Irradiation

Les échantillons sont irradiés dans des containers en magnésium sous atmosphère d'hélium. On évite ainsi, grâce à l'excellente conductibilité thermique de l'hélium, l'échauffement et l'oxydation de l'uranium.

Les containers sont vidés puis remplis d'hélium (sous 2 kg/cm²) au moyen d'un tube de cuivre brasé au couvercle, qui est ensuite pincé et coupé (voir fig. 3).

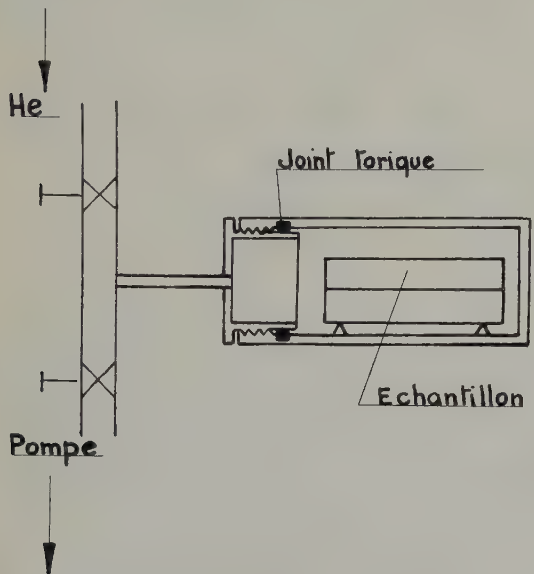

Fig. 3. Container d'irradiation pendant le remplissage d'hélium.

Les irradiations sont faites dans les canaux de radioéléments des piles EL 1 (ZOE) de Fontenay aux Roses et EL 2 de Saclay.

Les plus fortes irradiations (8 jours dans EL 2) correspondaient à un flux de neutrons de 1.6×10^{18} neutrons/cm², soit un taux d'irradiation d'environ 3 MWJ/tonne (il s'agit d'uranium naturel).

2.3. Mesures

La résistivité supplémentaire due aux défauts de réseau étant à peu près indépendante de la température — donc relativement plus importante aux basses températures (loi de Matthiesen) — les mesures de résistance sont faites à la température de l'azote liquide.

Nous utilisons un pont de Kelvin qui permet une précision de 10^{-4}.

Les mesures sur les échantillons irradiés sont faites 8 jours environ après sortie de pile. Leur activité est suffisamment réduite pour qu'on puisse les manipuler derrière de faibles épaisseurs de plomb.

Pendant le raccordement (par brasure à l'étain) du circuit de mesure aux 4 fils de cuivre de l'échantillon irradié, celui-ci se trouve dans une boite en plomb (fig. 4).

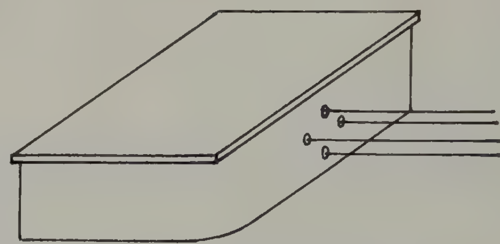

Fig. 4. Disposition de l'échantillon pendant son raccordement au circuit de mesure.

Pendant la mesure, cette boite sert de couvercle au vase Dewar plein d'azote liquide. Le vase est lui-même entouré d'une gaine de 15 mm de plomb (fig. 5).

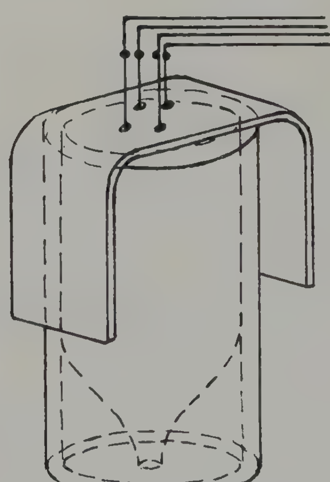

Fig. 5. Disposition de l'échantillon pendant la mesure.

L'ensemble se trouve dans une sorbonne munie d'une vitre au plomb.

Tous les appareils de mesure sont à l'extérieur de la sorbonne.

3. Resultats

Nous avons porté sur la figure 6:

En ordonnées, le rapport $\triangle R/R_0$ où R_0 est la résistance d'un échantillon avant irradiation et $\triangle R$ sa variation de résistance par irradiation.

En abscisses, le flux intégré de neutrons thermiques.

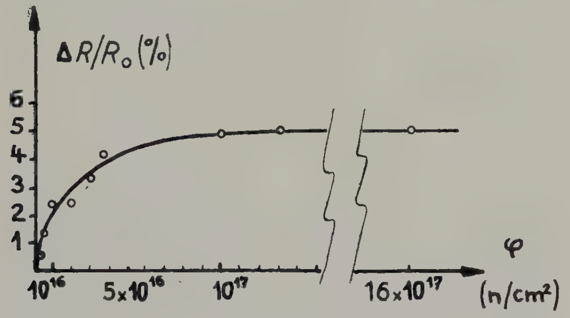

Fig. 6. Variation relative de résistance par irradiation (résultats bruts).

On voit que la saturation de l'excès de résistivité est atteinte pour environ 2×10^{17} neutrons/cm².

Nous pouvons déduire de cette courbe un ordre de grandeur du volume v de la pointe de fission.

Désignons, en effet, par:

$N(t)$ le nombre de défauts par unité de volume (essentiellement des défauts ponctuels) au temps t. $(N(0)=0)$;

ν le nombre de fissions par unité de temps dans l'unité de volume;

K le nombre de défauts créés par unité de temps dans l'unité de volume d'uranium (K est proportionnel à ν).

Nous savons (loi de Matthiesen) que

$$\left(\frac{\Delta R}{R_0}\right)_t \propto N(t).$$

Or, la variation de $N(t)$ entre le moment t et le moment $t+\mathrm{d}t$ est déterminée par:

La création de $K\mathrm{d}t$ défauts;

La disparition de $\nu\, v\, N\mathrm{d}t$ défauts balayés dans le volume total $\nu\, v\mathrm{d}t$ des pointes de fission.

Soit donc:

$$\mathrm{d}N(t)=K\,\mathrm{d}t-\nu\, v\, N(t)\mathrm{d}t$$

dont la solution (avec la condition $N(0)=0$) est: $N(t)=N(\infty)[1-\exp(-\nu\, vt)]$ où

$$N(\infty)=\frac{K}{\nu v}.$$

Pour les variations de résistivité, nous avons alors une loi analogue:

$$\left(\frac{\Delta\varrho}{\varrho_0}\right)_t=\left(\frac{\Delta\varrho}{\varrho_0}\right)_\infty\cdot[1-\exp(-\nu\, vt)].$$

Si $\sum_f$ est la section efficace macroscopique de fission de l'uranium utilisé,

φ le flux intégré de neutrons au moment t,

$\varphi_{\frac{1}{2}}$ le flux intégré correspondant à la demi-saturation, nous avons:

$$\left(\frac{\Delta\varrho}{\varrho_0}\right)_t=\left(\frac{\Delta\varrho}{\varrho_0}\right)_\infty\cdot[1-\exp(-v\textstyle\sum_f\varphi)]$$

et, en particulier:

$$\tfrac{1}{2}=1-\exp(-v\textstyle\sum_f\varphi_{\frac{1}{2}})$$

soit

$$v=\frac{\log 2}{\sum_f\cdot\varphi_{\frac{1}{2}}}=\frac{3.95\ \mathrm{cm}}{\varphi_{\frac{1}{2}}(\mathrm{neutrons/cm^2})}$$

avec $\sum_f=0.175\ \mathrm{cm^{-1}}$ pour l' uranium naturel.

Nous voyons sur la figure 6, que nous pouvons prendre $\varphi_{\frac{1}{2}}=1.6\times 10^{16}$ d'où une valeur approximative, pour v, de $2.5\times 10^{-16}\ \mathrm{cm}^3$ qui va nous être utile pour la discussion.

3.1. Discussion de $\triangle R/R_0$

La courbe de la figure 6 nous indique la variation du nombre de défauts avec l'irradiation.

Aux deux causes de variations que nous avons mentionnées au début:

Création de défauts par irradiation;

Annihilation de défauts par agitation thermique dans la pointe de fission,

il faut ajouter l'évolution naturelle des défauts à température d'irradiation (qui est la température ambiante).

On peut connaître cette évolution en dehors de la pile, en suivant la résistance d'un échantillon, après défournement, en fonction du

temps. Nous avons observé une rapide saturation de cette évolution (fig. 7).

Cette courbe montre d'abord qu'en faisant les mesures 8 jours après la sortie de pile, nous commettions sur $\triangle R/R_0$ une erreur constante d'une mesure à une autre.

Ensuite, si nous la prenons pour modèle de l'évolution à température ambiante des défauts *pendant* l'irradiation, nous pouvons introduire cette évolution dans l'analyse du nombre total des défauts à un moment donné.

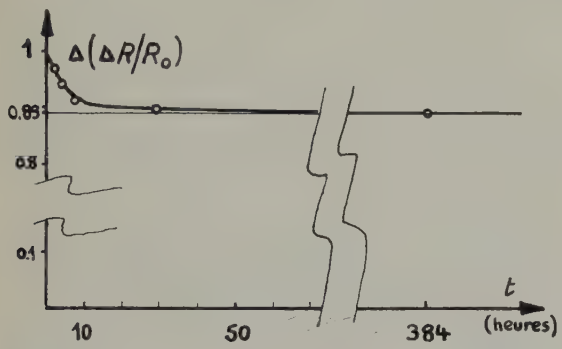

Fig. 7. Revenu de la résistance à température ambiante.

Nous admettons pour cela, qu'en première approximation, la fonction $f(t)$ (où $f(0)=1$) de la figure 7 représente le taux de disparition (ou de recombinaison) à la température ambiante des défauts apparus au moment $t=0$.

Cette probabilité, variable avec le temps, qu'ont les défauts d'évoluer après leur création, nous amène à chercher leur répartition en âge au cours de l'irradiation. Nous désignons par:

τ l'âge d'un défaut, c'est-à-dire le moment t où il a été formé (on aura toujours $\tau<t$).

$n(t, \tau)$ la répartition en âge des défauts: $n(t, \tau)\mathrm{d}\tau$ représente au moment t, le nombre de défauts apparus au moment τ pendant le temps $\mathrm{d}\tau$. $\mathrm{N}(t)=\int_0^t n(t, \tau)\mathrm{d}\tau$ est le nombre total de défauts au moment t.

Nous conservons aux constantes K, ν et v la signification précédemment donnée. Si nous nous intéressons à une tranche de population de défauts de même âge τ, les équations

$$n(\tau, \tau)=K \tag{1}$$

$$\frac{\partial n(t, \tau)}{\partial t}=n(t, \tau)\, f'_t(t-\tau)-\frac{1}{T}\, n(t, \tau) \text{ où } T=\frac{1}{\nu v} \tag{2}$$

décrivent

(1) la création au moment $t=\tau$ de défauts au rythme K.

(2) la disparition de ces mêmes défauts au cours du temps, le terme nf'_t se rapportant au recuit à température ambiante et le terme $-n/T$ exprimant l'annihilation par pointes de fission (ce dernier phénomène frappant évidemment les défauts sans distinction d'âge).

De (2), nous tirons:

$$n(t, \tau)=n_0(\tau)\ \exp\left[f(t-\tau)-\frac{t}{T}\right]$$

et de (1)

$$n_0(\tau)=K\ \exp\left(\frac{\tau}{T}-1\right)$$

d'où

$$n(t, \tau)=K\ \exp\left(\frac{\tau}{T}+f(t-\tau)-\frac{t}{T}-1\right). \tag{3}$$

Nous pouvons utiliser cette expression pour corriger les résultats expérimentaux en éliminant l'influence due au recuit pendant irradiation.

Ecrivons:

$$n(t, \tau)=n_1(t) \exp\left[\frac{\tau}{T}+f(t-\tau)\right] \text{ avec }$$

$$n_1(t)=K \exp\left(-\frac{t}{T}-1\right).$$

Pour une irradiation donnée, de durée t dans un flux de neutrons connu, T est approximativement connu (puisque $T=1/\nu v$ où nous prenons la valeur $v=2.5\times10^{-16}$ cm³).

Si nous traçons pour cette irradiation la courbe $n(\tau, f)=\exp\,[\tau/T+f(t-\tau)]$ dans le plan (n, τ), cette courbe représente la répartition en âge des défauts au moment t de fin d'irradiation, Si, sur le même graphique, nous traçons la courbe $n(\tau, 1)=\exp\,[(\tau/T)+1]$, nous avons l'image de la répartition s'il n'y avait pas recuit ($f\equiv1$). La figure 8 représente par exemple ces courbes pour une irradiation de 36 heures dans un flux de 2.4×10^{11} neutrons/cm$^{-2}\cdot$s (flux total 3.1×10^{16} neutrons/cm²).

La comparaison des aires $\mathscr{A}_f$ et $\mathscr{A}_1$ limitées par les courbes $n(\tau, f)$ et $n(\tau, 1)$ indique la proportion de défauts qui ont été éliminés par recuit pendant l'irradiation.

La correction $(\mathscr{A}_1-\mathscr{A}_f)/\mathscr{A}_f$ égale à 8 % dans le cas de la figure 8, a toujours été comprise entre 3 et 10.5 %. Elle est évidemment d'autant plus forte que le temps d'irradiation t est grand (par exemple 300 heures dans EL 2) ou que le flux de neutrons est faible (par exemple 0.4×10^{11} neutrons$\cdot$cm$^{-2}\cdot$s^{-1} dans EL 1).

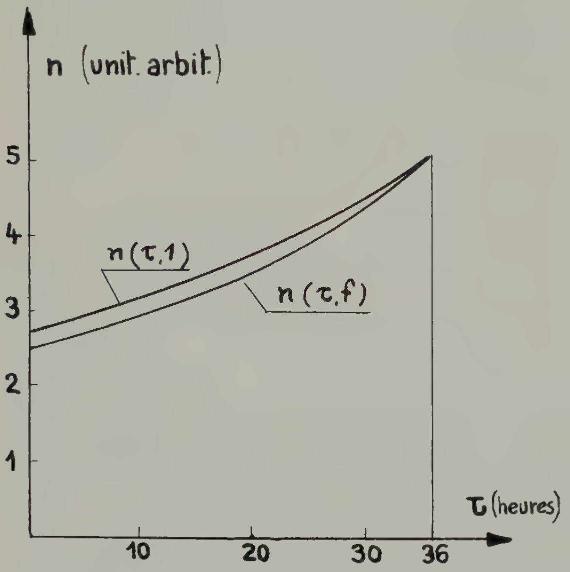

Fig. 8. Répartition en âge des défauts créés par irradiation.
$n(\tau,1)$ = répartition théorique (en l'absence de revenu).
$n(\tau,f)$ = répartition réelle.

Finalement, les résultats des mesures des résistance ont été majorés chacun

I. d'une correction constante $f(0)/f(\infty)=1/0.89$ qui ramène la mesure au moment de sortie de pile.

II. d'une correction $(\mathscr{A}_1-\mathscr{A}_f)/\mathscr{A}_f$ variable,

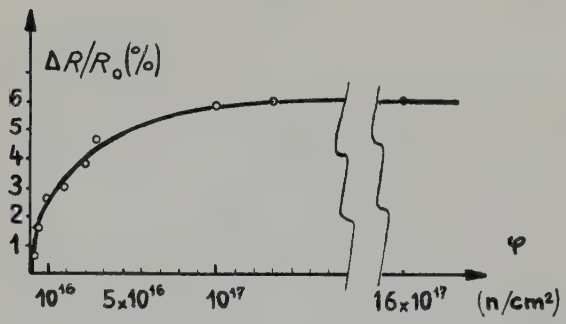

Fig. 9. Variation relative de résistance par irradiation (résultats corrigés).

tendant à éliminer l'évolution thermique des défauts pendant l'irradiation.

On obtient alors la courbe représentée sur la figure 9.

On pourra remarquer que les points ainsi obtenus sont *moins dispersés* que ceux de la figure 6.

3.2. Interprétation du taux d'irradiation

On sait que la réaction d'absorption qui, de ^{238}U aboutit à ^{239}Pu présente une section efficace résonnante pour les neutrons épithermiques.

Il existe de même plusieurs résonances épithermiques pour la fission de ^{235}U.

L'importance de ces phénomènes dépend du spectre de neutrons épithermiques de la pile qui n'est pas parfaitement connu.

Ces deux effets qui tendent:

Le premier à remplacer des atomes de ^{238}U par des atomes fissiles de Pu;

Le second à augmenter le nombre des fissions de ^{235}U,

peuvent jouer en surface un rôle non négligeable, augmentant l'un et l'autre le taux de combustion.

Il est donc important, pour des fils de 0.2 mm de diamètre, de savoir si l'on peut simple ment déduire ce taux de combustion du flux intégré de neutrons thermiques, sans faire d'erreur grossière.

Nous avons, pour cela, irradié en même temps un fil de 0.2 mm et un cube d'uranium de 5 mm d'arête. Nous avons ensuite prélevé au coeur du cube (par dissolution dans l'acide nitrique) une quantité d'uranium d'un poids équivalent à celui du fil et nous avons comparé l'activité du cube et celle du fil (par précipitation et comptage d'un des produits de fission, le baryum-140). Le fil, à poids égal, avait une activité d'environ 10 % supérieure à celle du cube, aussi bien pour une irradiation EL 1 que pour une irradiation EL 2.

Or, on peut calculer approximativement, par la théorie de la diffusion corrigée, la dépression de flux au centre du cube d'uranium: nous la trouvons égale à 9 %. Nous pouvons donc attribuer la différence d'activité trouvée entre

le fil et le cube à la dépression de flux dans ce dernier et prendre, comme taux de combustion des fils, celui qui correspond au flux intégré de neutrons qu'ils ont subi.

3.3. Volume de la pointe de fission

Nous pouvons maintenant interpréter la courbe de la figure 9 de façon simple.

L'équation de répartition

$$n(t,\tau) = K \exp\left(\frac{\tau}{T} + f(t-\tau) - \frac{t}{T} - 1\right)$$

devient, pour $f(t-\tau) \equiv 1$

$$n(t,\tau) = K \exp\left(\frac{\tau}{T} - \frac{t}{T}\right)$$

et alors

$$N(t) = \int_0^t n(t,\tau)\, d\tau = KT\left[1 - \exp\left(-\frac{t}{T}\right)\right].$$

Nous retrouvons évidemment la forme précédente

$$N(t) = KT[1 - \exp(-\nu v t)]$$

et de même $v = \dfrac{3.95 \text{ cm}}{\varphi_{1/2} \text{ neutrons/cm}^2}$, avec maintenant (fig. 9)

$$\varphi_{1/2} = (1.9 \times 10^{16} \pm 0.2 \times 10^{16}) \text{ neutrons/cm}^2$$

et alors

$$v = (2.1 \pm 0.2) \times 10^{-16} \text{ cm}^3.$$

4. Conclusions

La maille de l'uranium contenant 4 atomes pour 83 Å^3, le volume trouvé engloberait environ 10^7 atomes. Il est notablement plus fort que celui que Konobeevsky a déterminé mais ses mesures étaient relatives à des alliages U/Mo.

Il est important de remarquer que le "volume d'action" d'une fission dépend de la mesure physique qui prétend le déterminer. Nous avons ici défini la pointe de fission comme étant le volume dans lequel l'augmentation de résistivité était annihilée. A un autre paramètre correspondrait une définition du même type, mais le volume alors défini n'aurait pas de raison d'être le même que celui qui intervient pour la résistivité.

Notons enfin, l'intérêt qu'il y aurait à se débarrasser d'une correction de température ambiante en effectuant des irradiations à très basses températures.

Nous remercions ici M. Friedel et M. Blin des précieux conseils qu'ils nous ont donnés au cours de ce travail, et M. May (du Service des Radioéléments Artificiels) qui s'est chargé du comptage des fils irradiés.

Bibliographie

J. Blin, Effet de l'irradiation sur l'uranium. Semaine d'étude de la physique des métaux (CNAM, 1958)

J. Friedel, Action des rayonnements de grande énergie sur les solides, Défauts dans les cristaux (Gauthier Villars, 1956)

S. T. Konobeevsky, K. P. Dubrovin, B. M. Levitsky, C. D. Pantelev et N. F. Pravdyuk, On some physico chemical processes occuring in fissionable materials under irradiation (Seconde Conférence de Genève, 1958)

BOOK REVIEWS

F. P. Bowden and A. D. Yoffe, *Fast Reactions in Solids* (Butterworths Scientific Publications, London, 1958. 164 pages. 40s. Academic Press, New York, $ 7.00).

A chapter is included on the influence of corpuscular and electromagnetic radiations on the inception of explosions and on the kinetics of fast chemical reactions. Of the various unstable chemicals that have been investigated, only nitrogen iodide can be directly exploded, by corpuscular irradiation. The book as a whole gives a concise review of the fundamental aspects of explosions and detonations, and the chapter referred to serves to cast light on the general problem of the nucleation of explosions.

R. W. CAHN

Walter D. Wilkinson and William F. Murphy, with a chapter by Warren J. McGonnagle, *Nuclear Reactor Metallurgy* (D. van Nostrand Company, Princeton, 1958. viii + 382 pages).

This book was written to meet the specific needs of students of Argonne's International School of Nuclear Science and Engineering. Few of these students have any metallurgical knowledge, and the book thus seeks to inculcate the various elements of physical metallurgy at the points where they become necessary to an understanding of the text. This is inevitably an unsatisfactory procedure; many of the fragments of general metallurgy are far too concise to be entirely clear, and demand to be supplemented either by more spacious reading or else by the spoken word (as indeed they are at Argonne).

For readers already familiar with metallurgical concepts, however, the book is a most useful source of condensed information. Uranium is discussed fully, from ore-reduction to heat treatment, metallography and radiation damage. The chapter on uranium alloys is too brief to do justice to the importance of the subject. More technical topics such as corrosion and fuel element fabrication are also treated. Other metals such as beryllium and zirconium have chapters to themselves, and the chapter on ceramics includes several pages on uranium dioxide. There is an illuminatingly presented chapter on liquid metals which, however, omits mention of homogeneous liquid metal fuels.

While there are some references to British, French and Canadian work, the emphasis is very strongly on American contributions. This leads on occasions to serious omissions. Thus the chapter on canning of uranium makes no reference to the use of magnesium alloys, although this is standard practice in Britain and France. Zirconium as a canning material, on the other hand, receives full and detailed treatment.

In some details the text is, inevitably, not quite up to date. Thus the statement on p. 189 that alloying is not known to improve the dimensional stability of α-uranium is no longer correct. However, as a whole, this book is both an excellent introduction to its field and a useful source book of facts and figures.

R. W. CAHN

JOURNAL DES MATERIAUX NUCLEAIRES - 2 (1959) 211 - NORTH-HOLLAND PUBLISHING CO., AMSTERDAM

INSTRUCTIONS AUX AUTEURS

SOUMISSION DES TEXTES

Les manuscrits en français, anglais ou allemand doivent être envoyés en deux exemplaires à l'un des rédacteurs, soit directement, soit par l'intermédiaire de l'un des membres du Comité de Rédaction. Les résumés seront rédigés sur une feuille séparée fournie en quatre exemplaires.

Chaque volume pourra contenir un nombre limité d'articles d'ensemble rédigés sur la proposition des rédacteurs.

Les textes ne dépassant pas mille mots et ne comportant qu'un petit nombre de figures pourront être présentés comme "lettres à l'éditeur". Des commentaires sur les articles publiés dans le "Journal des Matériaux Nucléaires" seront les bienvenus et paraîtront sous forme de "lettres à l'éditeur".

Un effort particulier sera fait pour publier rapidement de telles lettres.

La possibilité de soumettre les manuscrits à un examen critique avant leur publication est laissée à la discrétion des rédacteurs. A ce sujet, aucun système n'a été formellement établi afin de faciliter une publication rapide.

Les auteurs doivent pouvoir déclarer que le manuscrit n'a pas encore été publié, ni partiellement, ni dans sa totalité.

Cependant, de brefs textes antérieurement présentés sous forme de "lettre à l'éditeur" dans "Nature" ou de note aux "Comptes Rendus" par exemple, pourront être développés dans le Journal des Matériaux Nucléaires. Il est entendu dans ce cas que l'auteur s'assure lui-même que les droits de publication ne seront pas enfreints par la parution de son article dans le Journal des Matériaux Nucléaires.

Si des rapports internes sont soumis au lieu de manuscrits, ils devront être soigneusement revus et présentés selon les règles exposées ci-dessous.

PRESENTATION

Le titre et le résumé seront dans la langue du texte; les lettres aux éditeurs ne nécessitent pas de résumé. Les résumés seront publiés en anglais, français et allemand; les rédacteurs se chargent de leur traduction (le résumé doit être compréhensible sans le titre qui ne sera pas traduit). Pour gagner de la place, éviter de couper un court résumé en plusieurs paragraphes.

Autant que possible éviter les renvois. S'ils sont employés, ne pas les numéroter mais les indiquer par les signes suivants: †, ††, ‡, ‡‡. Le renvoi devra être rédigé dans le texte même entre deux lignes, immédiatement sous la ligne contenant le signe correspondant.

Une attention particulière devra être portée sur la présentation de la partie expérimentale des travaux; on conseille d'user largement des appendices à cet effet afin d'éviter d'interrompre le texte. Une large utilisation de titres et de sous-titres facilite une compréhension rapide.

REFERENCES

Les références doivent être consécutivement numérotées dans le texte, par exemple: "selon Jones et Smith (6) . . ." et rassemblées à la fin du manuscrit (après les appendices). Autant que possible, citer de préférence des textes publiés plutôt que des rapports non publiés. Les exemples suivants illustrent la présentation des références:

1) W. Jones et J. Smith, J. Nucl. Mat. 1 (1959) 482.

2) G. Müller, Metallurgie der Nichteisenmetalle, Berlin, Springer, (1902), p. 231.

3) J. Adams, Argonne (USA) report ANL, 9347 (1955).

4) M. Dulong et G. Petit, Saclay (France) rapport CEA 4812, (1956).

5) T. Robinson, 2ème Conférence de Genève (1958) 15/P/8236.

Veiller à bien mentionner dans les références l'origine des rapports, conférences, etc . . . non publiés. Si un doute subsiste, écrire la référence avec le maximum de détails. Les organisations ne doivent être désignées par une notation abrégée que dans le cas où cette notation est admise sans confusion possible dans l'usage international.

FORMULES

Dans le texte, utiliser les *solidus* a/b et non les barres des fractions $\frac{a}{b}$; le symbole exp $(-x)$ et non e^{-x}. Ces règles ne concernent pas les formules exposées en évidence qui doivent être manuscrites pour faciliter le travail de l'imprimeur. Toutes les formules en cours de texte ou non doivent être ponctuées avec soin.

SYMBOLES ET ABREVIATIONS

L'attention des auteurs est particulièrement attirée sur les instructions suivantes qui, bien suivies, permettront de gagner beaucoup de temps.

En général, les auteurs sont invités à suivre les recommandations de la commission de nomenclature des symboles et unités de l'I.U.P.A.P., qui sont publiées dans Nuclear Physics 1 (1956) 539 et 7 (1958) 299.

Les symboles des grandeurs scalaires sont imprimés en italique; ils doivent toujours être soulignés dans le

texte tapé à la machine (par exemple: D pour une constante de diffusion, l pour une longueur, p pour la pression). Cette règle ne joue pas pour les formules exposées en milieu de page. Les symboles utilisés pour l'identification d'échantillons (par exemple: $B7$) seront de même imprimés en italique. Les vecteurs seront imprimés en plein trait, soulignés par un trait ondulé dans le texte ou les formules. Toutes les lettres ou groupes de lettres représentant des fonctions (exp, sin, log), les unités (cm, dyne, atm), les symboles chimiques ou toute abréviation ne représentant pas une grandeur (couche d, neutron = n), les noms de lieu ou d'organisations (AERE, CEA) sont imprimés en lettres ordinaires et ne doivent étre ni soulignés ni suivis de point dans le texte frappé (pas *cm.* mais cm). Il y a exception à cette règle dans le cas de quelques symboles composés qui doivent être écrits de la façon suivante: $\mathrm{g \cdot cm/sec^2}$, $\mathrm{kcal/cm^3 \cdot sec}$, $\mathrm{kg/cm^2}$ (et *non* kg/sq cm, $\mathrm{kg \cdot cm^{-2}}$ ou kg par $\mathrm{cm^2}$. Indiquer les isotopes de la façon suivante: U^{235}.

UNITES

Le système métrique sera utilisé. En particulier, les températures seront toujours indiquées en °C ou °K et non en °F. Exceptionnellement, les pressions et tensions pourront être exprimées en psi (livre par pouce carré), en raison de leur usage fréquent ($1\ \mathrm{kg/cm^2} = 14.223$ psi). Les tonnes du système métrique seront exprimées par le terme "tonne". Les pertes par corrosion seront données en $\mathrm{mg/cm^2}$.

Les flux de neutrons intégrés seront mentionnés avec le symbole nvt ($\mathrm{neutron/cm^2}$). Les taux de combustion seront exprimés en nombre d'atomes ayant subi la fission pour 100 atomes de l'élément combustible initial, de même pour les alliages combustibles.

La composition des alliages peut être donnée soit en poids pour cent (pds %) ou de préférence en atomes pour cent (at %). Ne jamais laisser le terme % seul.

Dans le texte, la composition des alliages doit être indiquée comme dans l'exemple suivant: Al/4.0 pds % Cu/0.5 pds % Mn.

Les symboles qui ne sont pas d'usage général comme ε pour "l'élongation à la rupture" ou R pour la "charge de rupture" ne doivent jamais être employés sans explication; cette règle est imposée par le caractère international du Journal des Matériaux Nucléaires. Si de tels signes sont utilisés, ils doivent toujours être expliqués dans les légendes ou sur les figures elles-mêmes.

SYMBOLES MATHEMATIQUES

Pour le logarithme népérien de x, écrire $\log x$ ou $\ln x$. Pour le logarithme à base dix, $\log_{10} x$ (les suffixes comme le 10 dans $\log_{10}$ x seront indiqués en veillant à ce qu'il n'y ait aucune confusion possible sur leur nature pour l'imprimeur). Pour "approximativement égal", utiliser le signe $\approx$.

LETTRES GRECQUES

Les lettres grecques doivent être expliquées dans la marge. Ceci est particulièrement important dans le cas de α qui peut être confondu avec le signe $\propto$ "proportionnel à".

DESSINS ET TABLEAUX

L'emplacement approximatif des figures et des tableaux doit être indiqué au crayon dans le texte tapé. Chaque tableau doit être envoyé sur une feuille séparée et doit avoir un titre en plus de son numéro.

Les traits des figures doivent être d'une seule ligne à l'encre de chine et les lettres en caractères gras. L'imprimeur ne peut pas préparer de plaques pour les dessins tels que ceux reproduits dans les rapports polycopiés après stencils. On est prié de veiller à une épaisseur de trait et une taille de lettre suffisantes pour pouvoir les réduire au moment de la mise en plaques. Les règles ci-dessus et les symboles concernant les unités doivent être aussi observés pour les figures.

Toutes les figures doivent avoir des légendes qui seront rassemblées dans une liste sur une feuille à part; des légendes bien détaillées facilitent la compréhension du texte.

PHOTOS

En présenter le minimum en raison du prix toujours plus élevé de leur reproduction.

Il est préférable pour la présentation des articles qu'un format uniforme soit maintenu. Le travail de l'imprimeur sera facilité si la largeur des photos est la même que celle des colonnes (3 pouces $\approx$ 7.5 cm), l'échelle d'agrandissement de toutes les photos sera signalée dans les légendes par exemple: (120 $\times$).

Les photos à reproduire ne doivent pas être encadrées sauf si elles font partie d'une figure composée; il est préférable de faire ressortir les contrastes qui seront atténués dans le texte imprimé. Si nécessaire, indiquer la partie supérieure de la photo par une croix au verso.

Il serait préférable de ne pas exposer de schémas ou photographies des équipements techniques et accessoires (loupes, boîtes à gants, équipement d'irradiation, fours de moulage) à moins qu'ils soient d'un intérêt nouveau.

TIRES A PART

Les auteurs seuls en recevront 25 exemplaires gratuits. Deux ou plusieurs auteurs en recevront 50. Les exemplaires supplémentaires devront être commandés au moment du renvoi des placards corrigés.